

Temperature Responsive Photonic Coatings based on Siloxane Liquid Crystals

Citation for published version (APA):

Zhang, W. (2021). *Temperature Responsive Photonic Coatings based on Siloxane Liquid Crystals*. [Phd Thesis 1 (Research TU/e / Graduation TU/e), Chemical Engineering and Chemistry]. Technische Universiteit Eindhoven.

Document status and date:

Published: 01/09/2021

Document Version:

Publisher's PDF, also known as Version of Record (includes final page, issue and volume numbers)

Please check the document version of this publication:

- A submitted manuscript is the version of the article upon submission and before peer-review. There can be important differences between the submitted version and the official published version of record. People interested in the research are advised to contact the author for the final version of the publication, or visit the DOI to the publisher's website.
- The final author version and the galley proof are versions of the publication after peer review.
- The final published version features the final layout of the paper including the volume, issue and page numbers.

[Link to publication](#)

General rights

Copyright and moral rights for the publications made accessible in the public portal are retained by the authors and/or other copyright owners and it is a condition of accessing publications that users recognise and abide by the legal requirements associated with these rights.

- Users may download and print one copy of any publication from the public portal for the purpose of private study or research.
- You may not further distribute the material or use it for any profit-making activity or commercial gain
- You may freely distribute the URL identifying the publication in the public portal.

If the publication is distributed under the terms of Article 25fa of the Dutch Copyright Act, indicated by the "Taverne" license above, please follow below link for the End User Agreement:

www.tue.nl/taverne

Take down policy

If you believe that this document breaches copyright please contact us at:

openaccess@tue.nl

providing details and we will investigate your claim.

Temperature Responsive Photonic Coatings based on Siloxane Liquid Crystals

PROEFSCHRIFT

ter verkrijging van de graad van doctor aan de Technische
Universiteit Eindhoven, op gezag van de rector magnificus prof.dr.ir.
F.P.T. Baaijens, voor een commissie aangewezen door het College
voor Promoties, in het openbaar te verdedigen op woensdag 1
september 2021 om 11:00 uur

door

Weixin Zhang

geboren te Guangdong, China

Dit proefschrift is goedgekeurd door de promotoren en de samenstelling van de promotiecommissie is als volgt:

voorzitter: prof.dr. F. Gallucci
1^e promotor: prof.dr. A.P.H.J. Schenning
2^e promotor: prof.dr. L.T. de Haan (South China Normal University)
copromotor: prof.dr. G. Zhou (South China Normal University)
leden: prof.dr. R.P. Sijbesma
dr. A.C. de Carvalho Esteves
prof.dr. J. Wang (Technical Institute of Physics &
Chemistry, Chinese Academy of Sciences)
adviseur: dr. J. Lub

Het onderzoek of ontwerp dat in dit proefschrift wordt beschreven is uitgevoerd in overeenstemming met de TU/e Gedragscode Wetenschapsbeoefening.

A catalogue record is available from the Eindhoven University of Technology Library.

ISBN: 978-90-386-5333-4

Copyright © 2021 by Weixin Zhang

Cover design by Weixin Zhang

Printed by ProefschriftMaken || www.proefschriftmaken.nl

This work has been financially supported by National Key R&D Program of China (2020YFE0100200), National Natural Science Foundation of China (Nos. 51561135014, U1501244), the Science and Technology Program of Guangzhou (Grant Nos. 2019050001), Science and technology project of Guangdong Province (No. 2018A050501012), Guangdong Provincial Key Laboratory of Optical Information Materials and Technology (No. 2017B030301007), National Center for International Research on Green Optoelectronics (IRGO), MOE International Laboratory for Optical Information Technologies, SCNU-TUE Joint Lab of Device Integrated Responsive Materials (DIRM), the 111 Project and Yunnan expert workstation (202005AF150028).

Table of Contents

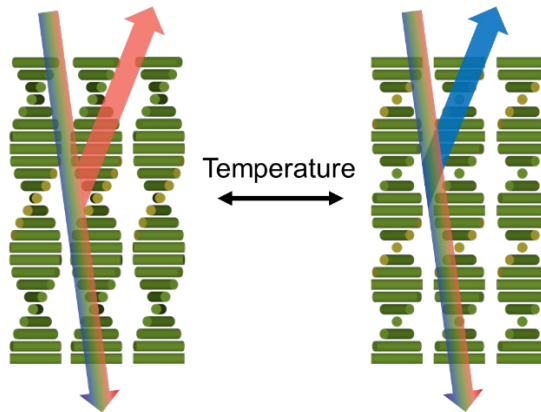
Chapter 1 <i>Introduction</i>	1
Chapter 2 <i>Easily processable temperature responsive infrared reflective coatings based on liquid crystal oligomers</i>	23
Chapter 3 <i>Polymer stabilized cholesteric liquid crystal polysiloxane for temperature responsive infrared reflective coatings</i>	39
Chapter 4 <i>Fully reversible thermochromic photonic coatings with a protective topcoat</i>	63
Chapter 5 <i>Thermochromic multicolored photonic coatings with linear polarized light dependent features</i>	79
Chapter 6 <i>Technology assessment</i>	95
Summary	109
Acknowledgements	111
Curriculum Vitae	115

Frequently used abbreviations:

CLC	cholesteric liquid crystals
TR-RC	temperature responsive reflective color
Ch	cholesteric
Sm	smectic A
T_{Sm-Ch}	smectic to cholesteric transition temperature
T_i	isotropic transition temperature
T_g	glass transition temperature
HTP	helical twisting power
PDLC	polymer-dispersed liquid crystals
PSLC	polymer-stabilized liquid crystals
NMR	nuclear magnetic resonance
DSC	differential scanning calorimetry
POM	polarized optical microscopy
n_{avg}	average chain length
MALDI-TOF-MS	matrix-assisted laser desorption/ionization-time of flight mass spectrometry
LPL	linear polarized light

Chapter 1

Introduction



Temperature responsive cholesteric liquid crystals (CLCs) are an important class of photonic materials that show dynamic reflection properties upon temperature changes. Such photonic materials are promising for applications in interactive decoration, sensors, and heat-regulating windows. Development of these materials into coatings would allow for scalable fabrication of products and a broader range of applications. This chapter reviews the different classes of temperature responsive CLC coatings, showing the different molecular systems and the corresponding mechanisms of the thermochromic behavior. The last part of this chapter describes the aim of the thesis: the development of easily-processable, robust, transparent, reversibly temperature responsive CLC coatings.

This chapter is partially reproduced from: Zhang, W.; Froyen, A. A. F.; Schenning, A. P. H. J.; Zhou, G.; Debije, M. G.; de Haan, L. T. Temperature-Responsive Photonic Devices Based on Cholesteric Liquid Crystals. *Adv. Photonics Res.* **2021**, 2 (7), 2100016.

Chapter 1

1. General introduction

Electromagnetic waves of different wavelengths are perceived by most eyes as different colors; this perception is ubiquitous to daily life as humans rely on light for visual recognition of objects, reception of signals, and appreciation of aesthetics. However, the visible spectrum makes up only a fraction of solar light: many wavelengths are invisible to the human eye but are still essential for life on Earth. Near-infrared light, for instance, is a major component of the sun's radiation reaching Earth, predominantly acting as a heating source.^[1]

Photonic structures are composed of highly ordered stacks of alternating materials with differing refractive indices. This periodic modulation creates a "Bragg reflector" that selectively reflects light of certain wavelengths. Common natural examples of static photonic structures include the alternating layers found in butterfly wings^[2,3], the opal-like structures of bird feathers^[4,5], and beetle carapaces^[6,7]. However, biology presents not only static but also dynamic color. Species such as sapphirinid copepods^[8,9], panther chameleons^[10], and neon tetra fish^[11] can alter their skin colors for camouflage or communication purposes. These dynamic, vivid colors rely on dynamic photonic structures. Decades of biomimetic studies have been conducted to develop iridescent reflectors in the laboratory.^[12-15] Helicoid structures that act as Bragg reflectors can be built using self-assembled nanocrystals^[16-19] or blue-phase liquid crystals^[20], but helicoid temperature-responsive devices are mostly realized by using cholesteric liquid crystals (CLCs).^[21,22]

Typical thermotropic, calamitic liquid crystals (LCs) consist of rigid mesogenic groups and flexible spacers (Figure 1.1). The rigid mesogenic groups (cores) often include aromatic or hexagonal rings, providing crystalline order. The cores are linked to soft spacer units, usually aliphatic tails. The combination of cores and tails results in a system with crystal-like order but liquid-like rheology due to the presence of both hard and soft moieties. By introducing chiral molecules to the achiral nematic (N) phase, the mesogens self-assemble into the cholesteric (Ch) phase, also referred to as the chiral nematic (N*) phase.^[23] The cholesteric phase is similar to the achiral nematic phase but with a small rotational offset of the anisotropic mesogenic units from neighboring units, yielding a helicoidal structure, due to the presence of chiral dopants that induce the helical twist in either a right- or left-handed manner, depending on the stereochemistry of the dopant's chiral center. Incident circularly

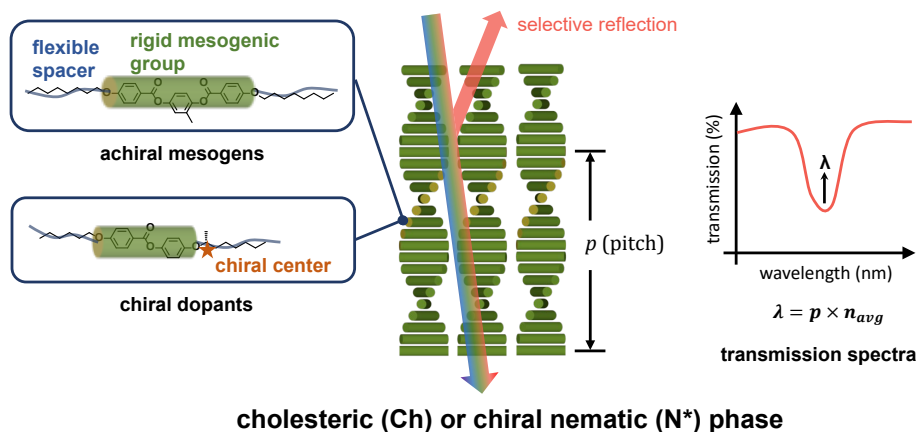


Figure 1.1 Schematic representation of the cholesteric phase with a demonstration of selective reflection. The central illustration demonstrates the general molecular structure of CLC systems. The chiral dopants have stereospecific centers that induce the helical twist in the host mesogens. A typical calamitic achiral LC molecule and a typical chiral dopant molecule are shown as an example (left), each with a rigid mesogenic group and flexible spacer unit(s). On the right is a schematic representation of the classical reflection band induced by planar-aligned CLCs, which is often characterized by transmission spectra. The notch in the transmission spectra represents the reflection center (λ).

polarized light (CPL) of the same handedness as the helix is reflected while the opposite handedness of CPL is transmitted. This means that for unpolarized incident light a maximum of 50% of the incoming light can be reflected. The Bragg reflection wavelength (λ) of such helical structures is a function of the helical pitch (p) and n_{avg} of the cholesteric phase. When observed normal to the surface of the cholesteric, the Bragg reflection equation can be simplified to Equation 2:

$$\lambda = p \times n_{avg} \quad \text{Equation 1}$$

where λ denotes the bandgap's central wavelength, n_{avg} the average refractive index. The pitch p is defined as the distance over which 2π (full) rotations take place. The helical pitch of CLCs is determined by the helical twisting power (HTP, in μm^{-1}) of the chiral units, the measure of the capacity of compelling the planes of LCs to rotate through the depth of the layer in the case of planar CLC alignment, the concentration of chiral units in the system (c), and its enantiomeric excess (ee) (Equation 3). In most cases, ee is 1, as absolute stereospecific compounds are used. The sign of the HTP is

Chapter 1

defined as the handedness induced by the dopant, where a plus sign (+) stands for right-handedness, and a minus sign (-) stands for left-handedness.

$$p = 1/(HTP \times c \times ee) \quad \text{Equation 2}$$

Photonic structures must consist of highly ordered periodic microstructures for proper Bragg reflection. For CLCs, a planar monodomain alignment is required to present selective reflection properties without light scattering. The advantage of using CLCs lies in their ability to self-assemble into photonic structures. Compared to other forms of photonic crystal structures such as opals, block copolymers and alternating refractive index layers,^[24–27] structural color from CLCs can be achieved without the presence of phase-separated materials. Furthermore, as a result of the liquid-like flow behavior, the alignment of CLCs can easily be realized by shear or capillary forces, or by use of alignment layers, enabling large-scale fabrication of CLCs into various device forms, including cells (material sandwiched between substrates), coatings (material on a single substrate), free-standing films, microcapsules, and even three-dimensional objects.

Technologies based on stimuli-responsive CLC systems that alter their reflective color are rapidly developing.^[22,25,28] In particular, “smart” temperature-responsive CLCs^[29] have found their way into numerous applications since they can alter their pitch length, and thus their reflective color, autonomously with a change in temperature. Such autonomously responsive CLC systems are desirable as temperature indicators^[30], interactive decorations^[31], smart safety labels,^[32,33] and energy regulating ‘smart’ windows.^[34]

2. Temperature responsive CLC coatings

Classical CLC systems involve only small mesogenic molecules, where the mesogens have a high degree of freedom to rotate and displace, which allows for drastically temperature responsiveness in reflection color (TR-RC). Although small mesogenic molecules have been thoroughly studied in cells, recent advances in small molecule systems have shifted the focus towards single-substrate devices, since coatings allow for easy scale-up of production and could be introduced in a broader range of applications (e.g. flexible devices) compared to cell-based CLC devices. Small

mesogenic molecular systems, however, suffer from poor performance stability over time due to their fluid-like behavior. There are many modifications to a CLC system to gain suitability for coating devices, including encapsulation of small mesogenic molecules, stabilizing with crosslinked network, or creating polymeric CLC systems. This section will discuss the state-of-the-art temperature responsive CLC coatings utilizing different molecular systems, driven by different mechanisms, and fabricated via different methods.

Small mesogenic CLC molecules often generate a temperature responsiveness through one of two mechanisms: thermal HTP variation and smectic transition. Both mechanisms are based on the winding/unwinding of the helix, which can achieve a large reflection band shift.

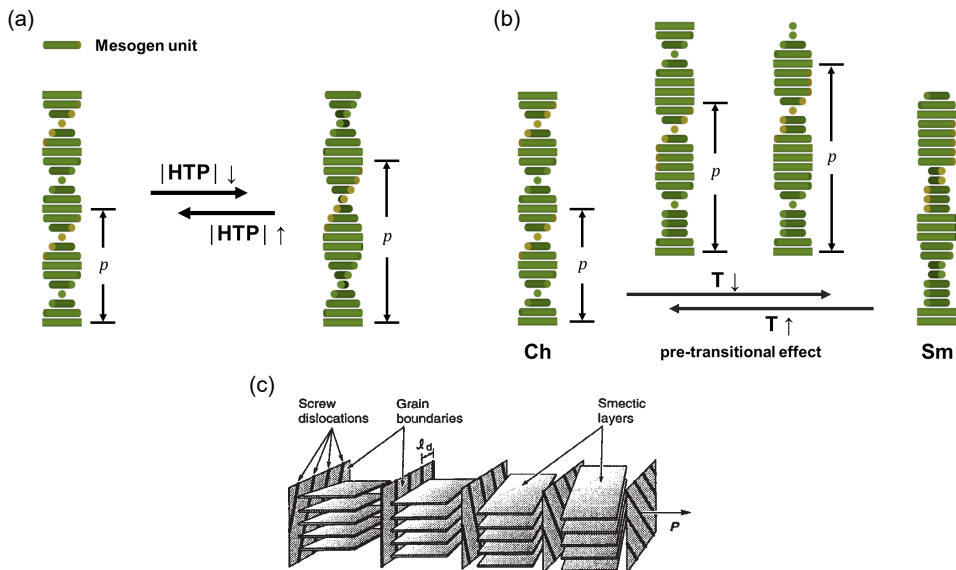


Figure 1.2 Schematic representations of two typical TR-RC mechanisms of temperature responsive CLCs: (a) Heat-responsive helical twisting power and (b) Smectic-cholesteric transition. (c) Schematic representation of TGBA (smectic A*) phase theory. Reproduced with permission.^[37] Copyright 2006, Taylor & Francis.

The HTP variation stems from different interactions between the changing molecular conformations of the chiral dopant with the host, which is mainly related to the

Chapter 1

chemical nature of the chiral center (Figure 1.2a). Some CLCs have a smectic A (Sm) phase transition at lower temperature, and passing through this phase transition can have a dramatic effect on the photonic structure. The pitch of the unwinding helices increases towards infinite with decreasing temperature (Figure 1.2b), resulting in an exceptionally large reflection band shift over a relatively small temperature range. An example of nematic E7 mixed with chiral dopant S811 in cells presents a large bandshift of ~500 nm by only a 0.2 °C change of temperature when closing to the transition point.^[35]

The smectic*-cholesteric effect is understood as the gradual growth of smectic moieties inside the cholesteric phase which causes an enlargement of the pitch. The smectic phase adopts a close-to-crystal order in layered structures. The CLC that has a smectic phase transition increases its helical pitch drastically towards infinite during cooling when the temperature approaches the smectic transition (Figure 1.2b). This effect is called the pre-transitional effect^[36], as it takes place above the smectic transition point over a wide temperature range.

The smectic-cholesteric transition mechanism is explained by the twist-grain-boundary phase (TGB) theory.^[37] The TGB theory reveals that the twisting of cholesteric phase serves as an external field similar to mechanical deformation.^[38] This cholesteric twist deformation, combined with the twist and bend deformation of mesogens near the smectic transition, leads to a “twisted smectic A” (smectic A*) structure, where smectic domains adopt a twisted pattern between layers (Figure 1.3c). These twisted smectic layers are bound to incur defects^[39] at their boundaries, called “grain boundary”. Therefore, the smectic A* phase is also named the TGBA phase. A defect-less smectic A phase should have no photonic structure, but a TGBA structure has helical twists due to the defects, and is thus photonic. Maintaining planar helical alignment upon temperature variations in these systems is essential for transparent devices. In some cases, rather than shifting the reflection band, the sharp transition between the smectic and cholesteric phases can instead result in disruption of the planar helical alignment into a focal conic state (multi-domain), resulting in scattering.^[40] This misalignment can be corrected by annealing in the cholesteric temperature range with the assistance of an alignment layer.^[41]

* The term “smectic” in this thesis particularly refers to the smectic A type.

The pre-transitional effect is a powerful mechanism for temperature responsive photonic systems due to the large response. The smectic-cholesteric transition effect is the thermochromic mechanism which drives the coating devices described throughout Chapters 2-5 of this thesis.

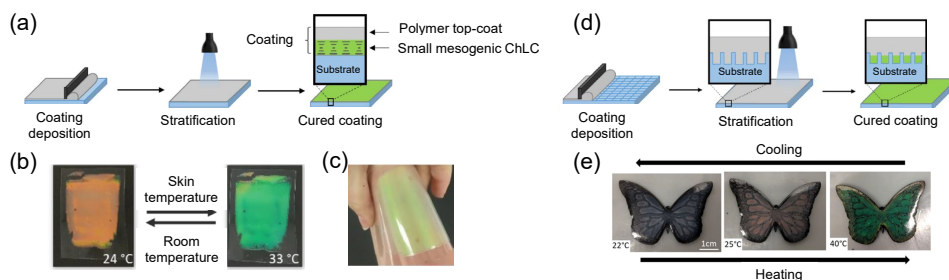


Figure 1.3 Demonstrations of photo-induced phase separation yielding a polymeric hard top-coat that protects the responsive CLC small mesogenic molecules underneath. (a) Scheme of a one-step photopolymerization-induced phase separation (also known as stratification). (b) The stratified coating shows a reflection color change upon heating. (c) Flexible devices were possible using a polycarbonate foil as a substrate. (d) Leakage of the CLC layer can be prevented by using a substrate with pre-designed trays. (e) A butterfly pattern was 3D printed on poly(lactic acid). A reversible TR-RC behavior was observed. Reproduced with permission. [42] Copyright 2019, Royal Society of Chemistry.

Adopting either HTP changing or smectic-cholesteric transition mechanisms, these small mesogenic molecules must be confined to prevent LC leakage. One possible route is by creating a stratified top layer. To prepare such layers, a temperature-responsive CLC mixture is blended with UV-curable acrylate monomers and a UV absorber.^[42] After applying a layer of the unreacted mixture on top of a substrate, subsequent photo-polymerization at a low intensity initiates a polymerization-induced phase separation (Figure 1.3a). The UV absorber creates a steep light intensity gradient through the film thickness, causing the UV-curable monomers to rapidly polymerize near the top surface, promoting the diffusion of additional monomer to the film surface, thereby forming a hard, polymeric topcoat. Thus, after photopolymerization, the CLC mixture is protected by a polymer layer and shows a reasonable degree of alignment. Upon heating, a blueshift was observed due to the HTP changing of chiral dopant included in the CLC (Figure 1.3b). The smectic-cholesteric type of CLCs are also applicable here.^[43,44] The devices were flexible since a thin polycarbonate sheet was used as substrate (Figure 1.3c). Additionally,

Chapter 1

substrates consisting of pre-designed trays were fabricated to prevent leakage and to enhance the structural integrity and robustness of the device (Figure 1.3d).^[42] Complex patterned substrates can be made in any arbitrary shape and pattern with a 3D printer, for example. Figure 1.3e gives an example of a phase-separated photopolymerized CLC coating on top of a printed substrate.

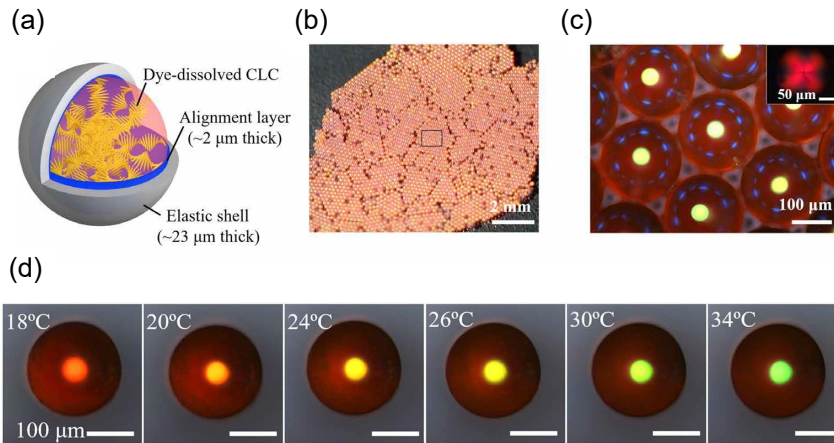


Figure 1.4 (a) Schematic of a photonic capsule composed of a CLC core with a dye dissolved into it, an inner alignment layer, and an outer elastic shell. (b,c) Photograph and optical microscopy image of dried CLC capsules. The capsules maintain their spherical shape and radially aligned helical axes, which results in photonic cross-communication. (d) TR-RC demonstration of the CLC microcapsules observed using microscopy. Reproduced with permission.^[45] Copyright 2018, Science (AAAS).

Encapsulation of small mesogenic CLCs can be also realized in spherical shells. This results in the development of angular independent TR-RC devices.^[45] Using a microfluidic production method, TR-RC CLC material is confined in elastic shells of photo-cured silicone methacrylate. Remnant glycerol and polyvinyl alcohol from the emulsion solution at the shell interface provide a surface with planar anchoring conditions for the alignment, with the helical axis extending in the radial direction (Figure 1.4a-c). Due to the radial CLC configuration, the reflection color of the particles is independent of the viewing angle. The TR-RC was preserved in these capsules, which showed a red-to-green color shift between 18 °C and 34 °C (Figure 1.4d). A fluorescent dye was doped into the LC phase to allow for lasing. The radial

alignment of the CLC leads to omnidirectional lasing, which can be used for imaging applications.

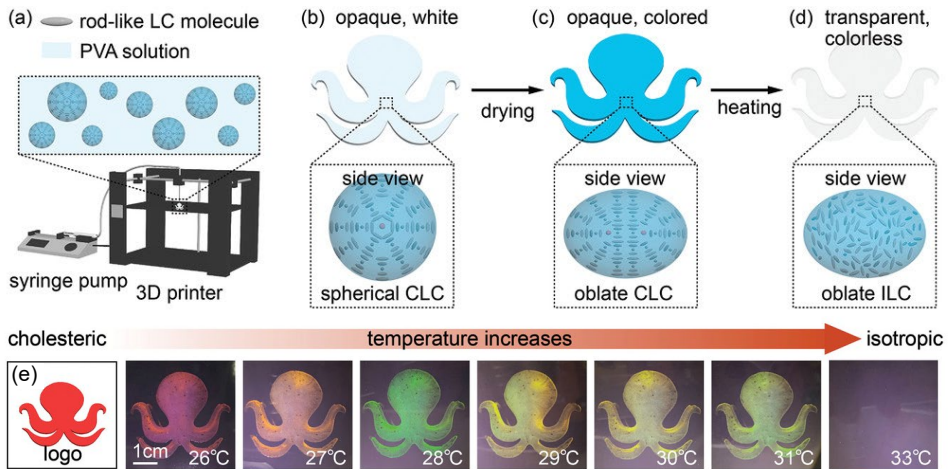


Figure 1.5 (a,b) the 3D printing procedure of the spherical-CLC-droplet-dispersed PVA solution into an octopus shape. (c) Upon water evaporation, spherical CLC droplets are squeezed into oblate CLC droplets and the opaque, white octopus pattern turns into an opaque-and-colored state. (d) Upon heating to the isotropic phase, the octopus pattern becomes transparent and colorless. (e) TR-RC behavior of the 3D-printed octopus' logo. Reproduced with permission. ^[48] Copyright 2021, John Wiley and Sons.

One can presume that such microcapsules can be dispersed in a polymeric binder to establish robust coatings.^[46,47] Such polymer-dispersed liquid crystal (PDLC) systems are often highly robust and can be produced without alignment layers, making them well-suited for all manner of applications. PDLC systems can be also created via emulsion that enables rapid fabrication of devices in a single production step. A recent example of 3D printable, emulsion-based PDLC coatings that exhibit a TR-RC response is based on CLCs having a smectic-cholesteric transition upon heating embedded in polyvinyl alcohol (Figure 1.5a-b),^[48] Upon emulsifying, the CLC material is dispersed as distributed-sized droplets due to the immiscibility between the aqueous solution and the CLC material. Although the CLC is planar-radially aligned, an opaque white reflection is shown at this stage due to polydisperse droplet size. After printing the emulsion, the coating is left to dry. Shrinkage of the deposited film, induced by water evaporation, promotes alignment into oblate spheroids due to the compression of the original CLC spheres (Figure 1.5c). The planar helix

Chapter 1

orientation is thereby acquired due to the solidification of the polymer, showing vivid reflection colors. The smectic-cholesteric type temperature response is obtained in these PDLC coatings, and while the temperature enters isotropic phase, the reflection disappears as the planar alignment is erased (Figure 1.5d-e).

Commercial products, such as Feverscan[®][30] (LCR Hallcrest) and SFXC[®] Liquid Crystal Sheets[31] (SFXC), have been developed using micro-encapsulated TR-RC CLC inks. The formulations of these inks are confidential, but the product descriptions (for example, the product sheets can be cut with scissors) strongly suggest these formulations are based on one of the PDLC methods explained above. These flexible temperature-responsive sheets can be applied directly to a substrate as a label by using an adhesive layer. The TR-RC inks can be bought separately and used to decorate a surface using spray coating and inkjet printing.^[49] Despite these promising PDLC applications, some major challenges remain. The development of uniformly sized CLC capsules/droplets on large scales is challenging, and they can become inhomogeneously distributed after coating and drying. Owing to the refractive index mismatch between the CLC spheres and the polymer binder, these films are prone to scattering, so this technique has not been used to develop transparent devices to date.

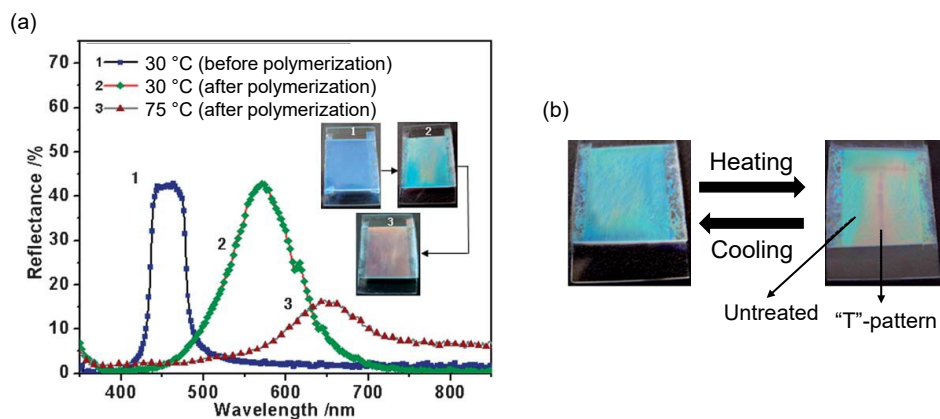


Figure 1.6 (a) Reflection spectra of the PSLC cell before/after polymerization at 30°C, and upon heated to 75°C after the polymerization. A red shift of reflection color upon heated is presented, as can be also seen by the photos. (b) The PSLC coating from the cell was demonstrated a drawn pattern when partially heated using a hot-pen. Upon cooling, the pattern disappeared. Reproduced with permission.^[55] Copyright 2010, Royal Society of Chemistry.

Besides PDLs, polymer-stabilized liquid crystals (PSLC) is an alternative category of CLC configuration, wherein the small mesogens are interpenetrated by the LC network. By stabilizing small mesogenic CLCs with a small amount of crosslinked LC network, the TR-RC functions of CLCs can be expanded, such as band-broadening^[50-53] or having both handedness of helices in one layer^[54], which have been realized in cells. Although PSLC systems utilize polymer networks, they primarily consist of small mesogenic molecules and are presumably not resistant enough to mechanical forces (e.g. touching) for use in coating applications. A rare example of a temperature-responsive PSLC applied as a coating is one using 20 wt % polymer network that includes a chiral crosslinker species with a thermo-sensitive HTP.^[55] The PSLC was prepared via a cell filling procedure, after which one glass plate was subsequently removed to obtain the coating. A redshift of color was observed after the polymerization. The coating demonstrated a reversible color shift from green to red (575-650nm) between 30 °C and 75 °C (Figure 1.6a). To demonstrate the versatility of the film, a red pattern was drawn on the coating using a hot-pen. The color change is reversed upon cooling, whereupon the pattern disappeared (Figure 1.6b). However, the robustness of the coating surface when exposed to external stresses was not demonstrated.

In contrast to small mesogenic molecules, the LC-to-crystal phase transition is normally suppressed in polymeric LCs, which instead display glass transitions. TR-RC coatings made of fully crosslinked CLC polymers or with oligomers are more often based on a change in layer thickness rather than on winding/unwinding of the helices (the HTP-changing and smectic-cholesteric mechanisms). Examples of the latter mechanisms are limited and can only be found in cells.^[56-59] An example of a PSLC coating with oligomers was obtained using a phase separation mechanism.^[60] The molecular system consists of an achiral siloxane oligomer that functions as a liquid crystal elastomer (LCE) and 21 wt % of reactive chiral mesogens (RM-1 and RM-2) that form a crosslinked network after photopolymerization (Figure 1.7a). The coating initially has a red color at room temperature (centered at 800 nm). Upon heating above the isotropic transition of the LCE, the coating reflection gradually blueshifts to 515 nm after 3.5 h as the LCE slowly diffuses towards the air interface (Figure 1.7b). A reversed shift is observed over a span of three weeks upon cooling below the isotropic temperature as the phase separated LCE slowly mixes back into the PSLC, causing swelling and thus the reversal of the band shift (Figure 1.7c).

Chapter 1

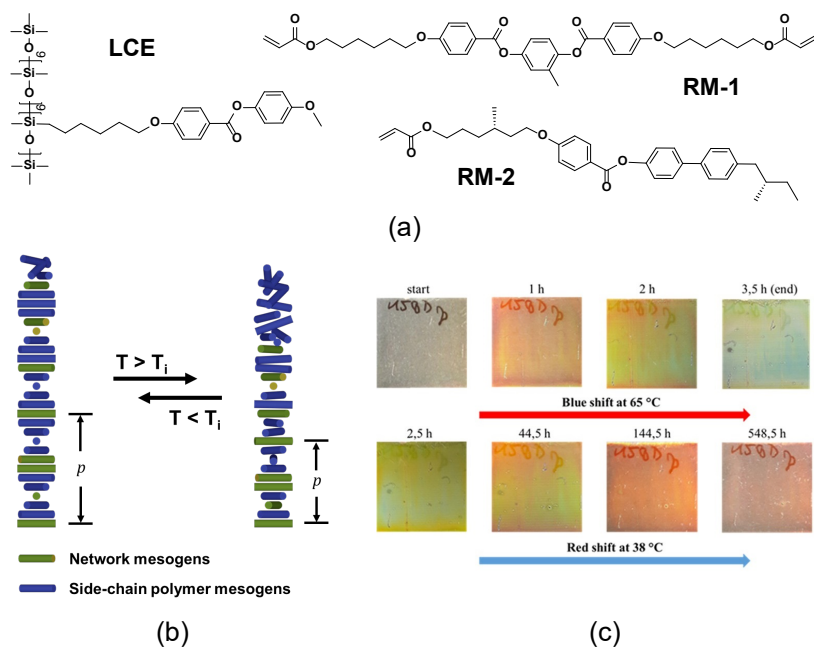


Figure 1.7 (a) Chemical composition of the TR-RC coating based on phase separation. (b) Representation of the phase separation mechanism between mesogenic molecules. (c) Photographs of the coating, showing the blue- and redshift during respectively heating above or cooling below the isotropic point. Reproduced with permission.^[60] Copyright 2019, American Chemical Society.

Phase separation of non-mesogenic molecules can also cause TR-RC. By including volatile, non-covalently bonded substances in the crosslinked network which may be removed by subsequent heating, the decreasing layer thickness results in a decrease in pitch length, and thus a blueshift of the reflection band (Figure 1.8a). The association of carboxylic acid groups via hydrogen bonds was exploited in a crosslinked polymeric CLC film by incorporating a non-reactive dicarboxylic acid (R)-(+)-3-methyladipic acid (MAA) chiral dopant.^[61] Raising the temperature above 160 °C disrupts the hydrogen bonds between the carboxylic groups, leading to the evaporation of MAA and collapse of the film with concurrent blueshifts of reflection color irreversibly from orange to green (Figure 1.8b). Such collapse is visible by mapping the surface topography (Figure 1.8c). The covalent crosslinking helps maintain the photonic structures during the collapse, allowing for color patterning

upon local heat exposure by using a laser beam as a “hot-pen” (Figure 1.8d). Upon base treatment of this coating, the carboxylic acid groups (-COOH) are converted into carboxylate groups (-COO⁻), disrupting the hydrogen bonds (Figure 1.8e). After drying, the coating becomes hygroscopic due to the presence of the ionic species. In

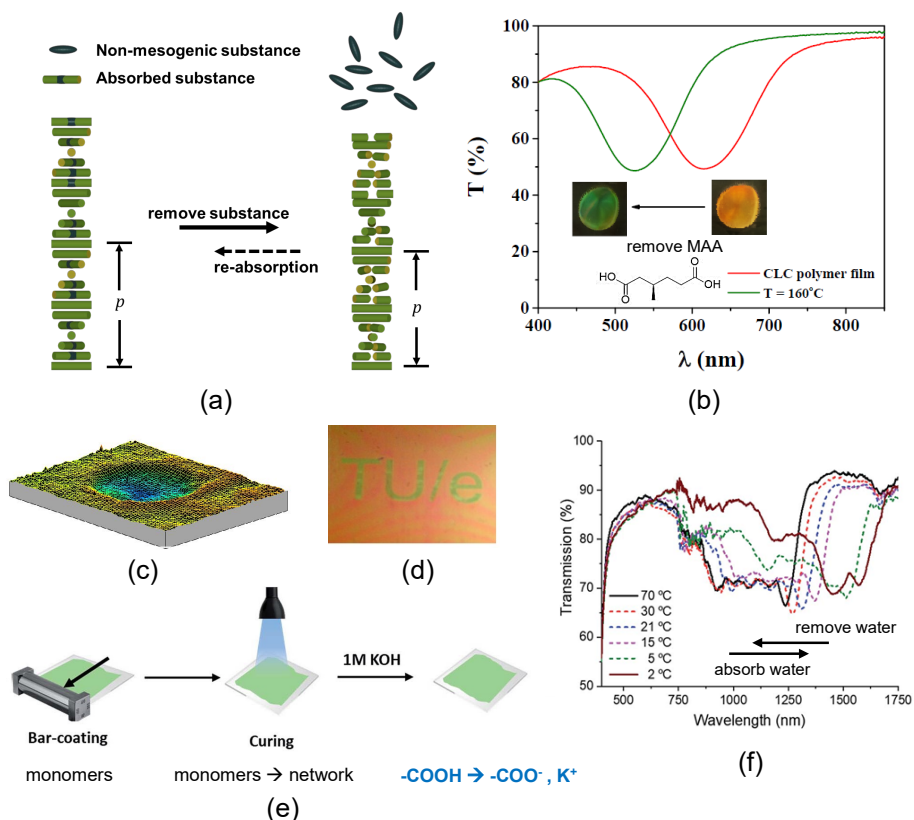


Figure 1.8 (a) Representation of the phase separation mechanism of non-mesogenic molecules. (b) Presentation of an irreversible TR-RC coating. Upon heating to 160 °C, a blue shift was observed, indicating the evaporation of the non-covalently bonded chiral dopant (MAA). (c) Three-dimensional surface topography map of the CLC polymer coating that was locally heated with a laser beam, revealing a temperature-induced reduction in coating thickness. (d) Local heat exposure allows for topographical changes and corresponding color patterns. Adapted with permission.^[61] Copyright 2016, Society of Photo-Optical Instrumentation Engineers (SPIE). (e) The preparation of the humidity-gated, reversible TR-RC coatings. (f) Temperature-induced band gap shift of the CLC coating at a constant relative humidity of RH = 75%. The coating was modified to have a broadband reflection (~400 nm bandwidth) by using a UV absorber. Reproduced with permission.^[62] Copyright 2019, Royal Society of Chemistry.

Chapter 1

this way, a humidity-gated, temperature-responsive CLC coating was developed.^[62] Experimental results show that when maintaining the RH at 75%, a band shift of 420 nm in the infrared region is seen as the temperature is varied between 70 °C and -2 °C. In contrast to the hydrogen-bonded coating using MAA, the color change of this coating is reversible by cooling if the RH is kept constant. Furthermore, by generating a chiral dopant concentration gradient using a UV absorbing dye during photopolymerization, the reflection bandwidth can be broadened to ~400 nm (Figure 1.8f). While the coatings were fabricated via bar-coating, an inkjet printing technique is also applicable to such materials.^[63]

Introducing a shape memory effect causes TR-RC behavior in crosslinked CLCs.^[64] In this process, the polymer chains are immobilized by maintaining the sample under its glass transition temperature (T_g) where the polymer has a higher modulus. Deformation in the CLC polymer above T_g can be induced via applying a mechanical force (such as embossing or stretching), reducing the pitch length and causing a blueshift in the reflection band, followed by cooling the sample to below T_g to fix the temporary shape (Figure 1.9a). The blueshifted reflection returns to its original value by heating the temporary shape above T_g , allowing the polymer to return to its initial shape as its elasticity recovers. By this principle, an irreversible, shape memory bulk coating was fabricated, which employs an acrylic CLC polymer network that has a T_g at around 60 °C.^[64] Further modification on this system by interpenetrating with a non-mesogenic polymer creates a wide glass transition range between 10-54 °C of the system.^[65] As a result, the coating presents a multi-stage shape recovery within the T_g range, and therefore a more gradual temperature response in color. Inspired by the encapsulated CLC droplets, shape memory CLC polymer particles were successfully synthesized^[66] as well and used to fabricate paintable coatings. These particles are embedded in a UV-curable acrylic binder for brush-paintable patterned coatings (Figure 1.9b-c). The deformation of the CLC particles by embossing could be observed using scanning electron microscopy (SEM) (Figure 1.9d). The planar-radial alignment of the cholesteric phase in these particles results in reflection colors independent of viewing angle.^[67]

Lastly, thermal deformation is also an important TR-RC mechanism of CLC polymers. Thermal deformation, usually manifested as an expansion with increasing temperature, is commonly seen in materials. For planar-aligned CLC polymers, anisotropic expansion occurs primarily along the director of the helix, leading to an expansion of pitch length and corresponding spectral redshift (Figure 1.10a).^[68] This process is usually reversible. Obvious thermal expansion of the pitch has been demonstrated in highly crosslinked cholesteric liquid crystal elastomers (CLCEs), such as temperature-responsive photonic CLCE film using an acrylic network.^[69] In Figure 1.10b-e is demonstrated another example of CLCE film consisting of crosslinked main-chain CLC oligomers^[70] where the color of the material changes from blue to red when heated from 25 °C to 200 °C. A physical thickening of the film was observed during this shift, which is proportional to the increase of reflection wavelength (Figure 1.10e). The magnitude of TR-RC can be controlled by the amount

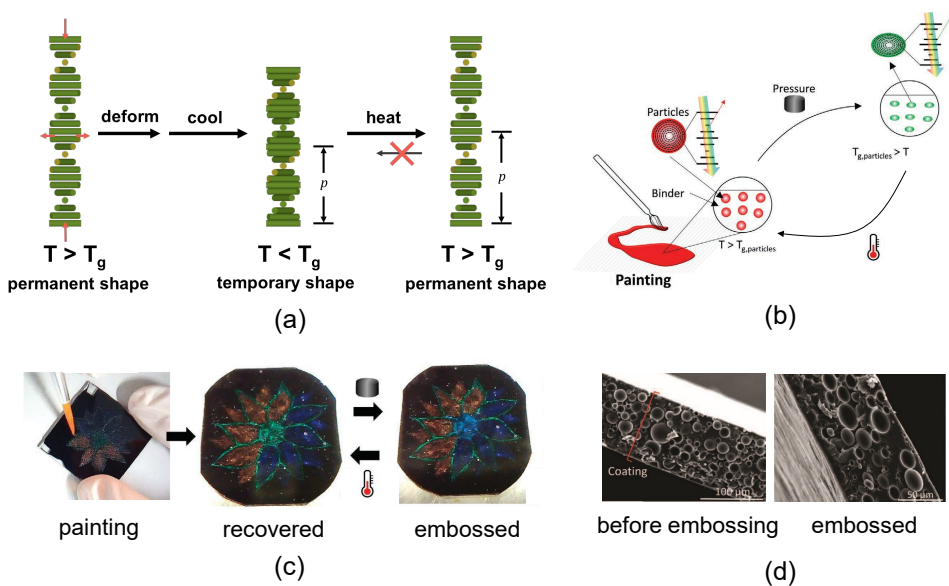


Figure 1.9 (a) Representation of the shape memory mechanism. (b) Schematic representation of the brush-paintable, shape-memory photonic coatings, in which the shape memory CLC polymer particles are embedded into a polymer binder. (c) TR-RC of the brush-painted multicolor coating. (d) Cross section SEM image of the coating before and after the first embossing step, showing the deformed shape of the particles. Adapted with permission.^[66] Copyright 2020, John Wiley and Sons.

Chapter 1

of chain extender (BDMT) added, which correlates to the crosslinking density of the material (Figure 1.10d). Although these examples exhibit their devices as free-standing films, fabrication of coatings from elastomers of such kinds are possible.^[71]

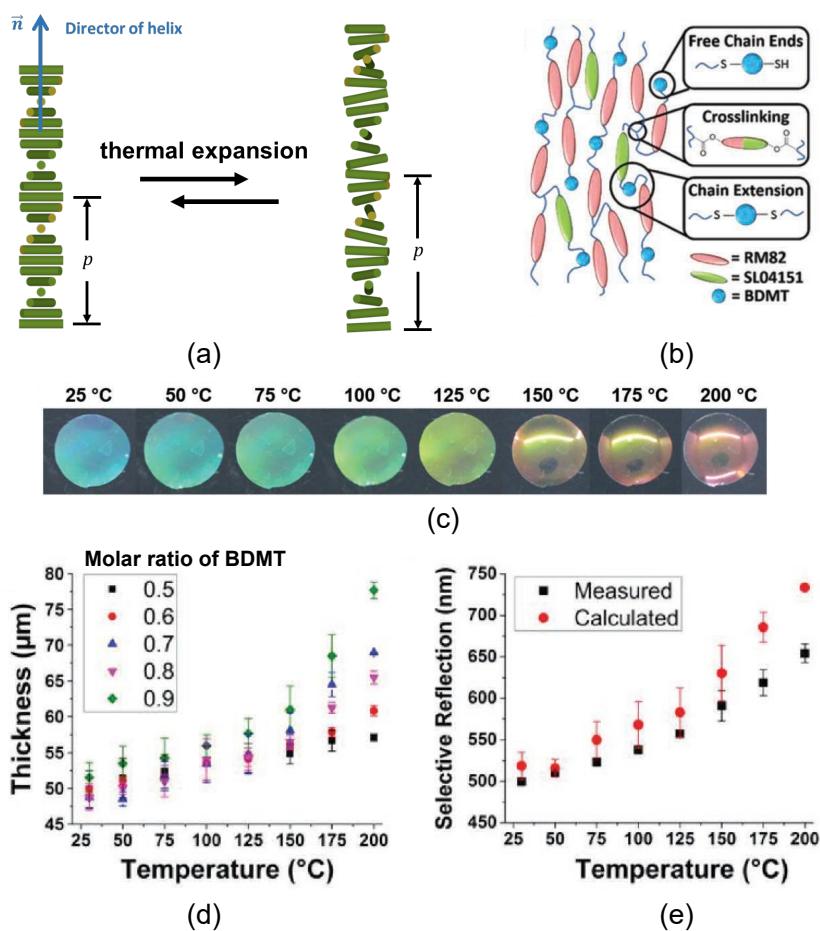


Figure 1.10 (a) Representation of the thermal expansion mechanism. (b) Schematic representation of the chain extended and crosslinked CLCE main-chain polymer. The chemical structures of the components are simplified as symbols. (c) Temperature-induced color changes observed in the CLCE film upon heating. The molar ratio of chain extender BDMT was 0.7. (d) Thickness variation along temperature change of the CLCE samples in different BDMT ratios. (e) Assuming an average refractive index of 1.65, the thickness changes were converted to an expected reflection wavelength and show close agreement with the optical measurements. Reproduced with permission.^[70] Copyright 2019, John Wiley and Sons.

3. Aim and outline of this thesis

As can be concluded from the review above, TR-RC devices from CLC materials have been developed in various configurations. Mesogenic molecule systems are preferably encapsulated under a topcoat or as dispersed droplets in a polymer binder to produce fast-responsive reflective coatings. Polymeric CLC TR-RC materials can be produced based on dimensional change of the helices rather than mesogen rotations. However, the fabrication of robust, easy processable TR-RC polymeric coatings with a wide color tuning range and fast, reversible response remains challenging. Since the existing CLC material systems do not gather all the above merits at once, a new design of molecular system is needed.

This thesis aims for the development of a temperature responsive CLC coating that satisfies all the requirements for scalable, daily-life products: easy processability, mechanically robust, wide color tuning range, operating at moderate temperatures, full reversibility, and fast response speed. In addition, transparent coatings are aimed for, enabling transparent devices, which would be competitive to the opaque PDLCs. Side-chain siloxane LCs are selected to be the main material. The particularly low T_g provided by polysiloxane backbones (usually below 0°C ^[72,73]) allows for processability and responsiveness of the material near room temperature. The smectic-cholesteric mechanism is adopted to create TR-RC effects. In Chapter 2, a simple, uncrosslinked siloxane CLC homopolymer is synthesized and a smectic-cholesteric type mixture is formulated by adding a chiral dopant. An infrared reflective, thermochromic coating is successfully fabricated with this mixture via a simple wire-coating method. The transparent coating presents a blue shift of the reflection band of ~ 1000 nm in the IR region upon heating, which is reversible between 16°C - 66°C . This demonstrates the possibility of creating easily-processable, thermochromic coatings using siloxane CLC materials.

In Chapter 3, a new polysiloxane CLC terpolymer containing crosslink units is synthesized. This terpolymer is bar-coated with the help of a mediator agent and is further polymerized to fabricate a crosslinked network. After removal of the mediator agent, a smectic-cholesteric type TR-RC coating free of small mesogenic molecules is obtained. With a considerable degree of crosslinking, the coating retains a large thermochromic response between 1400 nm to 800 nm, which is presented as an

Chapter 1

infrared reflective smart window. Stability of the coating is examined through multiple temperature cycles and long-term storage.

The ongoing evolution of the molecular system is focused on simplifying the chemistry and further enhancing device durability. In Chapter 4, a reversible, temperature-responsive photonic coating with a protective topcoat is fabricated. A smectic-cholesteric oligosiloxane CLC without a crosslinker was synthesized. A reactive mesogen was added to the oligosiloxane to allow the generation of a crosslinked network after coating. Planar cholesteric alignment of the material can be achieved via blade coating without any mediating agents. By stabilizing with 3 wt% of the crosslinked reactive mesogen network, the photonic coating shows a reversible color change from red to blue upon heating. The PSLC coating also features a fast response speed, high transparency, and full reversibility. Additionally, a protective topcoat of polysiloxane elastomer is directly applied on top of the cholesteric layer to shield it against mild damage.

In Chapter 5, more complex optical responsiveness of the PSLC system introduced in Chapter 4 is explored. Firstly, the responsiveness of a PSLC coating with 4 wt% of reactive mesogen network is manipulated via controlling the polymerization temperature. Thermochromic patterns are created by polymerization using photomasks at different temperatures. Secondly, using a dichroic initiator and performing the polymerization with linear polarized light, deformed helical structures are obtained yielding reflection colors which are also linear polarization dependent. A patterned, linearly polarized light dependent, and thermochromic coating was fabricated for demonstration, revealing the potential towards aesthetics and security of these CLC coatings.

In the final chapter, the potential of TR-RC polymer coatings for future product development is assessed. As siloxane CLC materials possess the merit of easy processability and flexibility of molecular design, commercial products from this material can be prospected.

4. References

- [1] Y. Wang, E. L. Runnerstrom, D. J. Milliron, *Annu. Rev. Chem. Biomol. Eng.* **2016**, *7*, 283.
- [2] R. A. Potyrailo, R. K. Bonam, J. G. Hartley, T. A. Starkey, P. Vukusic, M. Vasudev, T. Bunning, R.

- R. Naik, Z. Tang, M. A. Palacios, M. Larsen, L. A. Le Tarte, J. C. Grande, S. Zhong, T. Deng, *Nat. Commun.* **2015**, *6*, 1.
- [3] C. P. Barrera-Patiño, J. D. Vollet-Filho, R. G. Teixeira-Rosa, H. P. Quiroz, A. Dussan, N. M. Inada, V. S. Bagnato, R. R. Rey-González, *Sci. Rep.* **2020**, *10*, 1.
- [4] E. R. Dufresne, H. Noh, V. Saranathan, S. G. J. Mochrie, H. Cao, R. O. Prum, *Soft Matter* **2009**, *5*, 1792.
- [5] S. Yoshioka, S. Kinoshita, *Forma* **2002**, *17*, 169.
- [6] V. Sharma, M. Crne, J. O. Park, M. Srinivasarao, *Science (80-.)* **2009**, *325*, 449.
- [7] L. Fernández Del Río, H. Arwin, K. Järrendahl, *Thin Solid Films* **2014**, *571*, 410.
- [8] D. Gur, B. Leshem, M. Pierantoni, V. Farstey, D. Oron, S. Weiner, L. Addadi, *J. Am. Chem. Soc.* **2015**, *137*, 8408.
- [9] D. Gur, B. Leshem, V. Farstey, D. Oron, L. Addadi, S. Weiner, *Adv. Funct. Mater.* **2016**, *26*, 1393.
- [10] J. Teyssier, S. V. Saenko, D. Van Der Marel, M. C. Milinkovitch, *Nat. Commun.* **2015**, *6*, 1.
- [11] D. Gur, B. A. Palmer, B. Leshem, D. Oron, P. Fratzl, S. Weiner, L. Addadi, *Angew. Chemie - Int. Ed.* **2015**, *54*, 12426.
- [12] S. Tadepalli, J. M. Slocik, M. K. Gupta, R. R. Naik, S. Singamaneni, *Chem. Rev.* **2017**, *117*, 12705.
- [13] M. F. Land, *Prog. Biophys. Mol. Biol.* **1972**, *24*, 75.
- [14] B. M. Walton, A. F. Bennett, *Physiol. Zool.* **1993**, *66*, 270.
- [15] J. Huang, X. Wang, Z. L. Wang, *Nano Lett.* **2006**, *6*, 2325.
- [16] H. Wan, X. Li, L. Zhang, X. Li, P. Liu, Z. Jiang, Z. Z. Yu, *ACS Appl. Mater. Interfaces* **2018**, *10*, 5918.
- [17] Y. Ma, P. Oleynikov, O. Terasaki, *Nat. Mater.* **2017**, *16*, 755.
- [18] K. Yao, Q. Meng, V. Bulone, Q. Zhou, *Adv. Mater.* **2017**, *29*, 1701323.
- [19] S. N. Fernandes, P. L. Almeida, N. Monge, L. E. Aguirre, D. Reis, C. L. P. de Oliveira, A. M. F. Neto, P. Pieranski, M. H. Godinho, *Adv. Mater.* **2017**, *29*, 1603560.
- [20] J. Yang, W. Zhao, Z. Yang, W. He, J. Wang, T. Ikeda, L. Jiang, *ACS Appl. Mater. Interfaces* **2019**, *11*, 46124.
- [21] R. Balamurugan, J. H. Liu, *React. Funct. Polym.* **2016**, *105*, 9.
- [22] T. J. White, M. E. McConney, T. J. Bunning, *J. Mater. Chem.* **2010**, *20*, 9832.
- [23] R. Eelkema, B. L. Feringa, *Org. Biomol. Chem.* **2006**, *4*, 3729.
- [24] A. Seeboth, D. Löttsch, R. Ruhmann, O. Muehling, *Chem. Rev.* **2014**, *114*, 3037.
- [25] E. P. A. Van Heeswijk, A. J. J. Kragt, N. Grossiord, A. P. H. J. Schenning, *Chem. Commun.* **2019**, *55*, 2880.
- [26] J. Ge, Y. Yin, *Angew. Chemie - Int. Ed.* **2011**, *50*, 1492.
- [27] C. Li, X. Zhou, K. Wang, K. Li, M. Li, Y. Song, *Compos. Commun.* **2019**, *12*, 47.
- [28] J. E. Stumpel, D. J. Broer, A. P. H. J. Schenning, *Chem. Commun.* **2014**, *50*, 15839.
- [29] I. Sage, *Liq. Cryst.* **2011**, *38*, 1551.
- [30] "Color Changing Thermometer Strips & Temperature Indicator," can be found under <https://www.hallcrest.com/>, accessed: **January 2021**.
- [31] "Special FX Creative- Inks, Paints, Pigment, Plastic and Print – SFXC _ Special FX Creative," can be found under <https://www.sfcc.co.uk/>, accessed: **January 2021**.
- [32] K. Nickmans, D. A. C. van der Heijden, A. P. H. J. Schenning, *Adv. Opt. Mater.* **2019**, *7*, 1900592.
- [33] Y. Foelen, D. A. C. Van Der Heijden, M. Del Pozo, J. Lub, C. W. M. Bastiaansen, A. P. H. J. Schenning, *ACS Appl. Mater. Interfaces* **2020**, *12*, 16896.
- [34] H. Khandelwal, A. P. H. J. Schenning, M. G. Debije, *Adv. Energy Mater.* **2017**, *7*, 1602209.
- [35] S. Y. T. Tzeng, C. N. Chen, Y. Tzeng, *Liq. Cryst.* **2010**, *37*, 1221.
- [36] G. S. Chilaya, *Crystallogr. Reports* **2000**, *45*, 871.
- [37] R. Dhar, *Phase Transitions* **2006**, *79*, 175.
- [38] S. R. Renn, T. C. Lubensky, *Phys. Rev. A* **1988**, *38*, 2132.
- [39] P. G. de Gennes, *Solid State Commun.* **1993**, *88*, 1039.

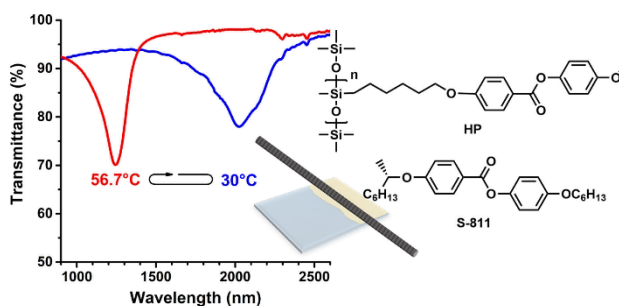
Chapter 1

- [40] F. Wang, H. Cao, K. Li, P. Song, X. Wu, H. Yang, *Colloids Surfaces A Physicochem. Eng. Asp.* **2012**, *410*, 31.
- [41] C. J. Tien, C. Y. Huang, Y. M. Kao, P. C. Yang, J. H. Liu, *Jpn. J. Appl. Phys.* **2009**, *48*, 071301.
- [42] E. P. A. van Heeswijk, T. Meerman, J. de Heer, N. Grossiord, A. P. H. J. Schenning, *ACS Appl. Polym. Mater.* **2019**, *1*, 3407.
- [43] H. Khandelwal, E. P. A. Van Heeswijk, A. P. H. J. Schenning, M. G. Debiije, *J. Mater. Chem. C* **2019**, *7*, 7395.
- [44] A. Ranjakesh, T.-H. Yoon, *ACS Appl. Mater. Interfaces* **2019**, *11*, 26314.
- [45] S. S. Lee, J. Bin Kim, Y. H. Kim, S. H. Kim, *Sci. Adv.* **2018**, *4*, eaat8276.
- [46] J. Guo, J. Zhang, Q. Zhang, N. Jiang, J. Wei, *RSC Adv.* **2013**, *3*, 21620.
- [47] M. Kim, K. J. Park, S. Seok, J. M. Ok, H. T. Jung, J. Choe, D. H. Kim, *ACS Appl. Mater. Interfaces* **2015**, *7*, 17904.
- [48] C. Yang, B. Wu, J. Ruan, P. Zhao, L. Chen, D. Chen, F. Ye, *Adv. Mater.* **2021**, 2006361.
- [49] J. Wang, J. Kolacz, Y. Chen, A. Jakli, J. Kawalec, M. Benitez, J. L. West, in *Dig. Tech. Pap. - SID Int. Symp.*, **2017**, pp. 147–149.
- [50] X. Yuan, L. Zhang, H. Yang, *Liq. Cryst.* **2010**, *37*, 445.
- [51] F. Wang, P. Song, H. Yang, X. Shao, *Liq. Cryst.* **2016**, *43*, 1732.
- [52] L. Xiao, H. Cao, J. Sun, H. Wang, D. Wang, Z. Yang, W. He, J. Xiao, H. Ding, H. Yang, *Liq. Cryst.* **2016**, *43*, 1299.
- [53] H. Yang, K. Mishima, K. Matsuyama, K. I. Hayashi, H. Kikuchi, T. Kajiyama, *Appl. Phys. Lett.* **2003**, *82*, 2407.
- [54] J. Guo, H. Wu, F. Chen, L. Zhang, W. He, H. Yang, J. Wei, *J. Mater. Chem.* **2010**, *20*, 4094.
- [55] F. Chen, J. Guo, Z. Qu, J. Wei, *J. Mater. Chem.* **2011**, *21*, 8574.
- [56] S. Relaix, M. Mitov, *Liq. Cryst.* **2008**, *35*, 1037.
- [57] X. Wu, L. Yu, H. Cao, R. Guo, K. Li, Z. Cheng, F. Wang, Z. Yang, H. Yang, *Polymer (Guildf)*. **2011**, *52*, 5836.
- [58] X. Wu, H. Cao, R. Guo, K. Li, F. Wang, Y. Gao, W. Yao, L. Zhang, X. Chen, H. Yang, *Macromolecules* **2012**, *45*, 5556.
- [59] F. Chen, J. Guo, O. Jin, J. Wei, *Chinese J. Polym. Sci.* **2013**, *31*, 630.
- [60] A. J. J. Kragt, N. C. M. Zuurbier, D. J. Broer, A. P. H. J. Schenning, *ACS Appl. Mater. Interfaces* **2019**, *11*, 28172.
- [61] M. Moirangthem, J. E. Stumpel, B. Alp, P. Teunissen, C. W. M. Bastiaansen, A. P. H. J. Schenning, in *Proc. SPIE 9769, Emerg. Liq. Cryst. Technol. XI*, Spie-Int Soc Optical Engineering, San Francisco, CA, **2016**, p. 97690Y.
- [62] E. P. A. Van Heeswijk, J. J. H. Kloos, N. Grossiord, A. P. H. J. Schenning, *J. Mater. Chem. A* **2019**, *7*, 6113.
- [63] N. Herzer, H. Guneyasu, D. J. D. Davies, D. Yildirim, A. R. Vaccaro, D. J. Broer, C. W. M. Bastiaansen, A. P. H. J. Schenning, *J. Am. Chem. Soc.* **2012**, *134*, 7608.
- [64] D. J. D. Davies, A. R. Vaccaro, S. M. Morris, N. Herzer, A. P. H. J. Schenning, C. W. M. Bastiaansen, *Adv. Funct. Mater.* **2013**, *23*, 2723.
- [65] M. Moirangthem, T. A. P. Engels, J. Murphy, C. W. M. Bastiaansen, A. P. H. J. Schenning, *ACS Appl. Mater. Interfaces* **2017**, *9*, 32161.
- [66] A. Belmonte, M. Pilz da Cunha, K. Nickmans, A. P. H. J. Schenning, *Adv. Opt. Mater.* **2020**, *8*, 2000054.
- [67] A. Belmonte, T. Bus, D. J. Broer, A. P. H. J. Schenning, *ACS Appl. Mater. Interfaces* **2019**, *11*, 14376.
- [68] M. Warner, E. M. Terentjev, *Liquid Crystal Elastomers*, Oxford University Press, **2007**.
- [69] H. Nagai, K. Urayama, *Phys. Rev. E* **2015**, *92*, 022501.
- [70] M. T. Brannum, A. M. Steele, M. C. Venetos, L. S. T. J. Korley, G. E. Wnek, T. J. White, *Adv. Opt. Mater.* **2019**, *7*, 1801683.

- [71] E. P. A. van Heeswijk, L. Yang, N. Grossiord, A. P. H. J. Schenning, *Adv. Funct. Mater.* **2020**, *30*, 1.
- [72] H. Ringsdorf, A. Schneller, *Makromol. Chem., Rapid Commun.* **1982**, *3*, 557.
- [73] H. Finkelmann, H. J. Kock, G. Rehage, *Die Makromol. Chemie, Rapid Commun.* **1981**, *2*, 317.

Chapter 2

Easily processable temperature responsive infrared reflective coatings based on liquid crystal oligomers



A temperature responsive near infrared (IR) reflective coating was fabricated based on a side-chain liquid crystal siloxane polymer by using a simple wired-bar method. The cholesteric liquid crystalline polymer film showed a blue shift of the reflection band of ~1000 nm in the IR region upon heating. The temperature responsive change of the reflection band was reversible. Compared to the same mixture system in an alignment cell, the coating showed a significantly faster response time. This research demonstrates an easy way to prepare a temperature responsive reflective coating that shifts its reflection to a shorter wavelength upon heating. As IR radiation of shorter wavelengths is more strongly represented in sunlight than longer wavelengths, this coating could be promising for a future application in smart climate control.

This chapter is partially reproduced from: Zhang, W.; Kragt, S.; Schenning, A. P. H. J.; De Haan, L. T. & Zhou, G. Easily Processable Temperature-Responsive Infrared-Reflective Polymer Coatings. *ACS Omega* **2017**, 2 (7), 3475–3482.

Chapter 2

1. Introduction

Near infrared light (IR), ranging from 700-2500 nm, makes up 50% of the total sunlight energy that reaches Earth and is a significant interior heating source of buildings.^[1] Transmission and reflection of near IR from sunlight can be regulated by specialized windows, which can reduce energy consumption for heating and cooling of buildings while still being transparent for visible light.^[2-5] Smart temperature responsive IR reflectors autonomously regulate the temperature of indoor spaces.^[6] As IR radiation of shorter wavelengths is more strongly represented in sunlight than longer wavelengths,^[7] a window that shifts its reflection to a shorter wavelength upon heating rejects more IR at higher temperatures, which reduces heating of the indoor space. If this can be done in a reversible and autonomous way, it would be a major step towards the construction of energy neutral buildings.

Temperature responsive photonic materials are the key to this kind of smart window, as such materials can change their reflection of light in response to temperature changes.^[8,9] Reported temperature responsive photonic systems are based on cholesteric liquid crystals,^[10,11] polymeric colloids^[12-14] or thermoplastic materials.^[15-17] Temperature responsive photonic hydrogel polymer coatings have been made for temperature sensors and indicators.^[18,19] These hydrogel coatings rely on swelling and de-swelling by water, and thus require specific humidity conditions. Devices based on CLCs have been discussed in detail in Chapter 1, but at the moment the development of a facile method to fabricate transparent temperature responsive polymer IR reflective coatings remains a challenge.

This chapter describes the fabrication of a temperature responsive IR reflecting coating using a simple wire-bar method. The photonic polymer film was based on a mixture of a side chain liquid crystalline polysiloxane homopolymer (HP)^[10,20,21] and 10% of chiral dopant S811, which has a smectic-cholesteric phase transition. A 1000 nm reversible blue shift of the reflection band within the IR region was observed upon increasing the temperature from room temperature to 60 °C. The same system in a cell showed a similar change of the reflection band as a function of temperature, but the coating showed a significantly faster response time. These results show that easily processable responsive photonic coatings can be fabricated that function similar to responsive systems in cells.

2. Results and discussion

2.1. Preparation and characterization of the LC mixture

The side chain liquid crystalline HP (which stands for “homopolymer”) was synthesized by grafting a liquid crystal with a vinyl end group onto a polymethylhydrosiloxane backbone in the presence of Karstedt’s catalyst.^[22,23] The structure of the HP was confirmed by attenuated total reflectance infrared spectroscopy (ATR-IR), gel permeation chromatography (GPC) and proton nuclear magnetic resonance (¹H-NMR). The average degree of polymerization was 6.3 while the polydispersity was 1.21. The detailed synthesis and characterization methods are given in the Experimental section in this Chapter. Differential scanning calorimetry (DSC) revealed that the polymer has both the desired smectic and nematic phases (G-8 Sm 20.7 N 75 I).

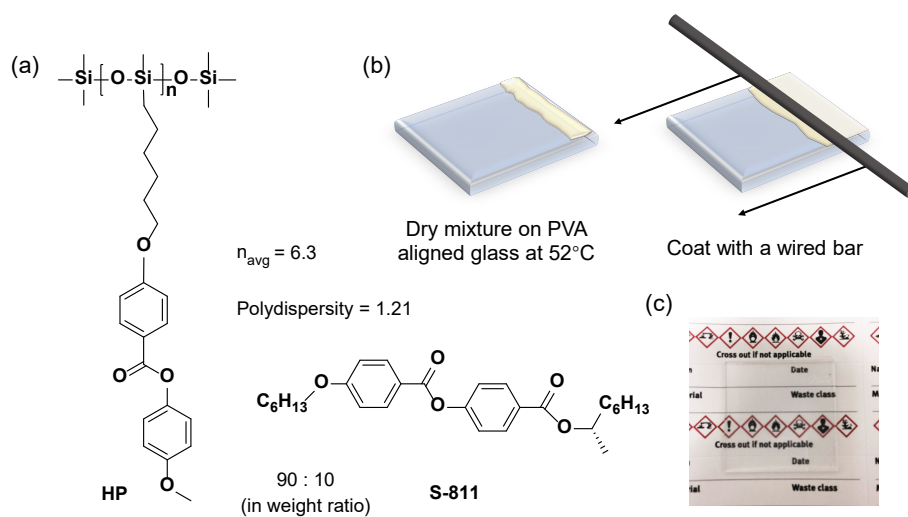


Figure 2.1 (a) Chemical structures of the LC polysiloxane-chiral dopant mixture, (b) schematic representation of the wire-bar coating method to fabricate the photonic coating, and (c) photograph of the photonic coating at 52 °C with a label as background to show the good transparency in the visible range. The photo was slightly adjusted in brightness.

An IR reflecting chiral nematic liquid crystal mixture was created by adding 10 wt% of chiral dopant S811 to the HP (Figure 2.1a), dissolving the mixture in dichloromethane, and evaporating the solvent overnight. The mixture had a cholesteric liquid crystalline phase between 22 °C and 64 °C, an intermediate

Chapter 2

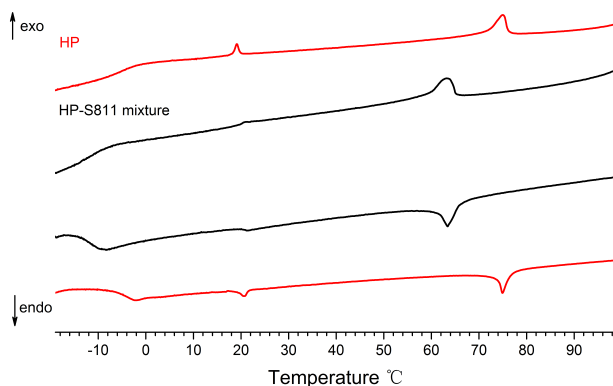


Figure 2.2 DSC traces of HP and the HP-S811 mixture. The heat flow (y-axis) is in arbitrary units.

mesophase between -10 and 22°C , and glass transition at -10°C , as determined by DSC (Figure 2.2). Wide-angle and small-angle X-ray scattering (WAXS and SAXS) measurements (Figure 2.3) showed a diffraction peak located at $q = 0.24 \text{ \AA}^{-1}$ ($2\theta = 3.386^{\circ}$, $d = 2.6 \text{ nm}$) at $\leq 60^{\circ}\text{C}$, which is a typical indication of the smectic order. The peak in the WAXS measurement at $q = 1.5 \text{ \AA}^{-1}$ represents the side-by-side intermolecular spacing which is present in both the nematic and smectic phase. The existence of smectic orders through the entire cholesteric temperature range, combined with a peak intensity increase with decreasing temperature, confirms a pre-transitional effect of this mixture, as introduced in Chapter 1.^[24,25]

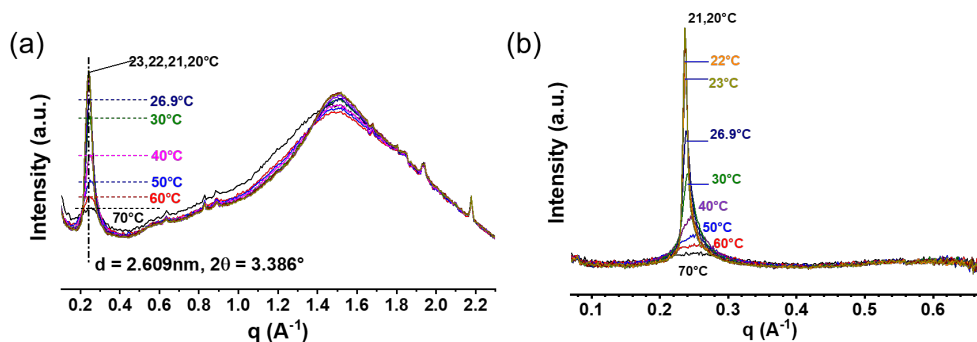


Figure 2.3 (a) WAXS and (b) SAXS of the HP-S811 mixture at different temperatures upon cooling.

2.2. Temperature response of the HP-S811 coating

The mixture of HP-S811 was coated at 52 °C on a glass surface with a PVA alignment layer using a wired bar(Figure 2.1b). After processing, a transparent colorless coating of 11.5 μm thick was obtained. Polarizing optical microscopy (POM) analysis showed typical planar cholesteric textures (Figure 2.4a). The stripes observed are originated from the micro pattern of the coating bar, and did not significantly influence coating transparency and properties.

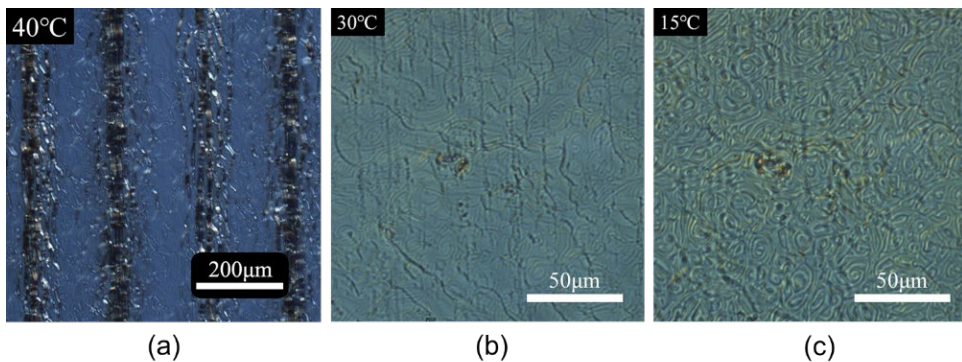


Figure 2.4 Polarizing optical microscopy (POM) images of the prepared HP-S811 coating, taken in the cholesteric phase (a, at 40 °C and b, at 30 °C) and in the smectic phase at 15 °C (c). The sample of (b) and (c) was processed by a 10 μm narrow gap applicator, for the sake of better texture clarity.

The TR-RC properties of the coating were investigated using UV/Vis/IR spectroscopy. Figure 2.5 presents the stabilized transmission spectra of a coating at different temperatures in two heating and cooling cycles. The bandwidth of each reflection peak was calculated from full width at half maximum (FWHM) reflection, and the Bragg reflection center (λ) was determined by the middle point of the FWHM line. The spectrum taken first at 47.5°C (Figure 2.5a, 47.5°C initial) had a reflection band centered at $\lambda = \sim 1380$ nm. The reflection band had a triangle-like shape with an FWHM of 210 nm. In the first cycle, between 56.7°C and 30°C the reflection band shifted from 1225 to 2026 nm. In the second cycle, upon further cooling to 16.5°C the reflection band did not disappear but was centered at 2310 nm (Figure 2.5b). During the two cycles, the reflection band showed a reversible change as a function of temperature (Figure 2.5c). Some scattering was also observed, which was visible as a lower transparency in the visible light region of the spectra. The scattering increased as the

Chapter 2

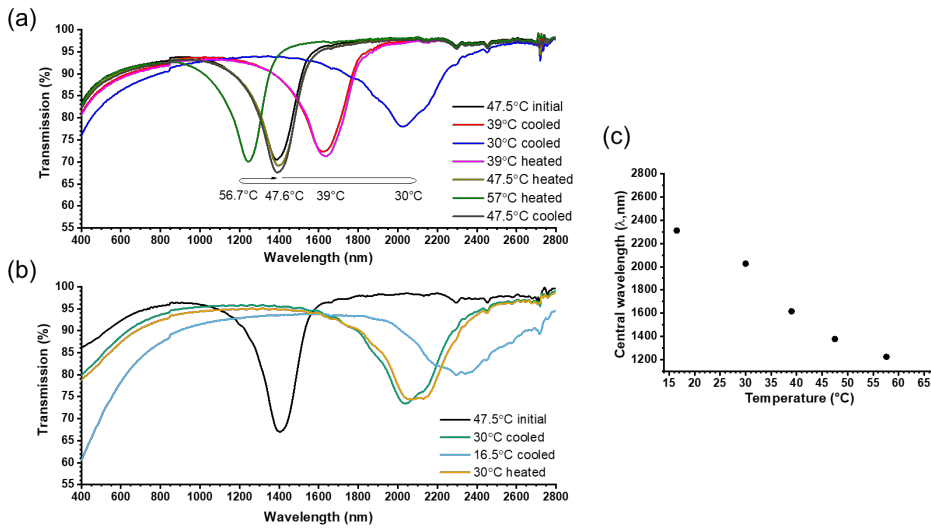


Figure 2.5 Transmission spectra of a single HP-S811 coating during two cycles of cooling and heating between (a) 56.7 °C and 30 °C, and (b) 47.6 °C and 16.5 °C. (c) Reflection wavelength (λ) of the HP-S811 coating as a function of temperature.

temperature decreased, and finally at 16.5 °C, below the smectic-cholesteric transition point, scattering reached the highest degree. POM images display a new “fingerprint” texture at lower temperatures, indicating a homeotropic alignment of the helices (Figure 2.4c), which could account for the scattering of the coating. This homeotropic alignment of mesogens at the air-coating interface could be more favorable due to lower surface tensions.^[26,27] In another experiment, the temperature was raised beyond the cholesteric to isotropic transition point. This wiped out the alignment of the molecules as expected. When the temperature was then lowered back to the cholesteric range, the liquid crystals re-aligned poorly, and the coating became highly scattering.

2.3. Temperature response of the HP-S811 cell

For comparison, TR-RC of the HP-S811 mixture was also studied in a cell. The spectrum of the cell exhibited an IR reflection peak centered at $\lambda = 1390$ nm at 52°C with a transmittance of 65%. The cell was fully transparent in the visible region, indicating planar alignment of the LCs. Compared to the coating, the FWHM of this band was much smaller (112 nm), and its shape was not triangular. This can be explained by the absence of a fingerprint texture, which doesn't form due to the lack

of an air interface, and leads to a sharper band and less scattering. The temperature of the cell was varied between 66 °C and 16 °C. Figure 2.6a shows the temperature dependent reflection spectra measured after stabilization. The spectra show the same gradual change of the reflection center along the temperature range as was observed in the coating. In the CLC temperature range, a 1000 nm red shift of λ was observed, i.e. λ increased from 1215 nm to 2190 nm. This wavelength shift was fully reversible between 66 °C and 30 °C. Below the smectic-cholesteric transition (22 °C) the reflection bands were only partially visible due to light absorption of the glass cell, but remained at the same position. This is similar to what was seen before in the coating.

Upon plotting the wavelength of the reflection band (λ) against temperature (Figure 2.6b), gradual reflection band shifts were observed. This behavior is different from the smectic-cholesteric systems reported earlier, where drastic reflection band shifting takes place within a few degrees of temperature.^[28] The gradual reflection band shift coincides with the gradual increase in smectic order in the CLC phase as observed by WAXS and SAXS (Figure 2.3). Most likely, as reported for other systems, this smectic order increase led to a gradual increase in pitch, leading to a red shift of the reflection band.^[29,30] Below the smectic-cholesteric transition the reflection band was not changing, revealing that the pitch did not change at these temperatures. It should be noted that the slight decrease of the helical twisting power of chiral dopant S811 with decreasing temperature will only have a minor contribution to the gradual λ change.^[31,32]

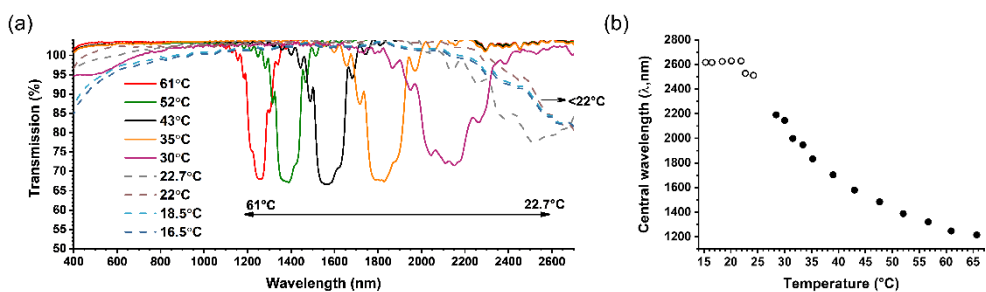


Figure 2.6 (a) stabilized transmission spectra, and (b) reflection wavelength (λ) of the HP- S811 cell as a function of temperature. Dashed lines and hollow dots refer to the spectra data partly out of machine detection range.

Chapter 2

2.4. Response time of the HP-S811 cell and coating

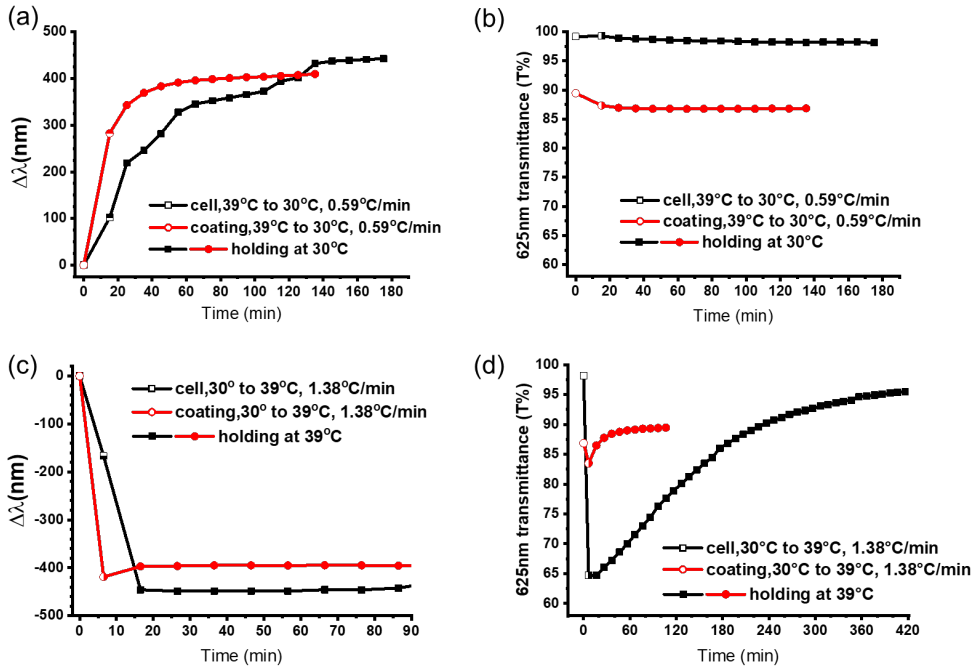


Figure 2.7 Response times of the HP-S811 cell and coating. (a) Change of the reflection band $\Delta\lambda$ and (b) change of the transmittance at 625 nm upon cooling from 39 °C to 30 °C. (c) Change of the reflection band $\Delta\lambda$ and (d) change of the transmittance at 625 nm upon heating from 30 °C to 39 °C. Time zero is the status of the sample before cooling or heating. Open symbols describe the data points collected during temperature ramp and the solid symbols describe data points collected once the temperature has stabilized.

The response time of the TR-RC of the polymer LC mixture was studied with respect to reflection band shift and transparency changes. Figure 2.7 shows a comparison of the response of both the coating and cell upon cooling from 39 °C to 30 °C (Figure 2.7a-b) and heating from 30 °C to 39 °C (Figure 2.7c-d). Interestingly, the responsive behavior of the coating was different when compared to the cell. Upon cooling the cell, the shift of the reflection band took place over 160 min (Figure 2.7a), while the transparency of the cell did not change and stayed high (Figure 2.7b). In contrast, upon heating the reflection band shifted in less than 10 min (Figure 2.7c), while the transparency initially dropped significantly due to scattering (from 98% to 65%) and recovered only after 410 min (Figure 2.7d). For the coating, the shift of the reflection

band was significantly faster upon cooling compared to the cell (60 min versus 160 min, Figure 2.7a), also without any drop in transparency (Figure 2.7b). Upon heating, the change of the reflection band was also faster compared to the cell (5 min versus 10 min, Figure 2.7c). The coating had a lower initial transparency compared to the cell, but upon heating its transmittance dropped by only 5% due to scattering (Figure 2.7d), and it quickly recovered in 20 min. At other temperatures the effects were similar, and this data is summarized in Table 2.1. At lower temperatures, a longer time was needed to obtain a transparent cell in the visible region. To make sure that the difference in kinetics between the cell and the coating was not caused by a temperature difference, we measured the temperature during and after the ramp. The temperature of the cell and coating differed by less than 1 °C, and vanished entirely after the ramp. This small temperature difference cannot be the cause for the large difference in kinetics that we observed.

Table 2.1 Thermal-optical response time of the HP-S811 cell and coating.

Process	Temperature change	Rate (°C/min)	Response Time* (min)	
			Cell	Coating
cooling	65.7°C→56.7°C	1.06	38.5	-
	56.7°C→47.6°C	0.91	50.0	30.0
	47.6°C→39°C	0.73	71.8	51.8
	39°C→30°C	0.59	175.3	105.3
heating	30°C→39°C	1.38	416.5	96.5
	39°C→47.6°C	1.29	106.7	86.7
	47.6°C→56.7°C	1.21	47.5	37.5
	56.7°C→65.7°C	1.06	58.5	-

*including time for heating/cooling.

2.5. Discussion of the mechanism of the temperature responsive infrared reflective cells and coatings

The thickness of the coating (11.5 μm) was shown to change only marginally with temperature. This reveals that the HP-S811 system undergoes helix winding and unwinding during pitch tuning without noticeable thermal expansion or shrinkage along the helical axis. The thickness in the cell is fixed by the cell gap and therefore the response mechanism of the cell and coating should be similar. We argue that the

Chapter 2

faster response of the coating stems from the lack of a top alignment layer. In the cell, where the stronger anchoring force determines alignment of the mesogens on both surfaces, helices can only wind or unwind by discontinuous jumps of integral π rotations,^[33,34] which may set an energy barrier to pitch changing. The evidence of discontinuous jumps has been observed in other cell systems. In the coating, winding and unwinding of helices can take place without integer π rotations and barriers are therefore removed, leading to a faster response. The scattering at intermediate temperatures is caused by the formation of focal conic defects. At a high temperature, the mixture has a low viscosity and the alignment, driven by the anchoring force of alignment layers, is fast. At a low temperature, where the helical pitch is long, planar alignment is thermodynamically favorable.^[35,36] However, at intermediate temperatures, neither is planar alignment favorable, nor is the viscosity low enough to quickly recover focal-conic defects. Remarkably, the reflection band did not disappear upon going from the cholesteric to the smectic phase, even though the temperature was still above T_g . We assume that below the transition temperature the mixture system adopts a twist grain boundary (TGB A*) phase, an intermediate phase of transition where smectic clusters form a macroscopic spiraling layer structure, which possesses helical pitches as well.^[22,37]

3. Conclusions

A mixture consisting of an LC polysiloxane and the chiral dopant S811 has been prepared to fabricate an easily processable temperature responsive IR-reflective coating. The photonic coating showed a blue shift in the reflection wavelength of light along a broad range in the IR region (2350–1250 nm) upon heating and was reversible. Interestingly, the response time of the coating was considerably faster compared to the same material in a glass cell. This makes such a coating appealing as a temperature responsive IR reflector that can autonomously regulate the temperature of indoor spaces. In the future, the reflection band of the coating can be fine-tuned to a different wavelength of IR by changing the amount of chiral dopant in the mixture.

The research shows that side-chain liquid crystal polymers can be applied as coatable temperature-responsive IR-reflective films, opening up a promising route towards the development of smart windows that can be applied directly on various surfaces. Since the temperature and optical response mechanisms of the coating are similar to the cell, this reveals that other response mechanisms already reported for a cell can

now also be applied to coatings, opening up new opportunities to fabricate temperature responsive polymers with novel properties.

4. Experimental

4.1. Polymer synthesis and characterization.

Materials. 4-hydroxybenzoic acid was purchased from J&K Chemical, China. 6-bromo-1-hexene was purchased from Heowns Biochem Technologies, China. 4-methoxyphenol and dicyclohexylcarbodiimide (DCC) were obtained from Adamas Reagent, Ltd, China. 4-Dimethylaminopyridine (DMAP) was received from Shanghai Macklin Biochemical Co., Ltd (China). Polymethylhydrosiloxane (PMHS, trimethylsilyl terminated, average Mn~390), Platinum (0)-1,3-divinyl-1,1,3,3-tetramethyldisiloxane complex solution in xylene, Pt ~2 % (Karstedt's catalyst), and anhydrous toluene were purchased from Sigma-Aldrich. Chiral dopant S811 was bought from Jiangsu Hecheng Advanced Materials Co., Ltd (China). All materials were used as received without further purification.

Characterization. The compounds were characterized by ATR-IR (Bruker VERTEX 70) and by ¹H-NMR (Varian as400, 400MHz) using chloroform-d. HP was analyzed by gel penetration chromatography (GPC, Waters e2695) equipped with an RI detector (Waters 2414) using tetrahydrofuran as eluent and monodisperse polystyrene calibration standards. Phase transition temperatures of HP were measured by differential scanning calorimetry (DSC, Mettler Toledo DSC 1) using heating and cooling rates of 2°C/min. The mixture was analyzed by both wide-angle and small-angle X-ray scattering (WAXS and SAXS, Ganesha lab instrument) at various temperatures.

The complete synthesis route of HP is presented in Figure 2.8.

Chapter 2

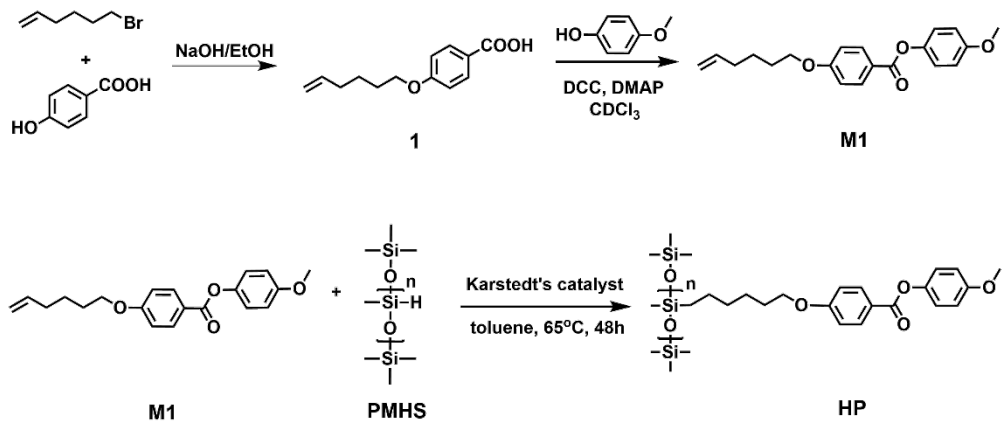


Figure 2.8 Synthetic route towards HP.

4-(5-hexenyloxy) benzoic acid (1) was prepared according to literature methods.^[38] Synthesis of **4-methoxyphenyl 4-(5-hexenyloxy) benzoate (M1)** was similar to this literature methods. In this step we used distilled chloroform as the solvent instead of dichloromethane, and 4-Dimethylaminopyridine (DMAP, 10 mol% to compound **1**) instead of 4-pyrrolidin-1-ylpyridine (POP).

Synthesis of homopolymer (HP): A 50 mL three-neck round-bottom Schlenk flask, which was fitted with a condenser pipe and a rubber septum, was dried according to standard Schlenk procedure and filled with argon. Into the flask was added liquid crystalline monomer **M1** (0.815g, 2.5 mmol), polymethylhydrosiloxane (PMHS, $M_n \sim 390$, 245 μ L, 0.8eq of Si-H group with respect to **M1**), and a magnetic stirring bar. The equipment was then further dried according to the Schlenk procedure and filled with dry argon. Through the septum 5 mL of anhydrous toluene was injected into the flask. The solution was stirred for 5 min to dissolve reactants completely. Then, into the stirring solution 50 μ L of Karstedt's catalyst was injected in one portion, and the mixture was brought to reflux at 65 °C in an oil bath for 48 h. The obtained brown solution was precipitated in toluene/cold methanol three times followed by centrifugation. The brown crude product was dried in vacuum, dissolved in 25 mL toluene, and 10 g of silica gel metal scavengers (Si-Triamine, SilicaMetS[®], Silicycle Inc.) was added, followed by vigorous stirring overnight to eliminate the platinum catalyst from the product. The silica gel was filtered off by toluene washing, and the obtained eluent was further filtered using a 0.45 μ m PTFE syringe filter, concentrated,

and precipitated in hexane and cold methanol once each, followed by centrifugation. The precipitate was finally dried at 70 °C in vacuum for 24 h, yielding a white sticky solid. Yield: 395.7mg, 44.1%. ATR-IR (cm⁻¹): 1732 (C=O), 1065 (Si-O-Si); extinction of vibrational band at 2160cm⁻¹ (Si-H) and 1640cm⁻¹ (C=C) from PMHS and M1, respectively. ¹H-NMR (400 MHz, chloroform-d, δ, ppm): 8.10 (2H), 7.08 (2H), 6.90 (4H), 3.99 (2H), 3.80 (3H), 1.78 (2H), 1.40 (4H), 1.40 (4H), 0.54 (2H), 0.02-0.13 (6H), GPC (THF, by RI detector, in polystyrene standards): Mn = 3305 Da, Mw = 4026 Da, Mw/Mn = 1.21.

Determination of the degree of polymerization

Monomer conversion (determined by residual Si-H), average degree of polymerization (aDP), and average molar mass (Mn) of HPs are calculated with the peak integrals measured in the NMR graphs, using Equation 3, 4 and 5, respectively. ΔSi-CH₃, ΔSi-CH₂ and ΔSi-H are designated as the peak integrals of Si-CH₃ (δ = 0.02-0.13), Si-CH₂ (δ = 0.54), and Si-H (δ = 4.7) chemical shifts of the HP graph, respectively.

$$\text{Residual Si-H } (r) = \frac{\Delta\text{Si-H}}{\frac{\Delta\text{Si-CH}_2}{2} + \Delta\text{Si-H}} \times 100\% \quad \text{Equation 3}$$

$$\text{aDP} = \frac{18(\Delta\text{Si-CH}_2 + \Delta\text{Si-H})}{\Delta\text{Si-CH}_3(2 - r) - 3(\Delta\text{Si-CH}_2 + \Delta\text{Si-H})} \quad \text{Equation 4}$$

$$\text{Mn} = 386 \times \text{aDP} + 162 \quad \text{Equation 5}$$

In Table 2.2 the calculated results from NMR of two batches of HPs used in the cell and the coating are listed. The coating and the cell used different batches of HP having mostly similar properties.

Table 2.2 Molecular information of HP, calculated from the NMR data.

Sample	Hydrosilylation completion (1-r)	aDP	Mn (Da)
HP used in the cell	99.3%	6.5	2671
HP used in the coating	98.1%	6.3	2594

Chapter 2

4.2. Coating fabrication and characterizations.

Preparation of the CLC polysiloxane mixture. 205.8 mg HP and 22.9 mg chiral dopant S811 (10 wt%) were dissolved in dichloromethane. The solvent was slowly evaporated on a 55 °C hot plate and further removed in high vacuum at 70 °C overnight to yield a homogenous polysiloxane chiral dopant mixture.

Fabrication of the IR reflective coatings. A few drops of a 5.0 wt % polyvinyl alcohol (PVA) in aqueous solution were spin-coated onto 3x3 cm clean glass plates at 2000 r.p.m for 30 seconds. The deposited films were dried at 60.0 °C for about 1 h and subsequently rubbed on a velvet textile cloth in one direction to induce alignment. The glass plate with PVA alignment layer was then placed on a hot plate at 52 °C. A coating bar having a surface microstructure with a waviness height of 24.4 μm and a wavelength of 202.6 μm was heated to 52 °C. The LC mixture was put on one side of the glass plate and coated by the bar in the direction antiparallel to the PVA layer rubbing direction. The bar was moved over the plate several times until the material was fully covering the plate. The resulting coating was stored on the hot plate at 52 °C.

Preparation of IR reflective cells. Two of the glass plates with rubbed PVA alignment layers were imposed antiparallel on each other and glued together by using a UV glue containing 15 μm silica particles as spacers. The mixture was filled into the cell at 52°C by capillary forces.

Characterization. Optical textures of the cells and coatings were investigated by polarizing optical microscopy (POM, Leica DM 7200P or Leica DM 2700M) with a hot stage (Linkam PE95/T95). Transmission spectra of the cells and coatings were obtained with a UV/VIS/NIR spectrometer (Perkin Elmer Lambda 950) with a 2D detector module. Temperature of the sample was controlled by a water-agent temperature controller (EYELA NCB-1200) and was calibrated by a thermoelectric couple. Thickness of the coating was measured by an interferometer (Forgale Zoomsurf 3D).

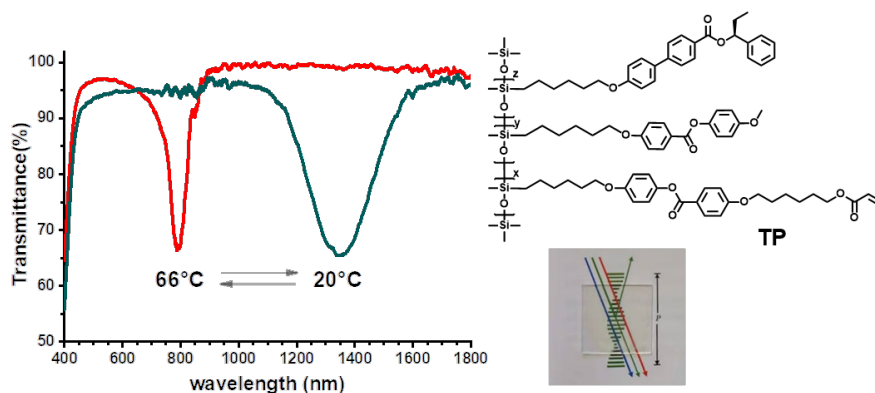
5. References

- [1] Y. Wang, E. L. Runnerstrom, D. J. Milliron, *Annu. Rev. Chem. Biomol. Eng.* **2016**, *7*, 283.
- [2] H. Khandelwal, R. C. G. M. Loonen, J. L. M. Hensen, A. P. H. J. Schenning, M. G. Debije, *J. Mater. Chem. A* **2014**, *2*, 14622.
- [3] H. Khandelwal, F. Roberz, R. C. G. M. Loonen, J. L. M. Hensen, C. W. M. Bastiaansen, D. J. Broer, M. G. Debije, A. P. H. J. Schenning, in *Proc. SPIE* (Ed.: I.C. Khoo), Spie-Int Soc Optical Engineering,

- San Diego, CA, **2014**, p. 91820S.
- [4] R. C. G. M. Loonen, M. Trčka, D. Cóstola, J. L. M. Hensen, *Renew. Sustain. Energy Rev.* **2013**, *25*, 483.
- [5] C. T. Riley, J. S. T. Smalley, J. R. J. Brodie, Y. Fainman, D. J. Sirbuly, Z. Liu, *Proc. Natl. Acad. Sci.* **2017**, *114*, 1264.
- [6] H. Khandelwal, A. P. H. J. Schenning, M. G. Debije, *Adv. Energy Mater.* **2017**, *7*, 1602209.
- [7] "Calculated from the data given at the website of National Research Energy Laboratory," can be found under <http://www.nrel.gov>, accessed: **October 2016**.
- [8] A. Seeboth, D. Löttsch, R. Ruhmann, O. Muehling, *Chem. Rev.* **2014**, *114*, 3037.
- [9] J. E. Stumpel, D. J. Broer, A. P. H. J. Schenning, *Chem. Commun.* **2014**, *50*, 15839.
- [10] H. Finkelmann, G. Rehage, *Makromol. Chemie-Rapid Commun.* **1980**, *1*, 733.
- [11] S. Y. T. Tzeng, C. N. Chen, Y. Tzeng, *Liq. Cryst.* **2010**, *37*, 1221.
- [12] H. Kawaguchi, *Polym. Int.* **2014**, *63*, 925.
- [13] Y. F. Yue, M. A. Haque, T. Kurokawa, T. Nakajima, J. P. Gong, *Adv. Mater.* **2013**, *25*, 3106.
- [14] J. Yoon, W. Lee, E. L. Thomas, *Macromolecules* **2008**, *41*, 4582.
- [15] J. Sussman, D. Snoswell, A. Kontogeorgos, J. J. Baumberg, P. Spahn, *Appl. Phys. Lett.* **2009**, *95*, 173116.
- [16] O. L. Pursiainen, J. J. Baumberg, H. Winkler, B. Viel, P. Spahn, T. Ruhl, *Opt. Express* **2007**, *15*, 9553.
- [17] S. Valkama, H. Kosonen, J. Ruokolainen, T. Haatainen, M. Torkkeli, R. Serimaa, G. Ten Brinke, O. Ikkala, *Nat. Mater.* **2004**, *3*, 872.
- [18] K. Ueno, K. Matsubara, M. Watanabe, Y. Takeoka, *Adv. Mater.* **2007**, *19*, 2807.
- [19] M. C. Chiappelli, R. C. Hayward, *Adv. Mater.* **2012**, *24*, 6100.
- [20] H. Finkelmann, G. Rehage, in *Adv. Polym. Sci.*, Springer Berlin Heidelberg, **1984**, pp. 99–172.
- [21] J.-W. Wang, B.-Y. Zhang, *J. Mater. Sci.* **2014**, *49*, 604.
- [22] H. Stevens, G. Rehage, H. Finkelmann, *Macromolecules* **1984**, *17*, 851.
- [23] H. Ringsdorf, A. Schneller, *Makromol. Chem., Rapid Commun.* **1982**, *3*, 557.
- [24] P. Davidson, *Prog. Polym. Sci.* **1996**, *21*, 893.
- [25] P. Becker, H. Siebert, L. Noirez, C. Schmidt, *Macromol. Symp.* **2005**, *220*, 111.
- [26] G. Agez, R. Bitar, M. Mitov, *Soft Matter* **2011**, *7*, 2841.
- [27] S. Nagano, *Chem. Rec.* **2016**, *16*, 378.
- [28] L. V. Natarajan, J. M. Wofford, V. P. Tondiglia, R. L. Sutherland, H. Koerner, R. A. Vaia, T. J. Bunning, *J. Appl. Phys.* **2008**, *103*, 093107.
- [29] K. A. Suresh, S. Chandrasekhar, *Mol Cryst Liq Cryst* **1976**, *40*, 133.
- [30] V. A. Mallia, N. Tamaoki, *Mol. Cryst. Liq. Cryst.* **2006**, *454*, 81.
- [31] Y. Huang, Y. Zhou, C. Doyle, S.-T. Wu, *Opt. Express* **2006**, *14*, 1236.
- [32] K. S. Shim, J. U. Heo, S. I. Jo, Y.-J. Lee, H.-R. Kim, J.-H. Kim, C.-J. Yu, *Opt. Express* **2014**, *22*, 15467.
- [33] I. Dierking, F. Gießelmann, P. Zugenmaier, W. Kuczynskit, S. T. Lagerwall, B. Stebler, *Liq. Cryst.* **1993**, *13*, 45.
- [34] H. G. Yoon, I. Dierking, H. F. Gleeson, *Phys. Rev. E - Stat. Nonlinear, Soft Matter Phys.* **2010**, *82*, 11705.
- [35] F. Wang, H. Cao, K. Li, P. Song, X. Wu, H. Yang, *Colloids Surfaces A Physicochem. Eng. Asp.* **2012**, *410*, 31.
- [36] F. Zhang, D. K. Yang, *Phys. Rev. E - Stat. Nonlinear, Soft Matter Phys.* **2002**, *66*, 041701/1.
- [37] G. S. Chilaya, *Crystallogr. Reports* **2000**, *45*, 871.
- [38] D. Lacey, H. N. Beattie, G. R. Mitchell, J. A. Pople, *J. Mater. Chem.* **1998**, *8*, 53.

Chapter 3

Polymer stabilized cholesteric liquid crystal polysiloxane for temperature responsive infrared reflective coatings



In this chapter is presented the development of a temperature responsive, infrared-reflective coating consisting of a polymer-stabilized cholesteric liquid crystal siloxane. First, a side-chain liquid crystal oligosiloxane containing acrylate, chiral and mesogenic moieties was successfully synthesized via multiple reaction steps. Subsequently, the coating was fabricated by bar-coating the cholesteric liquid crystal oligomer on glass, using a mediator liquid crystalline molecule to control the viscosity. After the UV-curing and removal of the mediator, a transparent, IR reflective coating was obtained. This fully cured, partially crosslinked transparent polymer coating retained a large temperature responsive color change of ~600 nm between 66°C and room temperature, and the shift was fully reversible.

This chapter is partially reproduced from: Zhang, W.; Lub, J.; Schenning, A. P. H. J.; Zhou, G.; de Haan, L. T. Polymer Stabilized Cholesteric Liquid Crystal Siloxane for Temperature-Responsive Photonic Coatings. *Int. J. Mol. Sci.* **2020**, 21 (5), 1803.

1. Introduction

In Chapter 2, a temperature responsive, infrared reflective coating was fabricated by blade-coating a mixture of oligomeric polysiloxane and a chiral dopant. This non-crosslinked CLC coating possessed a smectic-cholesteric phase transition, leading to a ~1200 nm bandshift within the IR region upon varying the temperature. However, a coating containing a low-molar-weight non crosslinked chiral dopant may suffer robustness, because dewetting and slow evaporation may occur. To obtain an industrially viable product, polymers are desired for a stable performance.^[1] Photonic coatings from non-polymerized CLC mixtures encapsulated in polymer binders or protective layers were reported, showing a good stability and large bandshift range by the smectic-cholesteric effect, but a subtle phase-separation process is required for their fabrication.^[2-4] Alternative ways to make temperature responsive color changing coatings from CLC polymers use either the humidity^[5,6] or heat expansion of the materials^[7,8], which are not able to induce a sensitive reflection band shift or rely on the presence of water.

Completely crosslinked LC polymers fail to retain any smectic-cholesteric effect that is present in their precursors^[9,10], but polymer-stabilized liquid crystal (PSLC) systems that are partially crosslinked may satisfy both coating stability and responsiveness.^[11-14] However, such coatings have never been realized. In this chapter, the development of a photopolymerizable, CLC polysiloxane mixture for the preparation of a temperature-responsive polymer network-stabilized photonic coating is described. A siloxane terpolymer (TP) with reactive acrylate mesogenic side groups was designed and prepared (Figure 3.1). The synthesis of the TP was performed via a three-step route: hydrosilylation, deprotection, and esterification. From the molecular weight of the final polydisperse terpolymer, an average estimated chain length of approximately 8~11 was determined. This TP was processable into planarly aligned cholesteric phase coatings by bar-coating, with the help of a nematic solvent that mediates the alignment. With the full conversion of the acrylate groups under UV-initiated polymerization, crosslinked networks were obtained in the coating. This partially crosslinked polymer coating still shows a ~600 nm reflection band shift within the IR region in response to a temperature change between 20–66 °C, owing to the smectic-cholesteric phase transition. Such temperature-responsive polymer-

stabilized polysiloxane photonic coatings would be attractive for a variety of applications including foils for energy-saving windows^[15–21]

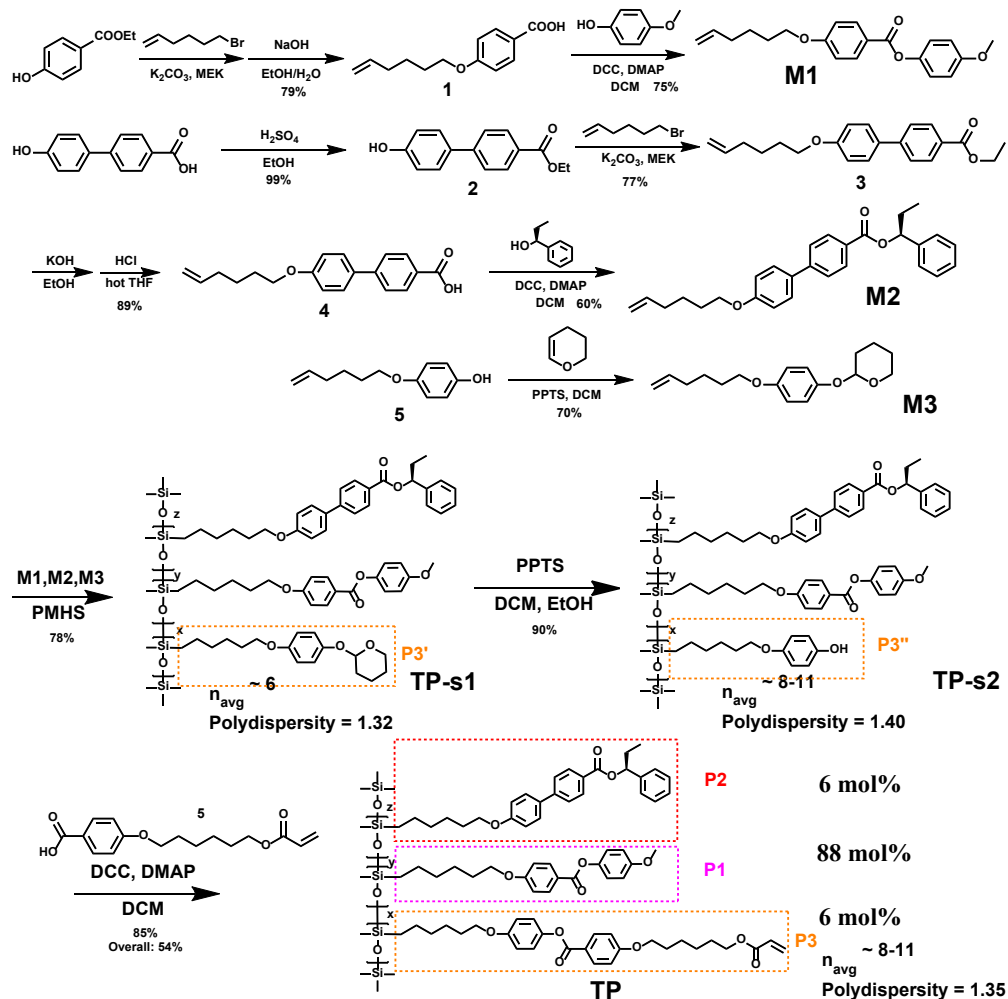


Figure 3.1 Synthetic routes for the preparation of the terpolymer (TP) and the required precursors M1, M2, and M3.

2. Results and discussion

2.1. Synthesis and characterization of the crosslinkable CLC siloxane (TP)

A side-chain polysiloxane LC terpolymer with both cholesteric and smectic LC phases which is crosslinkable was designed (TP, Figure 3.1). This polysiloxane-derived terpolymer contained three mesogenic side groups (P1, P2, and P3) prepared from three precursor molecules (M1, M2, and M3), which were attached to the polysiloxane backbone by hydrosilylation. Mesogenic side group P1 induces a smectic-nematic transition in the polysiloxane polymer^[22,23], the chiral side group P2 induces a cholesteric phase, and the acrylate-containing mesogenic group P3 enables photopolymerization. Monomers M1, M2 and M3 were synthesized and fully characterized by ¹H NMR and ¹³C NMR (See session 4.1). Although the complete synthesis of M1 has been reported^[24,25], here, we use a new approach to synthesize the intermediate product, 4-(hex-5-en-1-yloxy)benzoic acid (1) with a higher yield, by using ethyl 4-hydroxybenzoate as the reactant followed by dehydration of the ester group. The chiral dopant M2 is a new molecule designed to achieve a prominent helical twisting effect at low concentration. Synthesis of M2 was performed in four steps, with an overall yield of 40.7 %. The helical twisting power (HTP) of M2 was estimated to be $\sim 21 \mu\text{m}^{-1}$ in E7 (by wt%). M3 contains a protecting group which was used to prepare

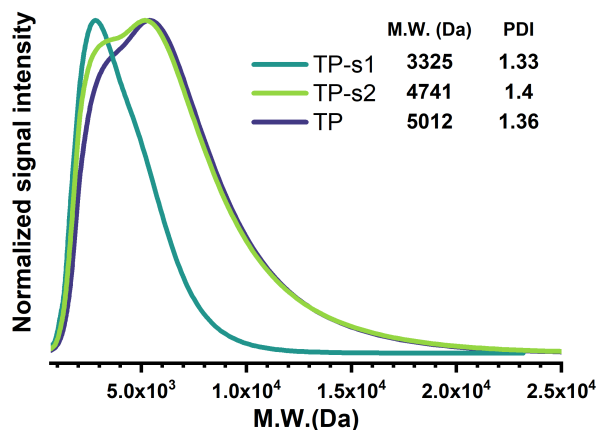


Figure 3.2 GPC molecular distributions of each synthesis step product of TP. Normalized by signal maximum. The molecular weight (M.W.) and polydispersity (PDI) are also given.

the acrylate-containing mesogenic group after the hydrosilylation reaction. It was used instead of the final mesogenic group to avoid participation of the acrylate group during the hydrosilylation.

The TP was obtained from the precursors and poly(methylhydroxylsiloxane) (PMHS) in three steps of synthesis (Figure 3.1). M1 represented the vast majority of precursor used (88 mol%), while M2 represented 6 mol% of the amount of precursor to obtain a cholesteric phase with a reflection band in the IR region. The amount of precursor M3 was 6 mol% in order to induce a low crosslink ratio after photo-polymerization and to maintain a proper pre-transitional effect. The PMHS used had an average chain length (n_{avg}) of 3.9. The polymer backbone was determined to be short in order to obtain only a small mol% of crosslinkable oligomers, which also maintained a low

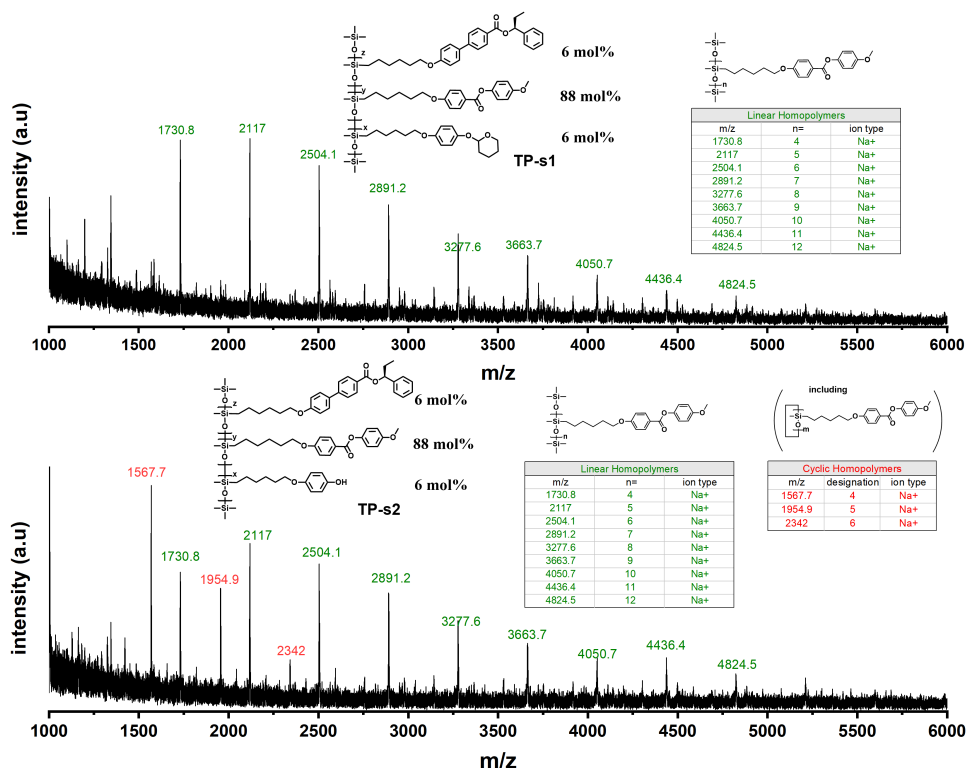


Figure 3.3 Matrix-assisted laser desorption/ionization-time of flight mass spectrometry (MALDI-TOF-MS) spectra of TP-s1, TP-s2. Assignments of the P1 homopolymer signals are specifically listed.

Chapter 3

crosslinked ratio in the coatings. In the first synthesis step, TP-s1 was made through a hydrosilylation reaction of M1, M2, and M3 with PMHS, in a yield of 77.6%. The product TP-s1 was found to have a n_{avg} of approximately 6, calculated based on the ^1H NMR spectrum, by Equation 4. The increase of n_{avg} is most likely due to the loss of the low-mass fraction during precipitation. In the second step, the tetrahydropyran (THP)-protecting group was removed in the presence of pyridinium *p*-toluenesulphonate and ethanol to form TP-s2. This deprotection reaction that formed the free phenolic group was completed without affecting the other mesogen side groups. However, gel permeation chromatography (GPC) of TP-s2 (Figure 3.2) revealed that the average molecular weight (M.W.) of TP-s2 had increased by 42% compared to TP-s1. Furthermore, a wider molecular weight distribution (polydispersity increased from 1.33 to 1.40) was observed. This molecular weight increase was disproportional to the weight loss of this step (yield = 90%). Moreover, a considerable number of cyclic oligomers was found in the matrix-assisted laser desorption/ionization-time of flight mass spectrometry (MALDI-TOF-MS) spectrum, which was absent in TP-s1 (Figure 3.3). Among the signals of the cyclic oligomers, the most intense ones are found at 1568, 1955, and 2342 Da and can be attributed to the four-ring, five-ring, and six-ring homo-oligomer of P1 as $\text{M}\cdot\text{Na}^+$ adducts, respectively. Trace signals of cyclic co-oligomers with one and two P2 or P3'' units are present in the spectrum as well. The Si-OH group or trifunctional branching silicon atoms could not be detected using the ^{29}Si NMR of TP-s2. Based on these results and literature reports on similar phenomena^[26], we assume that an exchange of the Si-O-Si bonds among the siloxane backbones was catalyzed by the mildly acidic PPTS, resulting in the appearance of both longer chains and cyclic compounds.

The third reaction step, the esterification of the phenol groups in TP-s2 with carboxylic acid building block 5 using *N,N'*-dicyclohexylcarbodiimide (DCC) and *N,N*-4-dimethylaminopyridine (*N,N*-4-dimethylaminopyridine), yielded the desired terpolymer (TP). The ^1H NMR spectrum of TP (Figure 3.4) confirmed the correct chemical structure of the polymer. This data also confirmed the molar ratio of the smectic-nematic mesogen (P1), chiral dopant (P2), and acrylate mesogen (P3) units to be 88:6:6. The molecular weight of TP was found to be 5012 Da, with a polydispersity index of 1.36, by GPC (Figure 3.2).

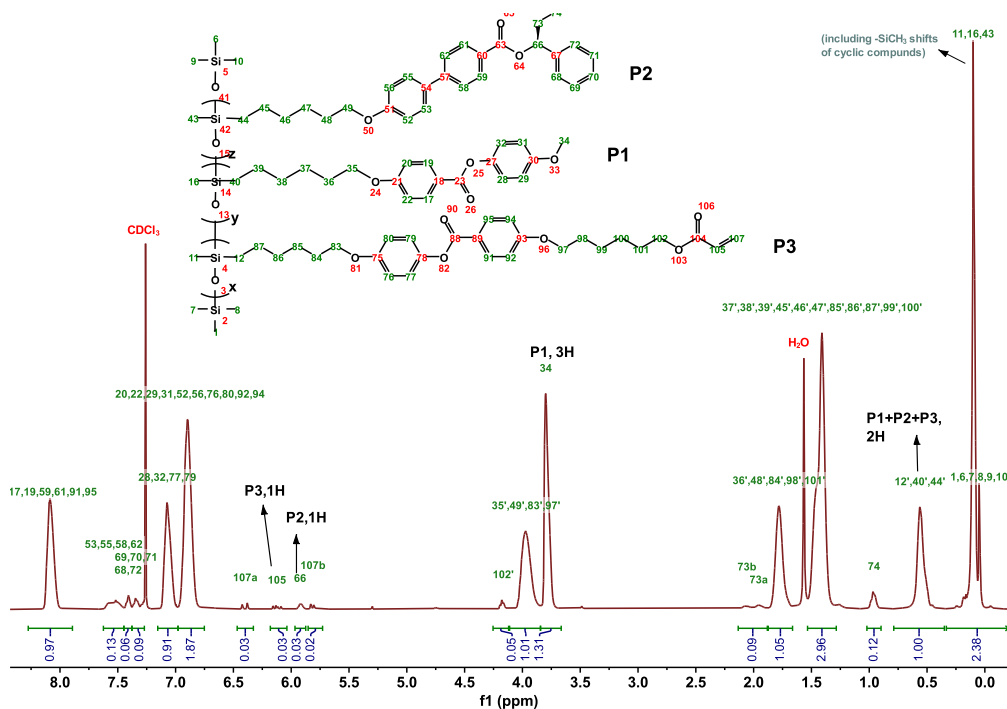


Figure 3.4 ^1H NMR spectrum of TP, with peak assignments and peak integral values.

Chapter 3

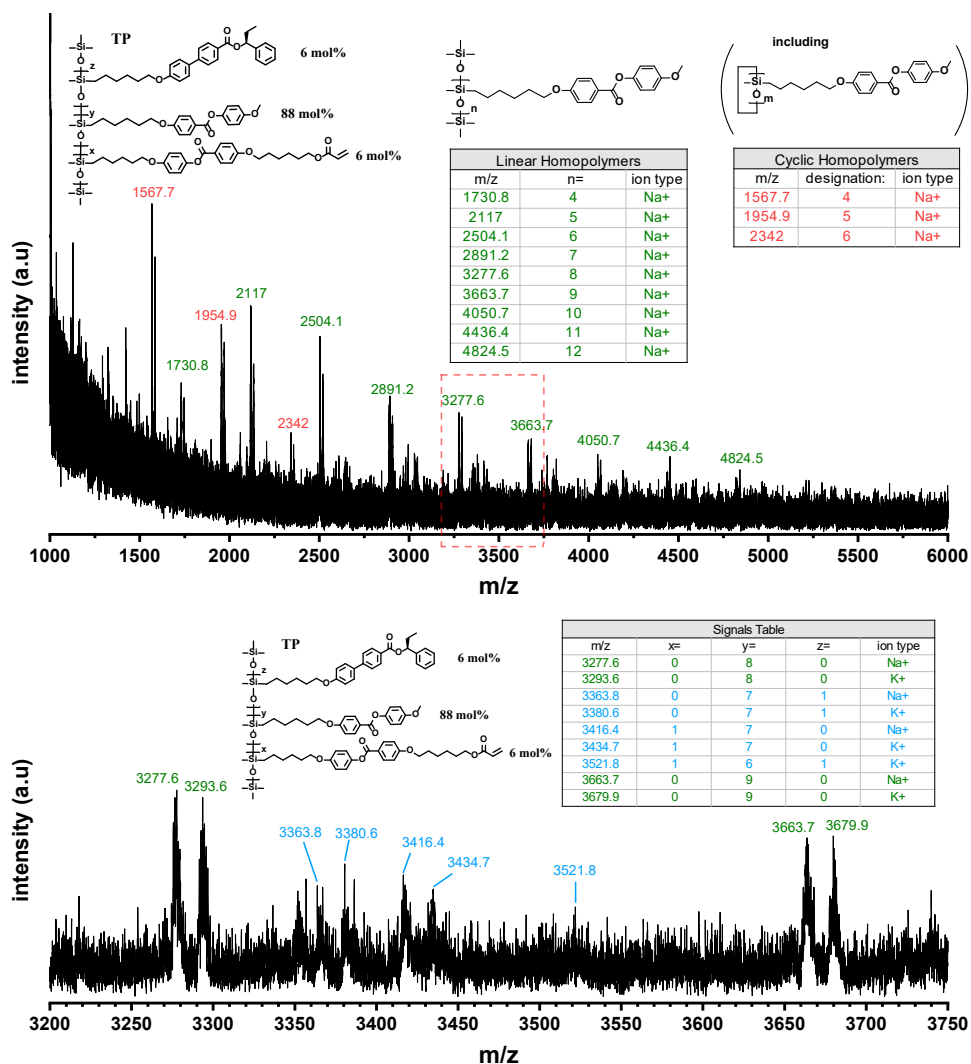


Figure 3.5 MALDI-TOF-MS spectrum (top) and zoom in (bottom) of TP, with captions indicating different species.

MALDI-TOF-MS spectra (Figure 3.5) confirmed the molecular weight of the differently distributed mesogenic species of the polymer. Cyclic chain oligomers generated during TP-s2 synthesis remained in the final product but were considered a minor fraction. Based on these results, we estimated an n_{avg} of the TP between 8 and 11. The rates of different chain lengths (n) in the TP that possess no acrylate group ($R_{0,n}$), one acrylate group ($R_{1,n}$), and more than two acrylate groups ($R_{2+,n}$) have been

calculated using the total concentration of crosslinker in the oligomers and are listed in Table 3.1. Formulas used for the calculations are given by Equation 6-8. From the estimated n_{avg} it can be seen that a considerable fraction of the oligomer molecules in the TP do not contain any acrylate group (50.6%–60.1%), and, therefore, these molecules will definitely not participate in the network formation. Creating a crosslinked network requires molecules that contain at least two acrylate groups. Through these calculations, we also find that the chance of TP oligomers having >2 acrylate groups is not trivial (7.9 mol% when $n_{\text{avg}} = 8$). Therefore, a rather high network fraction after crosslinking is expected.

Table 3.1 Calculated rates of different chain lengths¹ (n) in the TP that possess no acrylate group ($R_{0,n}$), one acrylate group ($R_{1,n}$), and more than two acrylate groups ($R_{2+,n}$). In mol%.

$n=$	$R_{0,n}$	$R_{1,n}$	$R_{2+,n}$
4	78.1%	19.9%	2.0%
5	73.4%	23.4%	3.2%
6	69.0%	26.4%	4.6%
7	64.8%	29.0%	6.2%
8	61.0%	31.1%	7.9%
9	57.3%	32.9%	9.8%
10	53.9%	34.4%	11.7%
11	50.6%	35.5%	13.9%
12	47.6%	36.5%	15.9%

¹ The actual TP has a wide distribution of chain lengths. Therefore, the general R_0 , R_1 and R_{2+} of TP may be significantly influenced by such a complex and can not be accurately specified. This table lists only the assumed most populated chain lengths of TP.

$$R_{0,n} = C_n^0 \times 0.94^n \quad \text{Equation 6}$$

$$R_{1,n} = C_n^1 \times 0.94^{n-1} \times 0.06 \quad \text{Equation 7}$$

$$R_{2+,n} = 1 - R_{0,n} - R_{1,n} \quad \text{Equation 8}$$

Chapter 3

The liquid crystalline properties of the TP were subsequently examined using differential scanning calorimetry (DSC). Despite being a complex mixture of various species, TP shows clear peaks of phase transitions on DSC curves (Figure 3.6a). The isotropic transition and smectic-cholesteric transition were observed at 78 °C and at 29.5 °C, respectively. The glass transition (T_g) of the material is around 0 °C. The TP has a clear cholesteric reflection band below 70 °C, which was measured by transmission spectroscopy of a TP-filled cell with planar alignment layers. Figure 3.6 shows that the reflection wavelength continuously increased as the temperature decreased and stabilized below the transition point of 29.5 °C. This confirmed a smectic-cholesteric pre-transitional effect in this liquid crystalline polymer.

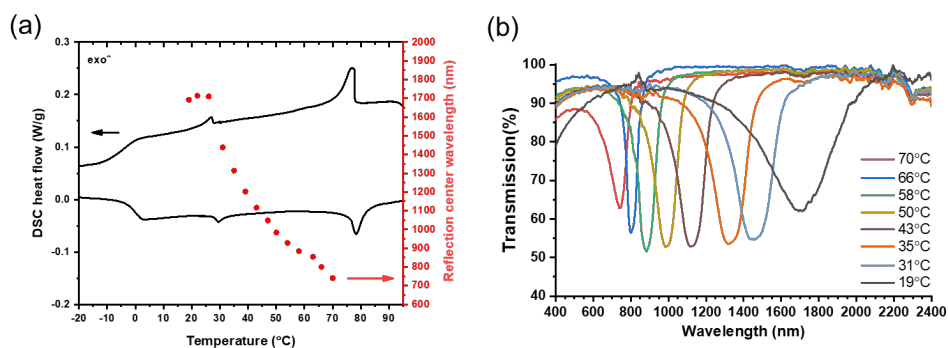


Figure 3.6 (a) DSC curves of TP (black lines), and center of the reflection band as a function of temperature (red dots). (b) Transmission spectra of the TP, when filled in an alignment cell.

2.2. Fabrication of a Polymer Stabilized Cholesteric Liquid Crystal Siloxane Coating

The TP was coated on a glass substrate using an easy-to-conduct bar-coating method. The fabrication of the coatings is shown in Figure 3.7a. The mixture was first bar-coated on glass prepared with a rubbed polyimide layer to obtain a planar cholesteric alignment. This was preferably performed right below the isotropic transition, where the material had a lower viscosity, in order to achieve planar cholesteric alignment under shear force^[27]. However, coating the pure TP did not result in a satisfying planar cholesteric alignment, as the viscosity was too high, causing all mesogens to be aligned uniaxially along the coating direction. To lower the viscosity and improve the alignment of the material, we added a coating mediator to the terpolymer. (Figure 3.7) The coating mediator is an apolar nematogenic molecule^[28] with structural

similarity to the majority mesogenic side group P1 of TP, which ensured good mixing without disrupting the LC phase. The mediator was lab-synthesized via a simple step of esterification. Indeed, a mixture of mediator with TP in a weight ratio of 1:3 was still liquid crystalline. This 1:3 mixture had the right properties to coat and align the material at the cholesteric temperature of 51 °C. In addition, a photoinitiator was added to the mixture to initiate photo-polymerization of the acrylate groups in the TP.

The coating was irradiated with UV under nitrogen, during which acrylate groups were polymerized. Finally, after cooling, the coating was washed in heptane multiple times to remove the mediator molecules from the coating. The fabricated pristine coating showed good visible light transparency at room temperature (Figure 3.7b). Polarized microscope images of the coating presented a planarly aligned cholesteric texture (Figure 3.7c), and a reflection band centered at ~1200 nm was seen in the transmission spectrum of the coating (Figure 3.7d). These results indicate that the fully cured coating retained a proper planar cholesteric alignment, even after the extraction of mediator with heptane.

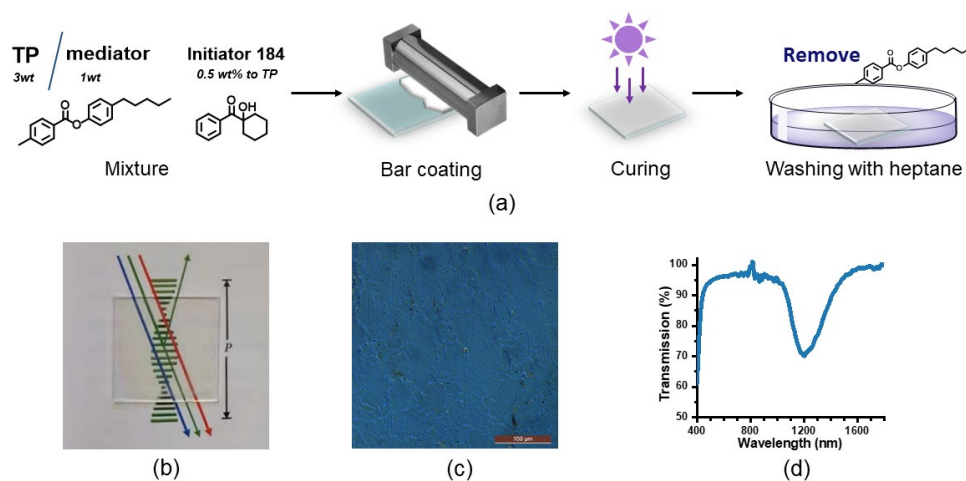


Figure 3.7 (a) Schematic of the preparation and UV curing of terpolymer coatings. (b) Image of a fully-cured TP coating at room temperature, with a colorful image as background showing good visible light transparency. (c) Polarizer microscopy (POM) image of a fully-cured TP coating at room temperature (transmission mode), showing a planar aligned cholesteric texture. The bluish color might be due to the reduced efficiency of the polarizers. (d) Transmission spectrum of the fully cured coating at room temperature, after the removal of the mediator.

Chapter 3

To ensure full crosslinking, we initially investigated the crosslinked fraction of the polymer coating as a function of photo initiator concentration (0.05wt% - 0.5wt%). The coatings were collected in 0.2 μm PTFE filters, and then filtrated by dichloromethane flushing. It was found that in all cases most of the coating dissolved, indicating that the crosslinked network was not continuous. Proton NMR spectra were recorded of the eluents after evaporation of the solvent (Figure 3.8a). When 0.05 wt% of photoinitiator was used, which corresponds to ~ 1 wt% compared to the total weight of the acrylic mesogens, it was found that acrylate groups were poorly converted, as the acrylate signals were still prominently present in the spectrum. When the photoinitiator concentration was increased, the peaks became less prominent, and at 0.25 wt% (5 wt% compared to the total weight of the acrylate groups), the acrylate signals were no longer observable, suggesting high conversion of the acrylate groups. The concentration of 0.5 wt% was consequently selected for sample fabrication to ensure the full conversion of the acrylate groups.

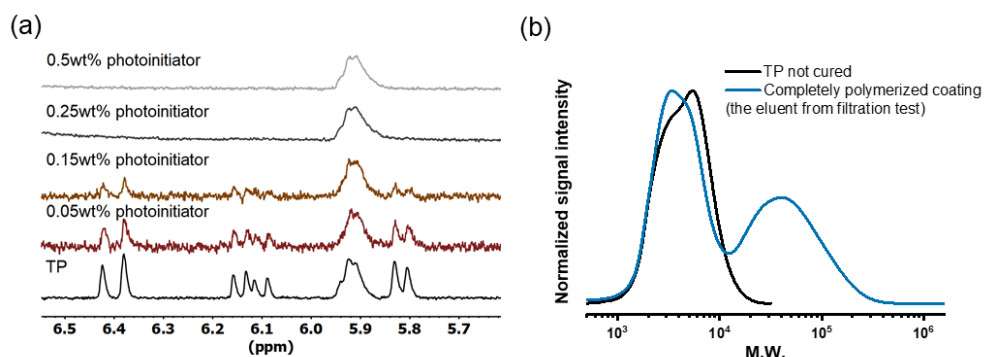


Figure 3.8 (a) ^1H NMR spectra of the processed coatings from mixtures with different initiator concentrations, showing the zoomed-in region where the acrylates signals are present. (b) GPC spectra showing the molecular weight distributions of the completely polymerized TP coatings, compared to the original TP. Normalized by the intensity maximum of the signals.

The crosslinked network fraction of the photonic coatings can be estimated during the filtration experiments. The remaining solid in the filter was the insoluble part of the coating, and was therefore considered as crosslinked polymers. 4 wt% of the original weight of the fully polymerized coating was left in the filter, while a control experiment of an uncured coating (made without using the photoinitiator and processed without the curing step) yielded 0 wt%. However, this 4 wt% does not represent all the reacted TP. The eluent from the filtration experiment contains a substantial amount of high M_w fraction as shown by GPC chromatography (Figure 3.8b), with molecular weights as high as 200 kDa. We assume this fraction contains larger macromolecules consisting of multiple linked TP molecules that can pass the filter pores.

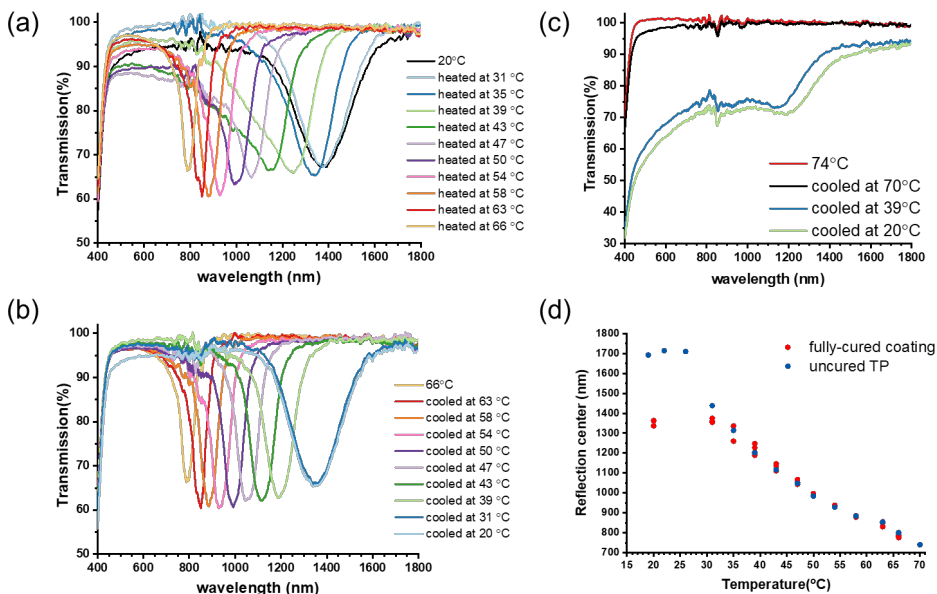


Figure 3.9 Transmission spectra of the fully cured TP coating recorded during heating (a) and cooling (b) between 20 °C and 66 °C, and (c) during cooling from an isotropic temperature (74°C). The thickness of the tested coating was 12 μm . (d) The reflection band center – temperature relation of the fully cured coating, compared to the uncured TP in an alignment cell.

Chapter 3

2.3. Temperature response of the polymer stabilized CLC siloxane coating

The temperature responsive color changing properties of the polymer-stabilized CLC coatings were investigated using UV-Vis-NIR spectroscopy. The absorption spectra of the coatings were measured at different temperatures during stepwise heating and cooling cycles. The results of the first cycle of heating and cooling were different from those of the rest of the cycles. It is most likely that the cholesteric helix reassembles from the collapse caused by the removal of mediator during the fabrication of the coating. Further heating and cooling give the same temperature-responsive optical changes, and multiple cycles of heating and cooling show repetitive results. Figure 3.9 shows the spectra of the coating during the second heating and cooling cycle. Increasing the temperature stepwise from 31 °C to 66 °C resulted in a ~600 nm blueshift of the reflection band center, from 1363 nm to 775 nm (Figure 3.9a). A reversed redshift was seen during the cooling steps (Figure 3.9b). Below 31 °C, the reflection band redshift ceased. This TR-RC is irreversible from the isotropic temperature, and upon cooling from 74 °C the coating did not reverse to the transparent-reflective state but instead adopted an intensely light-scattering state (Figure 3.9c), indicating that the planar cholesteric structure was destroyed. The fully-polymerized coating maintained a similar responsiveness between 31~66 °C compared to the uncured polymer, except that the polymerized one ceases at a lower temperature (Figure 3.9d).

2.4. Discussion of the temperature responsiveness of the TP coating

The DSC curve of the fully cured coating reveals a transitional peak present at 29 °C, which is right around the temperature threshold at which the reflection band ceases to shift. This, together with the similar temperature responsive color changing behavior of the coating compared to the uncured one, suggest that the smectic-cholesteric transition is still the driving force behind the reflection band shifting of the TP coating after crosslinking.

It is interesting to see this well-preserved pre-transitional effect in this polymer-stabilized PSLC coating, as the effect is usually strongly suppressed and in most cases disappears completely after crosslinking has been applied. In a previously reported example of a PSLC system in a cell containing small LC molecules and a 5% crosslinked reactive mesogens (RM) network, the pre-transitional effect of the smectic-cholesteric LCs was strongly reduced after the network was formed ^[11], and

in crosslinked polymer networks with no small molecules present, the pre-transitional effect has never been observed at all. In the PSLC coating presented here, 31.1–35.5% of the TP has one acrylate side group and 7.9–13.9% has two, implying a higher crosslink density; however, it maintained most of the pre-transitional effect after crosslinking.

The above investigations on the composition of the fully cured coating show that it consists of unreacted TP (presumably without an acrylate side group), large macromolecules consisting of multiple TP molecules linked together, and a continuously crosslinked network. This is different from traditional PSLC systems which only contain small molecules and a continuous network.^[29,30] We propose that the polymerization mechanism of the current system is very different from the traditional PSLC systems in which continuous polymer networks are observed^[29,30], as the high viscosity of the material and low concentration of acrylate groups limits polymer chain propagation. As a result, most of the short networks are hindered from connecting with each other to form larger networks, and only a relatively small fraction of the TP becomes part of the continuous network. However, it seems that the responsiveness of the TP coatings benefits from the different way of crosslinking in this system, though some of the improvements can be attributed to the more flexible siloxane backbone compared to RMs.

3. Conclusions

A polysiloxane smectic-cholesteric LC terpolymer with acrylate groups covalently linked to one of the mesogenic side-groups was successfully synthesized via a three-step route. The terpolymer obtained had an unexpectedly increased backbone chain length, and some formation of cyclic oligomer compounds was observed—both of which are side effects of the deprotection step. We propose the mechanism of these side reactions takes place through catalysis by PPTS. A temperature-responsive IR reflective coating was successfully fabricated from this terpolymer. This approach features easy processability using a bar-coating method. We have also found that a coating mediator can assist in the formation of planar alignment of cholesteric polysiloxane LCs during bar-coating. The fully cured terpolymer coatings retained ~600 nm of reversible reflection band shift by heating and cooling. The partially retained temperature responsiveness of the coatings was still caused by the inherent smectic-cholesteric transitional effect of TP.

Chapter 3

The approach of using a polymer-stabilized polysiloxane smectic-cholesteric type LC polymer to fabricate a temperature-responsive photonic polymer is promising. By adjusting the chiral component fraction in the CLC siloxane, a reflection color in the visible region may also be achieved, further broadening the range of potential applications. However, as far as applications are concerned, the difficult synthesis and relying on a mediator provide limiting factors. Mechanical stability of the coating is not satisfying at higher temperature, either (data not shown here). These issues are to be solved in the next chapter.

4. Experimental

4.1. Synthesis of TP

Materials. Ethyl 4-hydroxybenzoate and 3,4-Dihydropyran were purchased from Shanghai Macklin Biochemical Co., Ltd. 6-bromohex-1-ene, 4'-hydroxy-[1,1'-biphenyl]-4-carboxylic acid, p-toluic acid and 4-pentylphenol were obtained from Beijing HWRK chemical Co., Ltd. 4-Dimethylaminopyridine DMAP, Dicyclohexylcarbodiimide (DCC), (S)-(-)-1-phenyl-1-propanol and 1-ethyl-(3-dimethylaminopropyl)carbonyldiimide hydrochloride (EDC•HCl) were obtained from Sigma-Aldrich. 4-(5-hexenyloxy)phenol (**5**) was synthesized by Philips Research Laboratories.^[31] Pyridinium p-toluenesulfonate (PPTS) was purchased from Acros Organics. Poly(methyl hydrogen siloxane) (PMHS), trimethylsilyl terminated, average $M_n \sim 390$, was purchased from Sigma-Aldrich (as the "OMHS"). n_{avg} of the received OMHS was found to be 3.88 by NMR. Platinum(0)-1,3-divinyl-1,1,3,3-tetramethyldisiloxane (Karstedt's catalyst), 2% in xylene solution, was purchased from Sigma-Aldrich. Anhydrous toluene was purchased from Acros Organics. 4-(6-acryloxy-hex-1-yloxy)benzoic acid was purchased from SYNTHON Chemicals GmbH & Co. KG.

Characterizations. NMR spectra were recorded on a 400 MHz Bruker Avance III HD spectrometer. For ^{29}Si measurements, Chromium(III) acetylacetonate and tetramethylsilane were added to the sample, and the measurements were performed under the inverse-grated mode. Matrix-assisted laser desorption/ionization time-of-flight mass spectrometry (MALDI-TOF MS) was performed on a Bruker Autoflex Speed MALDI-MS instrument, with a DCTB as matrix agent. Differential scanning calorimetry (DSC) curves were measured with a DSC Q2000, TA Instruments. Gel

penetration chromatography (GPC) was performed on a Shimadzu LC-2030C.3D instrument equipped with a PDA-254 nm detector, using chloroform as the eluent and monodisperse polystyrene calibration standards.

Syntheses

Synthesis of 4-(hex-5-en-1-yloxy)benzoic acid (1)

A solution was made of 50 g (0.3 mol) ethyl 4-hydroxybenzoate, 53 g (0.32 mol) 6-bromohex-1-ene and 52 g (0.376 mol) potassium carbonate in 750 mL butanone. The mixture was stirred at 85 °C overnight, then cooled to room temperature. After cooling, the solution was filtered, and the solvent was evaporated. The residue was dissolved in 200 mL chloroform. The chloroform solution was extracted three times with an aqueous 1 N NaOH solution (3×200 mL) and with brine (2×200 mL). The organic phase was dried with magnesium sulfate, then a pale-yellow liquid was collected by solvent evaporation. This product was mixed with sodium hydroxide (25.2 g, 0.63 mol) ethanol (400 mL) and water (400 mL), and was refluxed for 12 hr. After being cooled to room temperature, the solution was acidified to a pH of 2 with concentrated HCl. The resulting precipitate was collected and recrystallized from ethanol (500 mL) as a white solid. Yield: 49 g, 79 %.

$^1\text{H NMR}$ (500 MHz, CDCl_3) δ 8.08 (d, $J = 8.9$ Hz), 6.95 (d, $J = 8.9$ Hz), 5.85 (ddt, $J = 16.9, 10.2, 6.6$ Hz), 5.04 (d, $J = 2.2$ Hz), 4.06 (t, $J = 6.5$ Hz), 2.20 – 2.13 (m), 1.95 – 1.76 (m), 1.73 – 1.51 (m).

Synthesis of 4-methoxyphenyl 4-(hex-5-en-1-yloxy)benzoate (M1)

To a solution of 8 g (36.3 mmol) 4-(hex-5-en-1-yloxy)benzoic acid (1), 4.66 g (37.6 mmol) 4-methoxyphenol and 0.42 g (3.44 mmol) DMAP in 220 ml DCM was added 8.73 g (42.3 mmol) DCC in 30 ml of DCM. The mixture was stirred overnight at room temperature. The suspension was filtered, and the solid was dried. The crude product was recrystallized three times from methanol, followed by column chromatography (pentane/DCM = 1:1). The final product was a white solid. Yield: 8.93 g, 75.4 %.

$^1\text{H NMR}$ (400 MHz, CDCl_3) δ 8.13 (d, $J = 8.8$ Hz, 2H), 7.12 (d, $J = 9.0$ Hz, 2H), 6.96 (d, $J = 8.9$ Hz, 2H), 6.93 (d, $J = 9.0$ Hz, 2H), 5.84 (ddt, $J = 16.9, 10.2, 6.6$ Hz, 1H), 5.05 (dd, $J =$

Chapter 3

17.1, 1.7 Hz, 1H), 4.99 (dd, $J = 10.2, 1.5$ Hz, 1H), 4.05 (t, $J = 6.5$ Hz, 2H), 3.82 (s, 3H), 2.20 – 2.09 (m, 2H), 1.90 – 1.78 (m, 2H), 1.65 – 1.54 (m, 2H).

Ethyl 4'-hydroxy-[1,1'-biphenyl]-4-carboxylate (2) was prepared according to literature methods.^[32] Yield: 98.5 %.

Synthesis of ethyl 4'-(hex-5-en-1-yloxy)-[1,1'-biphenyl]-4-carboxylate (3)

8.00 g ethyl 4'-hydroxy-[1,1'-biphenyl]-4-carboxylate (**2**) (33 mmol), 6.00 g 6-bromo-1-ene (37 mmol), and 8.25 g K_2CO_3 (60 mmol) were dissolved in 180 mL butanone, followed by stirring at 85 °C for 42 h. After cooling, the solution was filtered, concentrated, dissolved in $CHCl_3$ (150 mL), washed with 1 N aqueous NaOH (~200 mL), then washed with 1N aqueous NaCl (~200 mL), then washed with water (~200 mL), and dried with $MgSO_4$. After filtration, the solvent was removed under reduced pressure to give the crude product. The product was recrystallized from methanol to obtain the product as a white solid. Yield: 8.26 g, 77 %.

1H NMR (400 MHz, $CDCl_3$) δ 8.08 (d, $J = 8.2$ Hz, 2H), 7.61 (d, $J = 8.2$ Hz, 2H), 7.56 (d, $J = 8.5$ Hz, 2H), 6.98 (d, $J = 8.7$ Hz, 2H), 5.84 (ddt, $J = 16.9, 10.2, 6.6$ Hz, 1H), 5.05 (dd, $J = 17.2, 1.7$ Hz, 1H), 4.98 (dd, $J = 10.2, 1.8$ Hz, 1H), 4.39 (q, $J = 7.1$ Hz, 2H), 4.02 (t, $J = 6.4$ Hz, 2H), 2.20 – 2.09 (m, 2H), 1.89 – 1.77 (m, 2H), 1.66 – 1.53 (m, 2H), 1.41 (t, $J = 7.1$ Hz, 3H).

Synthesis of 4'-(hex-5-en-1-yloxy)-[1,1'-biphenyl]-4-carboxylic acid (4)

To a solution of 8.26 g ethyl 4'-(hex-5-en-1-yloxy)-[1,1'-biphenyl]-4-carboxylate (**3**) (25.5 mmol) in ethanol (100 mL) was added dropwise 9 g KOH (160 mmol) in ethanol (250 mL), followed by reflux for 40 h. After cooling, the precipitate was collected, rinsed with water, and then dissolved in hot THF and acidified with 2 N HCl. After cooling the precipitate was collected, washed with water, and recrystallized once from acetic acid. The resulting product was a white solid. Yield: 6.71 g, 88.9 %.

1H NMR (400 MHz, $DMSO-d_6$) δ 12.94 (s, 1H), 7.98 (d, $J = 8.3$ Hz, 2H), 7.75 (d, $J = 8.4$ Hz, 2H), 7.68 (d, $J = 8.7$ Hz, 2H), 7.04 (d, $J = 8.8$ Hz, 2H), 5.84 (ddt, $J = 16.9, 10.2, 6.6$ Hz,

1H), 5.04 (dd, J = 17.1, 1.8 Hz, 1H), 4.98 (dd, J = 10.2, 1.9 Hz, 1H), 4.03 (t, J = 6.5 Hz, 2H), 2.16 – 2.05 (m, 2H), 1.80 – 1.68 (m, 2H), 1.59 – 1.46 (m, 2H).

¹³C NMR (101 MHz, DMSO-d₆) δ 167.67, 159.44, 144.44, 139.02, 131.55, 130.41, 129.26, 128.58, 126.55, 115.46, 115.44, 67.84, 33.31, 28.59, 25.20.

Synthesis of (S)-1-phenylpropyl 4'-(hex-5-en-1-yloxy)-[1,1'-biphenyl]-4-carboxylate (M2)

0.72 g of (S)-(-)-1-phenyl-1-propanol (5.28 mmol), 0.063 g of DMAP (0.518 mmol) and 1.565 g of 4'-(hex-5-en-1-yloxy)-[1,1'-biphenyl]-4-carboxylic acid (**4**) (5.28 mmol) was dissolved in 30 ml of dichloromethane. 1.088 g DCC (5.28 mmol) dissolved in 5 ml DCM was added dropwise to the mixture. The mixture was stirred at room temperature overnight. The resulting mixture was concentrated slightly, refrigerated, and then filtered. The eluent was collected, dried and further purified by column chromatography (DCM/pentane 3 : 5). Recrystallizing 3 times from methanol gave the final product as a white solid. Yield: 1.31 g, 60 %.

¹H NMR (400 MHz, Chloroform-d) δ 8.19 (d, J = 8.4 Hz, 2H), 7.68 (d, J = 8.5 Hz, 2H), 7.61 (d, J = 8.8 Hz, 2H), 7.52 – 7.45 (m, 2H), 7.45 – 7.38 (m, 2H), 7.38 – 7.30 (m, 1H), 7.04 (d, J = 8.8 Hz, 2H), 6.00 (t, J = 6.8 Hz, 1H), 5.90 (ddt, J = 16.9, 10.2, 6.6 Hz, 1H), 5.11 (dd, J = 17.1, 1.8 Hz, 1H), 5.05 (dd, J = 10.3, 1.8 Hz, 1H), 4.06 (t, J = 6.4 Hz, 2H), 2.25 – 2.17 (m, 2H), 2.19 – 2.05 (m, 1H), 2.03 (ddq, J = 13.9, 7.4, 6.3 Hz, 1H), 1.95 – 1.82 (m, 2H), 1.71 – 1.58 (m, 2H), 1.04 (t, J = 7.4 Hz, 3H).

¹³C NMR (101 MHz, CDCl₃) δ 165.86, 159.38, 145.31, 140.73, 138.50, 132.28, 130.16, 128.58, 128.44, 128.34, 127.82, 126.49, 126.46, 114.93, 114.81, 77.82, 67.91, 33.45, 29.63, 28.71, 25.34, 10.01.

Synthesis of M3

To a solution of 5 g of 4-(5-hexenyloxy)phenol (26 mmol) and 0.654 g PPTS (2.6 mmol) in 100 mL DCM was added 3.55 mL 3,4-dihydropyran (39 mmol), and the solution was stirred for 4 h at room temperature. Then the solution was concentrated, diluted with 200 mL diethyl ether, and washed with brine and water. Column chromatography over silica gel (pentane/DCM 5:3) resulted in a pale-yellow liquid product. Yield: 5 g, 69.6 %. Density: 1.047 g/mL at 25°C.

Chapter 3

^1H NMR (400 MHz, DMSO-d_6) δ 6.91 (d, $J = 9.1$ Hz, 2H), 6.80 (d, $J = 9.1$ Hz, 2H), 5.79 (ddt, $J = 16.9, 10.2, 6.6$ Hz, 1H), 5.27 (t, $J = 3.5$ Hz, 1H), 5.01 (dd, $J = 17.2, 1.9$ Hz, 1H), 4.94 (dd, $J = 28.1, 17.2$ Hz, 1H), 3.87 (t, $J = 6.4$ Hz, 2H), 3.81 – 3.70 (m, 1H), 3.54 – 3.43 (m, 1H), 2.17 – 1.99 (m, 2H), 1.92 – 1.34 (m, 10H).

^{13}C NMR (101 MHz, CDCl_3) δ 154.16, 151.15, 138.72, 117.90, 115.36, 114.82, 97.48, 68.41, 62.23, 33.60, 30.65, 28.96, 25.49, 25.41, 19.09.

Synthesis of TP-s1

Monomers **M1**, **M2**, and **M3** were put into a Schlenk flask in a molar ratio of 88 : 6 : 6, for a total of 11 mmol. 0.92 g OMHS was added to the flask, in which the amount of Si-H bonds was approximately 9 mmol. The components in the flask were flushed continuously with argon. 25 mL of anhydrous toluene was injected under argon atmosphere to dissolve the reactants. A catalytic amount of Karstedt's catalyst was then injected to start the reaction. The content of the flask was brought to reflux at 65 °C under argon atmosphere. The reaction was continued until sampling NMR showed no residual Si-H groups at $\delta=4.7$. The finished reaction was cooled, and the product solution was precipitated in toluene/cold methanol (-20 °C) 3 times. After removal of the solvent in vacuum, the resulting solid was dissolved in toluene, and an adequate amount of silica gel metal scavengers (Si-Triamine, SilicaMetS, Silicycle Inc.) was added. This was followed by vigorous stirring overnight to remove the platinum catalyst from the product. The silica gel was removed through filtration and washed with toluene. The eluent was evaporated, yielding a white, viscous solid product. Yield: 3.01 g, 77.6 %. N_{avg} calculated from NMR using a literature method^[25]: 6.12.

^1H NMR (400 MHz, CDCl_3) δ 8.10, 7.59, 7.52, 7.41, 7.35, 7.08, 6.90, 6.78, 5.93, 5.25, 3.99, 3.80, 3.56, 2.07, 1.96, 1.79, 1.65, 1.48, 1.41, 0.97, 0.55, 0.17, 0.10, 0.05. Molar ratio of **P1**, **P2**, **P3'** units are confirmed as 88 : 6 : 6.

^{29}Si NMR (79 MHz, CDCl_3) δ 7.09, -22.29, -22.88, -22.99.

Synthesis of TP-s2

3 g of **TP-s1** (containing ~0.47 mmol THP group) was dissolved in 40 ml DCM. 4 ml of ethanol (~100 mol. equiv. to THP amount) was added to the solution, 0.47 g of PPTS (0.188 mmol) was then added into the mixture with vigorous stirring. After 4.5 days the solution was precipitated into DCM/cold methanol three times. The product was a white and viscous solid. Yield: 2.7 g, ~90 %.

^1H NMR (400 MHz, CDCl_3) δ 8.10, 7.58, 7.52, 7.41, 7.35, 7.26, 7.08, 6.90, 6.70, 5.92, 3.97, 3.81, 2.06, 1.96, 1.78, 1.47, 1.41, 0.97, 0.56, 0.10, 0.05. Molar ratio of **P1**, **P2**, **P3''** units are confirmed as 88 : 6 : 6.

^{29}Si NMR (79 MHz, CDCl_3) δ 7.09, -19.96, -22.29, -22.87, -22.99.

Synthesis of TP

2.51 g **TP-s2** (containing ~0.4 mmol phenol group) was dissolved in 30 ml DCM. 0.585 g of 4-(6-acryloxy-hex-1-yloxy)benzoic acid (2 mmol, ~5 equiv.) and 0.0244 g DMAP (0.2 mmol) were added to the mixture. 0.412 g DCC (2 mmol, ~5 equiv.) was dissolved in 10 ml solution and added dropwise to the mixture. The mixture was stirred vigorously overnight. The solution was then concentrated and precipitated 3 times from DCM/cold methanol and once from toluene/heptane. Yield: 2.04 g, 85 %.

^1H NMR (400 MHz, CDCl_3) δ 8.07, 7.58, 7.41, 7.35, 7.07, 6.90, 4.16, 3.97, 3.80, 2.06, 1.96, 1.78, 1.46, 1.41, 0.97, 0.56, 0.19, 0.10, 0.05. Peak assignments and integral values are given in Figure 3.4.

^{29}Si NMR (79 MHz, CDCl_3) δ 7.11, -20.09, -22.28, -22.47, -22.86, -22.98.

Synthesis of the coating mediator

A solution of 1.36 g p-toluic acid (10 mmol), 1.64 g 4-pentylphenol (10 mmol), and 122 mg DMAP (1 mmol) in 100 mL DCM was cooled to 0 °C under argon, and 1.92 g (10 mmol) of EDC·HCl was added. After stirring overnight at RT, the solvent was removed under reduced pressure until 75 mL was left, and extracted subsequently with 50 mL of a saturated NaHCO_3 solution, 50 mL of water, and 50 mL of brine. After drying over anhydrous MgSO_4 , the solvent was removed under reduced pressure.

Chapter 3

The crude product was then purified by column chromatography (hexane/DCM 7 : 1) and obtained as a white solid. Yield: 2.51 g, 89 %.

$^1\text{H NMR}$ (600 MHz, CDCl_3) δ 8.09 (d, $J = 7.9$ Hz, 2H), 7.31 (d, $J = 8.0$ Hz, 2H), 7.22 (d, $J = 8.2$ Hz, 2H), 7.11 (d, $J = 8.7$ Hz, 2H), 2.62 (t, $J = 7.6$ Hz, 2H), 2.45 (s, 3H), 1.67 – 1.59 (m, 2H), 1.40 – 1.29 (m, 4H), 0.91 (t, $J = 6.9$ Hz, 3H).

$^1\text{H NMR}$ (400 MHz, CDCl_3) δ 8.10, 7.58, 7.52, 7.41, 7.35, 7.08, 6.90, 5.93, 3.99, 3.81, 2.08, 1.96, 1.79, 1.47, 1.41, 0.97, 0.55, 0.10, 0.05.

4.2. Preparation of TP coatings

Materials. Photoinitiator Irgacure 184 was purchased from Ciba Specialty Chemicals Inc.

Mixtures. The TP and the mediator were weighed in brown glass vials, in a weight ratio of 3:1. Subsequently, initiator 184 was added via solution in a volumetric flask (2 mg/mL in unstabilized THF), precisely 0.5 wt% to the weight of TP. More unstabilized THF was then added to dissolve all components, leading to a solution of ~45 wt% in the end.

Preparation of Rubbed Polyimide Coated Glass Substrates. The same procedure was followed as in ^[33].

Preparation of Coatings. An RK PrintCoat Instruments K control coater was used to prepare the coatings. The mixtures were applied on polyimide-rubbed glass substrates and placed at 60 °C for 1 h to evaporate the solvent. Then, the coatings were applied using a 30 μm gap (4-sided applicator, ZFR 2040.8030, Zehntner), which was pushed forward over the mixture automatically by the coater. The temperature of the substrate surface during the application was approximately 51 °C. The speed of the applicator movement was 0.5 cm/s. The coatings were then cooled down to 43–47 °C at the surface, flushed with nitrogen constantly for 1.5 h, and illuminated with UVA using an EXFO Omnicure S2000 mercury lamp, at an intensity of 20 mW/cm² for 10 min. After the exposure, the coatings were kept in nitrogen atmosphere for 1h, and were cooled down to room temperature. The coating mediator was removed from the coatings completely, by dipping the coatings in heptane for at least 16 h, with an exchange of solvent three times. The coatings were then collected and dried in air.

The thickness of the obtained coatings was measured using a Fogale Zoomsurf 3D interferometer. The coatings fabricated for optical measurements were ~11–13 μm in thickness.

For the control experiment of the mixture without using initiator 184, the coating was cooled to room temperature right after the coating application without UVA curing.

For the samples used in the crosslink fraction tests, the mixtures were coated on 9 x 12 cm clean glass substrates without polyimide layers. A larger portion of materials was used to create larger coating samples.

Characterizations. NMR, DSC, and GPC measurements follow the same methods as above. Polarizer microscopy (POM) images were taken on a Leica microscope DM2700 in transmission mode, equipped with polarizers.

Polymeric Distribution Analysis of the Coatings. The coatings were collected in 0.2 μm PTFE filters and weighed to find approximately 20 mg of materials on average. The filters containing these materials were flushed with a continuous flow of dichloromethane by syringes at room temperature, and then dried in a 40 °C oven. The flush-dry cycle was run until the weight of the dried filters did not reduce anymore. The crosslink fractions were calculated from the weight of the material left in the filter divided by the initial weight of material in the filter. The eluents were collected and analyzed with proton NMR and GPC.

Vis–NIR Transmission Spectra of the Coatings Over Temperature. Transmission spectra of the coatings were measured on a Shimadzu UV-3102 PC UV/Vis/NIR spectrophotometer equipped with an MPC-3100 sample compartment and a Linkam TMS93 temperature controller. A polyimide coated glass substrate was used as baseline. The actual temperature of the coating was calibrated using a thermometer probe (Comark KM340). A scan of spectrum started exactly every 5 min when the coating was kept at one temperature, until the new spectrum was identical to the previous one.

5. References

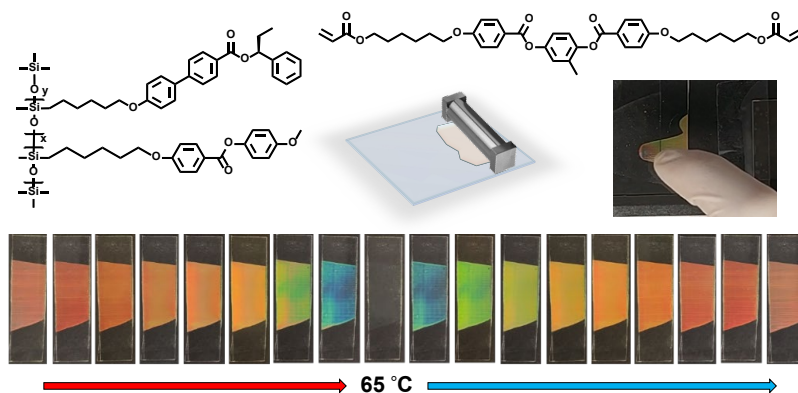
- [1] E. P. A. van Heeswijk, A. J. J. Kragt, N. Grossiord, A. Schenning, *Chem. Commun.* **2019**, 55, 2880.
- [2] H. Khandelwal, E. P. A. van Heeswijk, A. P. H. J. Schenning, M. G. Debije, *J. Mater. Chem. C* **2019**, 7, 7395.
- [3] A. Ranjkesh, T.-H. Yoon, *ACS Appl. Mater. Interfaces* **2019**, 11, 26314.
- [4] E. P. A. van Heeswijk, T. Meerman, J. de Heer, N. Grossiord, A. P. H. J. Schenning, *ACS Appl.*

Chapter 3

- Polym. Mater.* **2019**, *1*, 3407.
- [5] E. P. A. Van Heeswijk, J. J. H. Kloos, N. Grossiord, A. P. H. J. Schenning, *J. Mater. Chem. A* **2019**, *7*, 6113.
- [6] N. Herzer, H. Guneyasu, D. J. D. Davies, D. Yildirim, A. R. Vaccaro, D. J. Broer, C. W. M. Bastiaansen, A. P. H. J. Schenning, *J. Am. Chem. Soc.* **2012**, *134*, 7608.
- [7] H. Nagai, K. Urayama, *Phys. Rev. E* **2015**, *92*, 022501.
- [8] M. T. Brannum, A. M. Steele, M. C. Venetos, L. S. T. J. Korley, G. E. Wnek, T. J. White, *Adv. Opt. Mater.* **2019**, *7*, 1801683.
- [9] P. Zhang, A. J. J. Kragt, A. P. H. J. Schenning, L. T. De Haan, G. Zhou, *J. Mater. Chem. C* **2018**, *6*, 7184.
- [10] L. Zhang, M. Wang, L. Wang, D. K. Yang, H. Yu, H. Yang, *Liq. Cryst.* **2016**, *43*, 750.
- [11] B. Zhang, X. Lin, Y. You, X. Hu, L. de Haan, W. Zhao, G. Zhou, D. Yuan, *Opt. Express* **2019**, *27*, 13516.
- [12] X. Wu, H. Cao, R. Guo, K. Li, F. Wang, Y. Gao, W. Yao, L. Zhang, X. Chen, H. Yang, *Macromolecules* **2012**, *45*, 5556.
- [13] S. Relaix, M. Mitov, *Liq. Cryst.* **2008**, *35*, 1037.
- [14] G. Agez, M. Mitov, *J. Phys. Chem. B* **2011**, *115*, 6421.
- [15] S. Y. Li, G. A. Niklasson, C. G. Granqvist, *Thin Solid Films* **2012**, *520*, 3823.
- [16] Y. Ke, J. Chen, G. Lin, S. Wang, Y. Zhou, J. Yin, P. S. Lee, Y. Long, *Adv. Energy Mater.* **2019**, *9*, 1902066.
- [17] X. Liang, S. S. Guo, S. S. Guo, M. Chen, C. Li, Q. Wang, C. Zou, C. Zhang, L. Zhang, H. Yang, *Mater. Horizons* **2017**, *4*, 878.
- [18] X. Liang, C. Guo, M. Chen, S. Guo, L. Zhang, F. Li, S. Guo, H. Yang, *Nanoscale Horizons* **2017**, *2*, 319.
- [19] Y. Zhou, Y. Cai, X. Hu, Y. Long, *J. Mater. Chem. A* **2014**, *2*, 13550.
- [20] Y. Zhou, Y. Cai, X. Hu, Y. Long, *J. Mater. Chem. A* **2015**, *3*, 1121.
- [21] H. Khandelwal, A. P. H. J. Schenning, M. G. Debije, *Adv. Energy Mater.* **2017**, *7*, 1602209.
- [22] H. Stevens, G. Rehage, H. Finkelmann, *Macromolecules* **1984**, *17*, 851.
- [23] H. Finkelmann, G. Rehage, *Makromol. Chemie-Rapid Commun.* **1980**, *1*, 733.
- [24] D. Lacey, H. N. Beattie, G. R. Mitchell, J. A. Pople, *J. Mater. Chem.* **1998**, *8*, 53.
- [25] W. Zhang, S. Kragt, A. P. H. J. Schenning, L. T. De Haan, G. Zhou, *ACS Omega* **2017**, *2*, 3475.
- [26] S. Nishihama, H. Yamada, H. Nakazawa, *Clay Miner.* **1997**, *32*, 645.
- [27] A. J. J. Kragt, D. J. Broer, A. P. H. J. Schenning, *Adv. Funct. Mater.* **2018**, *28*, 1704756.
- [28] J. P. Van Meter, B. H. Klanderman, *Mol. Cryst. Liq. Cryst.* **1973**, *22*, 271.
- [29] A. S. Sonin, N. A. Churochkina, *Polym. Sci. Ser. A* **2010**, *52*, 463.
- [30] C. V. Rajaram, S. D. Hudson, L. C. Chien, *Chem. Mater.* **1995**, *7*, 2300.
- [31] H. T. A. Wilderbeek, M. G. M. Van Der Meer, M. A. G. Jansen, L. Nelissen, H. R. Fischer, J. J. G. S. Van Es, C. W. M. Bastiaansen, J. Lub, D. J. Broer, *Liq. Cryst.* **2003**, *30*, 93.
- [32] S. H. Kang, K. S. Jang, P. Theato, R. Zentel, J. Y. Chang, *Macromolecules* **2007**, *40*, 8349.
- [33] A. J. J. Kragt, D. C. Hoekstra, S. Stallinga, D. J. Broer, A. P. H. J. Schenning, *Adv. Mater.* **2019**, *31*, 1903120.

Chapter 4

Fully reversible thermochromic photonic coatings with a protective topcoat



The fabrication of reversible and stable thermochromic coatings remains challenging. In this chapter, a stable thermochromic photonic coating with a protective topcoat is fabricated. A cholesteric oligosiloxane liquid crystal possessing a smectic-to-cholesteric phase transition temperature response is synthesized. Planar alignment of its cholesteric phase can be achieved with blade coating. By stabilizing with 3 wt% of a crosslinked liquid crystal network, the photonic coating shows a fully reversible color change ranging from red to blue upon heating. A transparent polysiloxane layer can be directly applied on top of the cholesteric layer to protect it against damage without affecting the optical properties. This approach satisfies the basic requirements of thermochromic polymer coatings, as it combines easy processability, stability, and a reversible temperature response.

This chapter is partially reproduced from: Zhang, W.; Schenning, A. P. H. J.; Kragt, A. J. J.; Zhou, G.; de Haan, L. T. Reversible Thermochromic Photonic Coatings with a Protective Topcoat. *ACS Appl. Mater. Interfaces* **2021**, 13 (2), 3153–3160.

Chapter 4

1. Introduction

Chapter 3 presents a complex CLC terpolymer that was partially crosslinkable to form a polymer stabilized photonic coating. This coating showed a temperature responsive reflection band shift of about 600 nm. However, further improvements are needed towards applications. Firstly, the thermochromic response is irreversible when the coating is exposed above the isotropic phase transition temperature. Secondly, the coating could not be coat-aligned (in planar cholesteric texture) without the help of small molecule liquid crystal mediator.

On top of that, the crosslinked terpolymer coating still suffers from mechanical damage at elevated temperatures. It can be imagined that the mechanical robustness of the material is contradictory to the freedom of movement of the mesogens. Instead of fully crosslinking the polymers, a solid top layer can be added for protection instead. Protective top layers were successfully formed onto low molecular weight CLC systems using chemical reaction-induced phase separation.^[1-3] For polymeric materials, direct methods of adding an elastomeric topcoat might be possible^[4-6], which would make the fabrication process much easier.

The current chapter reports on a new approach for the preparation of temperature-responsive CLC photonic coatings with full thermal reversibility from the cholesteric-to-smectic and cholesteric-to-isotropic transitions, which also have a fast response and good optical transparency. A temperature-responsive siloxane CLC oligomer with a smectic-cholesteric transition (CP10, which stands for copolymer with 10mol% chiral compound, Figure 4.1) was synthesized, which can be directly blade-coated on glass. By introducing 3 wt% of crosslinked LC network into the CP10 coating, the optical properties of the coating become fully reversible even when passing the smectic and isotropic phase transitions, due to the stabilization of the planar alignment by the LC network. On top of the photonic coating, a transparent protective polymer layer was added via direct blade coating. The thermochromic response of the LC layer is unaffected by the topcoat, showing a reversible and continuous color change from blue to red between 53 °C and room temperature.

2. Results and discussion

2.1. Synthesis and characterization of the smectic-cholesteric oligosiloxane (CP10)

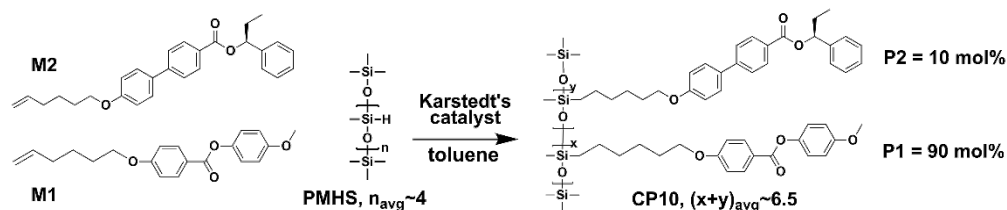


Figure 4.1 Synthetic route of CP10.

For the fabrication of the polymer stabilized liquid crystal coating, we synthesized a side-chain oligosiloxane LC with a low glass transition temperature^[7] and a smectic-to-cholesteric transition (CP10, Figure 4.1) using a one-step hydrosilylation reaction. The resulting oligomer is a random co-oligomer of mesogenic units P1 (90 mol%) and chiral units P2 (10 mol%). The synthesis of precursors M1 and M2 has been introduced in Chapter 3. The length of the siloxane oligomer backbone (n_{avg}) of PMHS was designed to be short ($n_{avg} \sim 4$) in order to obtain a moderate viscosity. This way it can be aligned in the CLC phase by coating, still has a fast response and is solid enough to apply the topcoat without affecting the alignment. The molecular structure and the correct ratio of P1/P2 have been confirmed by the ¹H NMR spectrum, and its n_{avg} is calculated to be about 6.5 (Equation 4). This increase of n_{avg} is presumably due to the

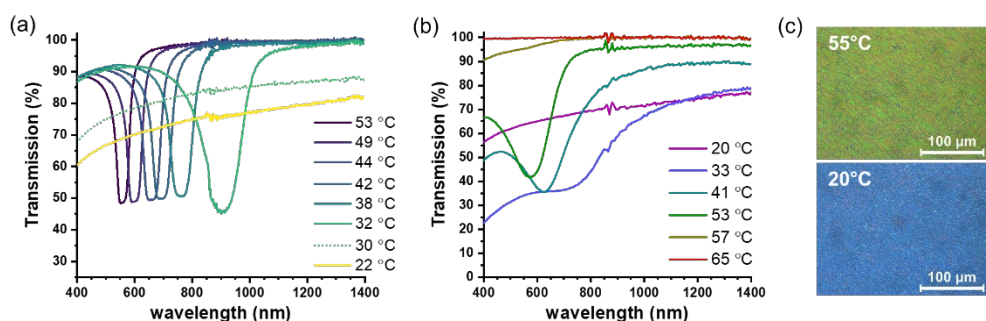


Figure 4.2 Transmission spectra of CP10 in a cell. (a) First cooling round from 55 °C (the temperature at which the cell was filled) to room temperature. (b) The second round of heating until isotropic. (c) POM image of CP10 in a cell, from a planarly aligned cholesteric phase at 55 °C to being cooled to 20 °C (smectic phase).

Chapter 4

loss of the low-molar fraction during precipitation, which is supported by the yield of 78%. When measured with GPC, CP10 shows a polydispersity of 1.18.

The oligomer has an isotropic transition (T_i) at 66 °C, a smectic-to-cholesteric transition ($T_{\text{Sm-Ch}}$) around 35 °C, and the glass transition (T_g) is around -6 °C. Transmission spectra of CP10 filled into a cell with planar alignment layers (Figure 4.2) show a clear reflection band below T_i . In the cholesteric LC phase, the central reflection wavelength shifted from 550 to 902 nm as the temperature decreased from 53 to 32 °C (Figure 4.2a), revealing the existence of the pre-translational effect. Below 31 °C the reflection band disappeared suddenly, followed by a loss of transparency. Polarization optical microscopy reveals that this scattering state is a result of a multidomain texture (Figure 4.2c). Hence, the disappearance of the reflection band and the strong scattering is caused by the formation of the multidomain state of the smectic phase.^[8-11] Despite having two alignment layers, the initial cholesteric alignment of CP10 does not recover completely upon heating back to the CLC phase (Figure 4.2b) or upon cooling from the isotropic phase (Figure 4.2c).

2.2. Polymer stabilized photonic coatings from CP10

The oligomer CP10 can be blade-coated at 60 °C to form planar cholesteric alignment, as the spectra show a clear reflection band with high transparency at cholesteric temperatures (Figure 4.3a). However, the cholesteric alignment is also lost when passing the phase transition temperatures. When heated up to the isotropic phase,

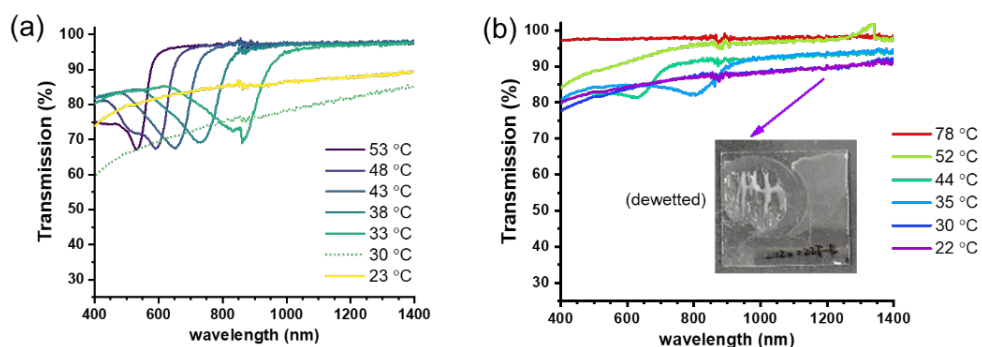


Figure 4.3 Transmission spectra of CP10 as a coating: (a) cooling to room temperature, immediately after coating at 60°C. (b) cooling from 78°C (isotropic phase).

apart from losing the cholesteric alignment, the coating irreversibly dewets (Figure 4.3b).

To stabilize the planar cholesteric alignment of CP10, we added a small amount of crosslinked LC network^[12-14] (Figure 4.4). A nematic diacrylate reactive mesogen was chosen as the monomer to prepare the network (the network monomer). We mixed the network monomer with CP10 in different ratios (1-4wt%) in order to study the stabilizing effect of different amounts of network. A photo-initiator was added to the mixture to initiate the network formation. The mixtures were blade-coated on glass substrates with planar alignment layers at the cholesteric temperature of 60 °C and then cured with UV irradiation to crosslink the network monomer and generate the network. The thickness of these coatings is about 10 to 12.5 μm as determined by interferometry. DSC measurements of these network-stabilized coatings show that their $T_{\text{Sm-Ch}}$ and T_i are preserved after crosslinking. As the network ratio is increased from 1wt% to 4wt%, $T_{\text{Sm-Ch}}$ and T_i decrease slightly from 31 to 26 °C and from 61 to 57 °C, respectively.

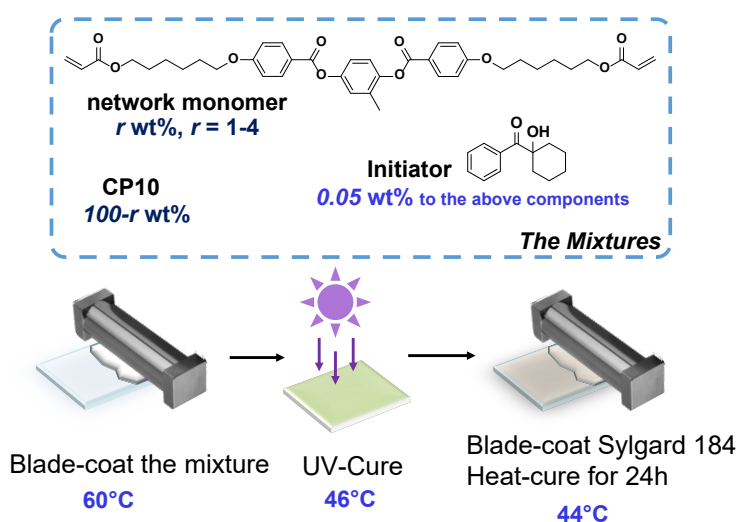


Figure 4.4 The composition of the mixtures using the smectic-cholesteric polymer CP10, and the fabrication of the network stabilized coatings with/without a protective topcoat.

Chapter 4

The thermo-optical response of the network-stabilized coatings containing 1, 2, 2.5, 3, and 4 wt% of the network monomer were investigated with UV-Vis-nIR spectroscopy over multiple rounds of heating and cooling from 22 °C (smectic phase) to 61 °C (isotropic phase). The stabilizing effect of the network was investigated by comparing the transparency levels of the coatings at room temperature before and after the first temperature cycle. We chose the transmission of 500 nm light as an indication of transparency. Notably, the coatings with a crosslinked network have a higher transmission of ~86% before the temperature cycle compared to a film without a network, which has a transmission of only ~72%. Even having 1 wt% of network significantly improves the transparency, with a clear reflection band (centered at

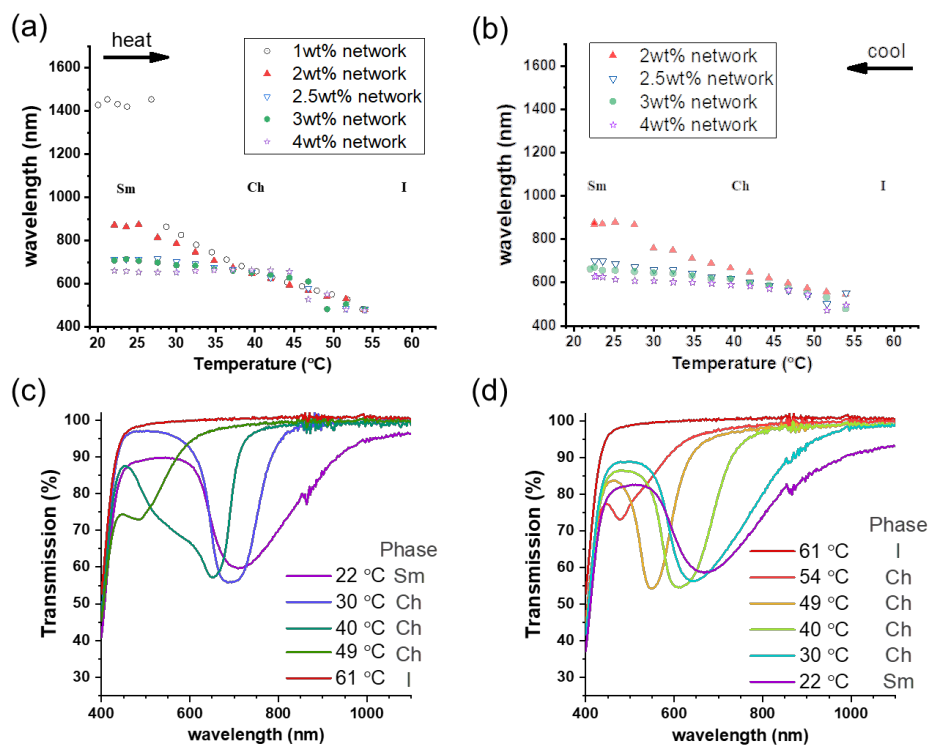


Figure 4.5 Thermo-chromic response of the CP10 coatings containing 1-4 wt% network. (a-b) Reflection band center wavelength during the first (a) heating and (b) cooling cycle between 22 °C (smectic) and 61 °C (isotropic). In (b), the data of the 1 wt% network coating is not shown due to strong scattering. (c-d) Transmission spectra of the fabricated coating with 3 wt% of network during the first (c) heating and (d) cooling cycle.

~1400 nm) at 22°C (smectic phase). However, after bringing it to the isotropic phase and cooling back to 22°C, the transparency of this film drops to 32% due to the scattering, indicating that 1 wt% of network is not enough to gain reversibility from the isotropic phase. Increasing the network content significantly improves the transparency of the coating after being cooled from isotropic, to 66%, 77%, 82% and 88% for 2, 2.5, 3 and 4 wt% of network, respectively.

Subsequently, we analyzed the temperature-responsive color change of these coatings by plotting the reflection band centers as a function of temperature (Figure 4.5a-b). In general, coatings containing 1-4 wt% of network show a continuous, reversible blueshift with increasing temperature within the cholesteric phase range due to the pre-transitional effect. For all coatings, the reflection wavelength reaches a minimum of ~480 nm (greenish-blue) at 54 °C, close to T_i . At 61 °C (above T_i) the reflection bands disappear. Dewetting in the isotropic phase was not observed in these samples. For 1 wt% of network the reflection bands became unrecognizable when cooled from isotropic due to irreversibility. For the other concentrations, upon cooling through the cholesteric temperature range the reflection centers red shift to 870, 690, 670, and 630 nm for 2, 2.5, 3 and 4 wt% of network, respectively. Below T_{sm-ch} , the reflection wavelength does not shift further. We propose that below the transition point, the LC layer is stable in a “twisted smectic A” structure (also known as the “twisted-grain-boundary” state)^[8,9,15], where the smectic A domains are twisted at the boundaries with their neighbors and maintain an overall helical structure. Based on this assumption, the decreased temperature response is most likely due to the suppressed pitch increase and smectic order formation by the network.

Although high transparency reversibility is obtained with 4 wt% network, its thermochromic response is limited so that obvious band shifts can only be observed above 45 °C. The coating with 2.5 wt% network has a similar thermochromic response as the one with 3 wt% but its transparency after the first temperature cycle is 10% less. Therefore, we consider 3 wt% of network as the optimal concentration for a good transparency and thermochromic responsiveness. It shows a reversible, full-color bandshift from ~480 nm (blue) to ~700 nm (close to infrared) from 54 to 20 °C, while keeping a transparency of 80% (Figure 4.5c-d). Compared to the cooling round, the reflection band during the heating round in the cholesteric temperature range (particularly 37-49 °C) is broader, and its band center shift is steeper at higher

Chapter 4

temperature. This hysteresis was also observed in the polymer-stabilized systems introduced in Chapter 3, which is believed to be generated by the network memory effect.

2.3. Application of the protective topcoat

On top of the network-stabilized coating layer of CP10 with 3 wt% the network monomer network we added a protective topcoat (Scheme 2) using Sylgard 184, a commercial silicone elastomer. The topcoat is about 17 μm thick as measured by interferometry. At room temperature (smectic phase), the resulting sandwiched coating presents a clear reflection band centered at ~ 700 nm.

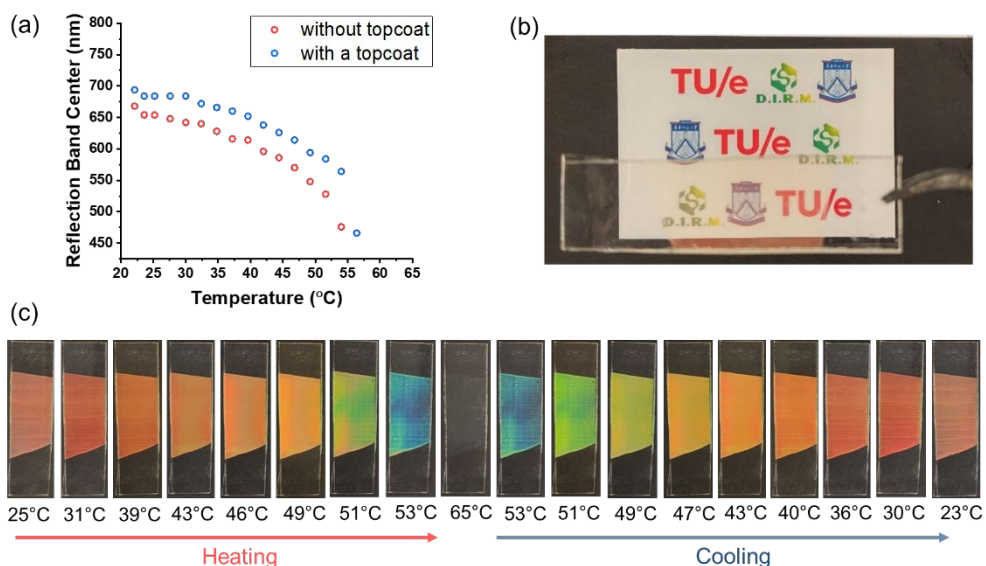


Figure 4.6 (a) Comparison of the reflection band shift of the 3 wt% network coating with and without topcoat. Data collected during the cooling round of the cycle. (b-c) Photographic images of the 3 wt% network coating with a topcoat (b) in front of a pictured background at a distance, and (c) on a black background during a temperature cycle to the isotropic phase.

The reflection band center of the coating with and without a topcoat has a similar trend of color change between 22 °C to 53 °C (Figure 4.6a), but the center wavelength position of the sample with a topcoat appears slightly redshifted (about 30 nm) compared to the sample without topcoat. We believe that this observation is caused by diffraction of the spectrometer light by the Sylgard topcoat and the corresponding

slight change of incident angle. The transparency remains at 80% after the cycle. As a control experiment, we fabricated the Siloxane-3wt% network coating material in an alignment cell and studied its thermochromic response. Similar to the topcoat, the cell configuration does not influence the temperature-response of the CLC material.

At room temperature, the coating shows a faded red color, due to a combination of reduced red reflection (the band is partially infrared) and minor scattering (Figure 4.6b). During heating, the coating shows a gradual thermochromic response, from 700 nm at room temperature (22 °C) to 480 nm (greenish-blue) at 53 °C, with various colors observed in between (Figure 4.6c). Upon entering the isotropic phase at 55 °C, the color disappears, and the coating becomes transparent. In the cooling round, the color reappears below T_i as greenish blue at 53 °C. The thermochromic response is reversed by cooling. When cooling back to 22 °C in the smectic phase, the faded-red color reappeared. The coating still has good transparency at room temperature after the full cycle. When the coating was cooled to room temperature from 50 °C, the

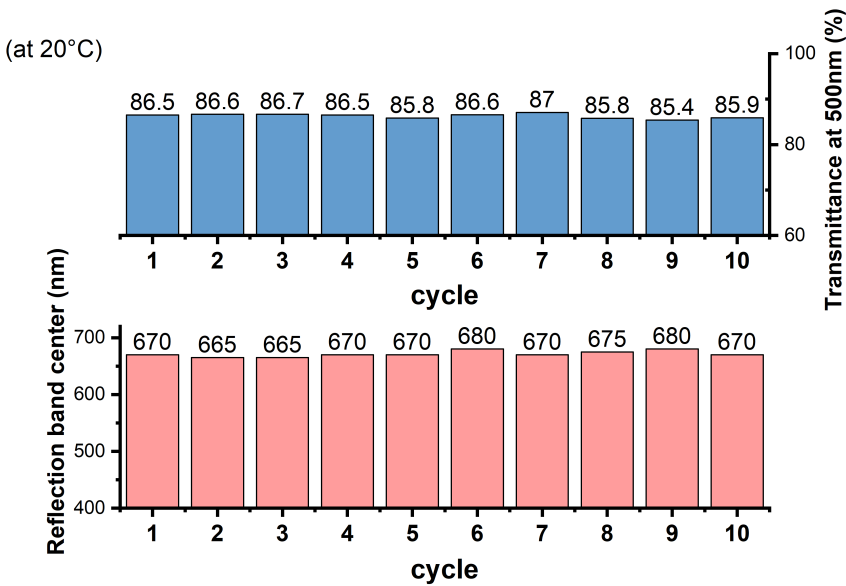


Figure 4.7 Transparency ($T\%$ at 500 nm) and reflection center wavelength of the CP10 - 3 wt% network coating with topcoat, at 20°C during 10 cycles of heating to isotropic and cooling to room temperature (the range was 20-65 °C for each cycle). Measurements started within 1 minute after the at target temperature was reached.

Chapter 4

original green color changed rapidly, and turned red within a minute, proving a fast responding speed.

Consistency in transparency and thermochromic response of the coating is confirmed after 10 heat-and-cool thermal cycles from room temperature to isotropic while measuring transmission spectra (Figure 4.7). At room temperature (20 °C) during each cycle, the 500 nm transmission is around 85%. Good consistency is seen in the reflection band centers too, with only small variations. The variation of band center position among cycles is probably due to the minor change of environmental temperature that could have impacted the actual sample temperature. Regardless of these variations, both transparencies and reflection centers at the same conditions were fluctuating only slightly over cycles and without drifting, which proves a long-term steadiness in performance.

After touching the coating with a finger several times, the color and surface of the coating area with Sylgard protection are intact (Figure 4.8). In contrast, on the area where the topcoat was removed visible fingerprints are observed, indicating a distorted surface. The Sylgard topcoat thus serves as a protective coating against surface damage.

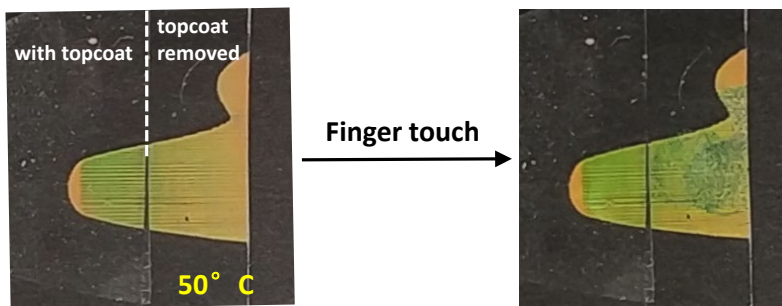


Figure 4.8 Images of the network stabilized coating with the topcoat partially removed before and after finger touching. The experiment was performed at 50 °C.

3. Conclusions

In this chapter is developed a facile approach to fabricate reversible temperature responsive CLC photonic coatings with a protective topcoat. A CLC oligosiloxane with a pre-transitional effect was successfully synthesized in one reaction step and blade-coated to obtain well-aligned CLC coatings. By adding a small amount of

crosslinked LC network, the alignment of the CLC phase is stabilized across phase transitions, at the cost of a bandshift range reduction. Through a systematic study, we optimized the network concentration and found 3 wt% to be optimal for the thermochromic response. The optimized coating shows a reversible reflection color change from ~700 nm at room temperature to ~480 nm at 54 °C, and its color is also reversible from the isotropic phase. The transparency of the coating is maintained over the entire temperature variation from smectic to cholesteric to isotropic.

A layer of PDMS elastomer (Sylgard) can be directly blade-coated on top of the CLC layer to obtain a protective topcoat. Due to this transparent PDMS topcoat, the coating receives proper protection against mechanical force, without losing device transparency. The thermochromic response of the LC layer is unaffected by this topcoat. We expect that other protective topcoats could also be applicable to this CLC system for different protective functions. The reflective coatings combine easy processability, coating robustness, and a fully reversible temperature response, making them appealing for a variety of applications.

4. Experimental

4.1. Synthesis of CP10

Materials. The monomers M1 and M2 were obtained from the experiments introduced in Chapter 3. Poly(methyl hydrogen siloxane) (PMHS), trimethylsilyl terminated, average $M_n \sim 390$, was purchased from Sigma-Aldrich. n_{avg} of the received PMHS was found to be 3.88 by NMR. Platinum(0)-1,3-divinyl-1,1,3,3-tetramethyldisiloxane (Karstedt's catalyst), 2% in xylene solution, was purchased from Sigma-Aldrich. Anhydrous toluene was purchased from Acros Organics.

Synthesis of CP10. 9.00 mmol of M1 and 1.00 mmol of M2 were combined in a Schlenk flask. 1026 μl of PMHS was added to the flask, in which the amount of Si-H bonds was approximately 8.50 mmol. The components in the flask were flushed continuously with argon. 15 mL of anhydrous toluene was injected under argon atmosphere to dissolve the reactants. One drop of Karstedt's catalyst was injected via syringe to start the reaction. The mixture was held at room temperature and terminated when NMR showed no residual Si-H groups at $\delta = 4.7$ ppm. The crude product was precipitated 3 times from toluene into cold methanol (-20 °C). After removal of the solvents in vacuum, the resulting solid was dissolved in toluene again,

Chapter 4

and 6.5g of silica gel metal scavengers (Si-Triamine, SilicaMetS, Silicycle Inc.) was added. This was followed by vigorous stirring overnight to remove the platinum catalyst from the product. The silica gel was removed through filtration and rinsed with toluene. The eluent that has turned colorless and was evaporated, yielding a white, viscous solid product. Yield: 2.92g, 78.6%.

$^1\text{H NMR}$ (400 MHz, CDCl_3) δ 8.10, 7.58, 7.52, 7.41, 7.35, 7.08, 6.91, 5.93, 3.99, 3.81, 2.06, 1.96, 1.79, 1.48, 1.41, 0.97, 0.56, 0.10, 0.05. The n_{avg} calculated according to Equation 4 is 6.52.

GPC (THF, detector: PDA254nm in polystyrene standards): $M_n = 3713\text{Da}$, $M_w = 4404\text{Da}$, $M_z = 5223\text{Da}$, $M_w/M_n = 1.186$.

Phase transitions (DSC) G -6 Sm 35 Ch 66 I.

4.2. Fabrication of coatings

Materials. The initiator Irgacure 184 was purchased from Ciba Specialty Chemicals Inc. The network monomer was purchased from Merck. Sylgard 184 was purchased from Dow Corning.

CLC coating mixture. In a tan glass vial was weighted CP10, the network monomer, and initiator in a weight ratio of 100-r : r : 0.05, in which $r = 1, 2, 2.5, 3, \text{ or } 4$. The network monomer and initiator were added into the mixture via diluted toluene solution in volumetric flasks. More toluene was then added, and the mixture was homogenized by stirring. The total solute comprises about 45 wt% of the mixture.

Topcoat mixture. In a vial was added Sylgard 184 base and the corresponding curing agent in an 8:1 weight ratio. The mixture was stirred vigorously to blend the components and was then degassed in vacuum at room temperature.

Preparation of rubbed polyimide coated glass substrates. Glass substrates of $3 \times 3 \text{ cm}^2$ size were prepared following a previously reported method.^[16] Those of $9 \times 9 \text{ cm}^2$ size were treated according to a similar procedure, but using a different spin coating rotation speed of 2000 rpm for 90 s.

Preparation of the coatings. An RK PrintCoat Instruments K control coater was used to prepare the coatings. Below is given an example of the fabrication procedure of a CP10 coating with a crosslinked network, and with a Sylgard topcoat:

On a $9 \times 9 \text{ cm}^2$ size glass substrate with rubbed polyimide was loaded $45 \mu\text{l}$ of the mixture, and it was placed at $100 \text{ }^\circ\text{C}$ for 40 min to evaporate the solvent. Then, the coating was applied using a $25 \mu\text{m}$ gap (4-sided applicator, ZFR 2040, Zehntner), which was pushed forward over the mixture automatically by the coater, at $60 \text{ }^\circ\text{C}$ on the substrate surface. The speed of the applicator movement was about 0.5 cm/s . The coating was then cooled down to $46 \text{ }^\circ\text{C}$ at the surface and was UV-cured using an EXFO Omnicure S2000 mercury lamp at an intensity of 20 mW/cm^2 for 10 min at $46 \text{ }^\circ\text{C}$ in a nitrogen environment. Afterwards, the coating was kept under nitrogen atmosphere at the same temperature for 30 min for post-curing. For application of the protective topcoat, the coating was transferred back to the coater. The freshly prepared Sylgard mixture was loaded onto the LC layer, and the layer was applied using a $60 \mu\text{m}$ gap (4-sided applicator, ZFR 2040.8030, Zehntner) at $44 \text{ }^\circ\text{C}$. The speed of the applicator movement was about 0.5 cm/s . After the application, the coating was kept at $44 \text{ }^\circ\text{C}$ for 24 h to cure the Sylgard and was then cooled to room temperature. The entire piece of coating was cut into several pieces for different tests using a glass cutter. The samples were annealed by a slow heat-cool process from room temperature to a maximum of $49 \text{ }^\circ\text{C}$ (CLC phase) prior to the tests. The heating and cooling rate of annealing was approximately $0.07 \text{ }^\circ\text{C/min}$.

For coatings without a Sylgard topcoat, the fabrication was finished by cooling the sample down to room temperature after the UV-curing step.

To prepare a coating without a network, a $3 \times 3 \text{ cm}^2$ glass substrate was used. CP10 was loaded on the substrate without the aid of solvents, and the coating was applied directly by the coater, using the same procedure as for the CLC layer described above. This procedure was assisted by other glass plates of equivalent thickness, as the applicator is larger in width than the substrate. Afterwards, the coating was brought to the pre-heated spectrophotometer immediately for transmission spectra measurements.

Preparation of the CLC cells. Cells were prepared by gluing together two $3 \times 3 \text{ cm}^2$ glass substrates with rubbed polyimide. The glue contained glass bead spacers of $10 \mu\text{m}$ diameter.

The cell containing CP10 was filled at $58 \text{ }^\circ\text{C}$ in the cholesteric phase. After filling the cell was brought to the pre-heated spectrophotometer immediately for transmission spectra measurements.

Chapter 4

The cell containing CP10 and 3 wt% of network monomers was filled in the CLC phase without solvent and UV-polymerized at 46 °C using the same conditions as for the coatings.

Characterization. Proton nuclear magnetic resonance (^1H NMR) spectra were recorded on a 400 MHz Bruker Avance III HD spectrometer. Gel permeation chromatography (GPC) was performed on a Shimadzu LC-2030C.3D instrument equipped with a PDA-254 nm detector, using tetrahydrofuran (THF) as the eluent and monodisperse polystyrene calibration standards. Differential scanning calorimetry (DSC) curves were measured with a DSC Q2000, TA Instruments. Polarizer microscopy (POM) images were taken on a Leica microscope DM2700 in transmission mode, equipped with crossed polarizers. Thicknesses of the coatings were examined using a Forogle Zoomsurf 3D interferometer.

Transmission spectra were performed in a PerkinElmer LAMBDA 750 UV/vis/NIR spectrophotometer with a 150 mm integrating sphere detector. Temperature control of the samples was realized via a Linkam THMS600 hot-stage with a customized aperture diameter of 6 mm. Heating and cooling of the hot-stage were programmed using a Linkam T96 controller.

Temperature calibrations. Temperature calibrations of the transmission spectra were performed using a Kane-May KM34O thermocouple with 1 °C precision. The temperature recorded on the surface of a blank glass plate mounted on the hot stage was considered as the actual temperature of the sample. When taking the photographic images, the temperatures were recorded simultaneously. For the transmission spectra, the temperature was pre-calibrated, resulting in a linear relationship between “the actual sample temperature (T_a , °C)” and “controller temperature setting (T_s , °C)”, as

$$T_a = 0.8014 T_s + 1.1203 \quad (R^2 = 0.9997, T_s > 30 \text{ }^\circ\text{C}) \quad \text{Equation 9}$$

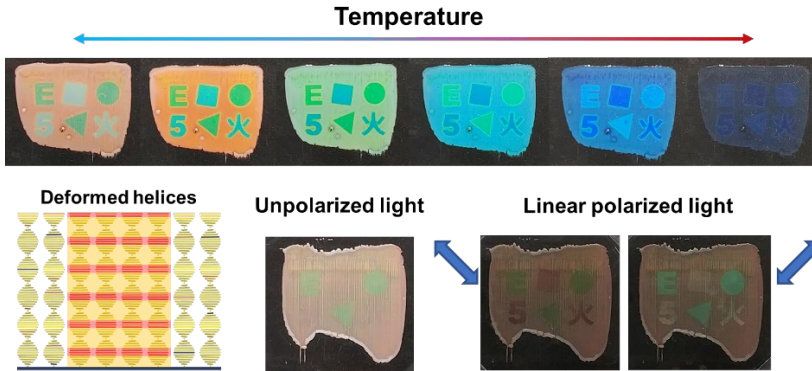
The actual temperatures of the samples were calculated from the controller setting using this formula. Nevertheless, due to the differences in calibration methods, and due to changes of the environmental temperature, 1~3 °C of difference in temperature designation among each test is expected.

5. References

- [1] A. Ranjkesh, T.-H. Yoon, *ACS Appl. Mater. Interfaces* **2019**, *11*, 26314.
- [2] H. Khandelwal, E. P. A. van Heeswijk, A. P. H. J. Schenning, M. G. Debije, *J. Mater. Chem. C* **2019**, *7*, 7395.
- [3] E. P. A. van Heeswijk, T. Meerman, J. de Heer, N. Grossiord, A. P. H. J. Schenning, *ACS Appl. Polym. Mater.* **2019**, *1*, 3407.
- [4] H. Zhou, H. Wang, H. Niu, A. Gestos, T. Lin, *Adv. Funct. Mater.* **2013**, *23*, 1664.
- [5] H. Wang, Y. Xue, J. Ding, L. Feng, X. Wang, T. Lin, *Angew. Chemie - Int. Ed.* **2011**, *50*, 11433.
- [6] D. Pyo, S. Ryu, K. U. Kyung, S. Yun, D. S. Kwon, *Appl. Phys. Lett.* **2018**, *112*, 061902.
- [7] H. Ringsdorf, A. Schneller, *Makromol. Chem., Rapid Commun.* **1982**, *3*, 557.
- [8] R. Dhar, *Phase Transitions* **2006**, *79*, 175.
- [9] M. Warren, M. Wilson, *Phys.Rev.E* **1998**, *57*, 5585.
- [10] F. Wang, H. Cao, K. Li, P. Song, X. Wu, H. Yang, *Colloids Surfaces A Physicochem. Eng. Asp.* **2012**, *410*, 31.
- [11] C. J. Tien, C. Y. Huang, Y. M. Kao, P. C. Yang, J. H. Liu, *Jpn. J. Appl. Phys.* **2009**, *48*, 071301.
- [12] J. Sun, H. Wang, L. Wang, H. Cao, H. Xie, X. Luo, J. Xiao, H. Ding, Z. Yang, H. Yang, *Smart Mater. Struct.* **2014**, *23*, 125038.
- [13] B. Zhang, X. Lin, Y. You, X. Hu, L. de Haan, W. Zhao, G. Zhou, D. Yuan, *Opt. Express* **2019**, *27*, 13516.
- [14] W. Huang, X. Zhang, J. Guo, L. Zhang, Z. Bian, D. Zhao, W. He, H. Cao, H. Yang, *Liq. Cryst.* **2009**, *36*, 497.
- [15] G. S. Chilaya, *Crystallogr. Reports* **2000**, *45*, 871.
- [16] A. J. J. Kragt, D. C. Hoekstra, S. Stallinga, D. J. Broer, A. P. H. J. Schenning, *Adv. Mater.* **2019**, *31*, 1903120.

Chapter 5

Thermochromic multicolored photonic coatings with linear polarized light dependent features



This chapter presents a thermochromic coating with light polarization dependent multiple structural colors by using a polymer stabilized cholesteric liquid crystal siloxane oligomer. Since the structural color change can be manipulated by the polymerization temperature, thermochromic multicolor patterns can be made via photomasks. The temperature response depends on the color and in case of a red color a maximal reversible reflection change from red to blue between 20°C and 56°C is obtained. On top of that, by using a dichroic photo-initiator and linear polarized UV light, linear polarized light dependency of the coating is obtained, too, showing different reflection colors varying the incident light polarization angles. A multicolor, thermochromic photonic coating with light polarization and structural color dependent features is therefore demonstrated.

This chapter is partially reproduced from: Zhang, W.; Kragt, S.; Schenning, A. P. H. J.; De Haan, L. T.; Zhou, G. Patternable thermochromic photonic coatings with light polarization dependencies. *Adv. Mater. Interfaces* (submitted).

1. Introduction

Multi-structural color patterns^[1-3] as well as light-polarization dependent color^[4,5] are present in many biology species. Inspired by nature, researches on helicoidal structures are dedicated to creating colorful patterns.^[6-11] So far, the scientific challenge remains to fabricate temperature responsive reflective color (TR-RC, or thermochromic) coatings with multi-color patterns from such materials. Patterned coatings have previously been created by photo-crosslinking oligomeric CLC precursors at different temperatures using photomasks^[12], or by painting CLC polymer particles of different colors^[13]. The latter example even presents an irreversible color shift by heating. However, the combined features of reversible thermochromic shift with multi-color patterns into one CLC coating remains a difficulty, as the mesogens mobility required for a reversible response can be easily lost by the addition of network which determines different colors.^[14] Although the printing of encapsulated CLC droplets of various ingredients might be viable ^[15,16] it would be more convenient if the thermal responses can be manipulated within a single formulation. Besides patterning, advanced optical effects such as linear polarized light (LPL) dependent color of CLC by deforming the circular helices into elliptical shapes, ^[17-21] would be appealing. A recent work of chemically deformed CLC coatings using achiral oligosiloxane LCs and chiral network monomers (>15wt%) feature in reflection color dependency of LPL with patternability, but is not thermochromic.^[19]

In this chapter a thermochromic patternable coating with a PSLC molecular system modified from Chapter 4 is presented. The smectic-cholesteric type CLC siloxane oligomer CP12 is stabilized by 4wt% of diacrylate LC network. Structural colored patterns can be made via polymerization at different temperatures using photomasks, and a three-color patterned coating was fabricated for demonstration. When heated, each color has its own temperature onset which causes the initially multicolored coating to become a single color at higher temperatures. In addition, linearly polarized light dependency can be obtained, and these stratified thermochromic coatings show changing colors when altering the polarization angles of incident LPL. We created a stratified two-color patterned coating for demonstration of its potential towards aesthetics and security applications.

2. Results and discussion

2.1. Thermochromic and multi-color pattern coatings

Mixtures containing an oligosiloxane CLC and a diacrylate LC monomer were prepared for the fabrication of thermochromic, multi-color patterned coatings (Figure 5.1a). The siloxane random co-oligomer of mesogenic (P1) and chiral dopant (P2) was synthesized according to the method introduced in Chapter 4. The molar ratio of P1/P2 is adjusted to be 88/12 in order to cover the full visible color range of response. The average backbone length is found to be approximately 6 (calculated from NMR), with a polydispersity of 1.21 (data from GPC). The oligomer undergoes a CLC-isotropic transition (T_i) at 65°C, a smectic-cholesteric transition (T_{sm-ch}) around 40°C, and a glass transition (T_g) around -2°C. When brought into a planar alignment cell, thermochromic behavior can be observed within the CLC temperature range due to the smectic-cholesteric transitional effect.

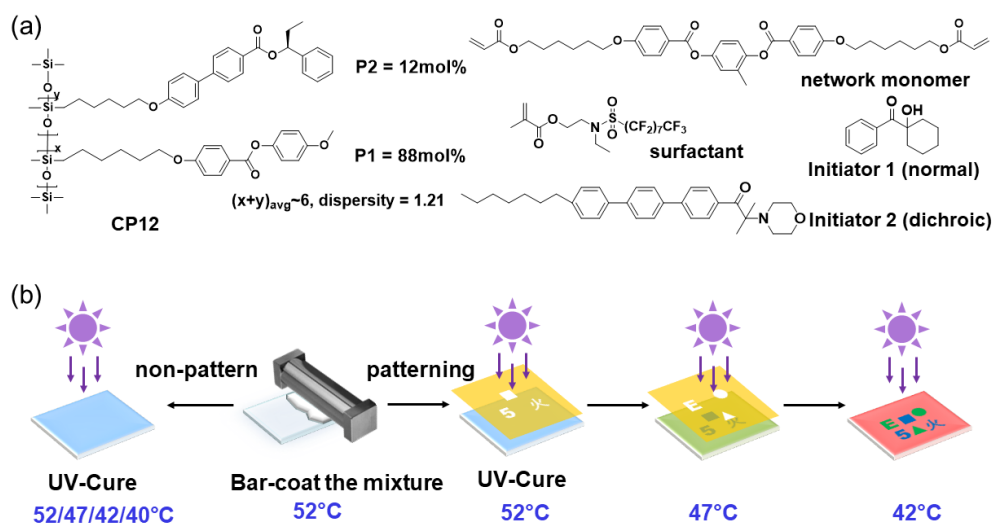


Figure 5.1 (a) Components used in the coating formulations. (b) Fabrication scheme of the patterned responsive photonic coating using initiator 1.

We chose the optimized network ratio of 4wt% referring to the amount of diacrylate LC in the mixture, to prepare thermochromic photonic coatings. Furthermore, 1 wt% of methacrylate surfactant was added to the mixture to assist planar cholesteric alignment of the coating at the coating-air interface, as well as 0.4 wt% of

Chapter 5

photoinitiator 1 to initiate network formation. Upon bar-coating the mixture at 52 °C on a glass substrate with a rubbed polyimide layer, a planarly aligned cholesteric coating was obtained. The smectic-cholesteric thermochromic response of the oligomer remains, showing blue (470 nm), green (520 nm), orange (585 nm), and red (630 nm) reflection at 52, 47, 42, and 40°C, respectively (Figure 5.1b). Via subsequent polymerization of the diacrylate LC monomer under UV light irradiation at these temperatures, polymer stabilized CLC coatings are formed. We initially prepared individual single-color coatings cured at 52, 47, 42, and 40°C, respectively, in order to investigate the thermochromic response of the different structural colors.

At room temperature (RT), the polymer stabilized CLC coating appears blue, green, orange and red, respectively (Figure 5.2b). The slight scattering at room temperature can therefore be explained by the formation of smectic domains. A slightly longer reflection wavelength than the uncured state is observed on spectra, due to the broader shape of the reflection bands (Figure 5.2a). This might be due to a certain degree of phase separation between the siloxane oligomer and the network.^[22] DSC of the cured coatings all reveal isotropic transition peak around 63 °C and smectic-cholesteric transitions around 39 °C, regardless of the curing temperature.

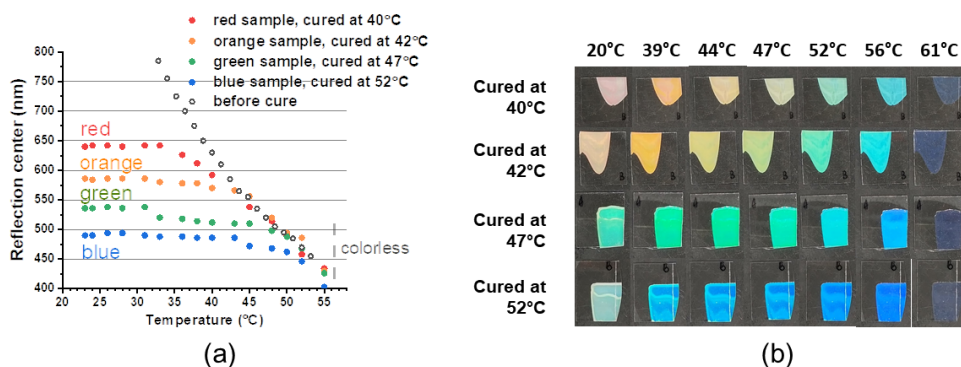


Figure 5.2 (a) Reflection center versus temperature of the coatings cured at 40, 42, 47, and 52°C during cooling, including a comparison to the uncured mixture. Slight variation in central wavelength among the samples at the same temperature is expected, as the actual temperature during each test might deviate slightly from calibration. (b) Images of the cured coatings at different temperatures during cooling.

Heating and cooling cycles were performed on these coatings to examine their thermochromic responses. Cycles between 20°C (smectic) and 61 °C (isotropic) demonstrate fully reversible thermochromic shift of these coatings, with each structural color showing its own unique thermochromic responsiveness (Figure 5.2a). For convenience, we first discuss the cooling cycles. When cooling from 61 °C (isotropic) to 55 °C (cholesteric), a reflection band appears centered at 402-440 nm (blue) for all these samples. Therefore, the planar cholesteric alignment is not lost due to the memory of the liquid crystal network. When the samples are further cooled the reflection color redshifts, following the same response as the uncured mixture until reaching the according curing temperatures. Below that temperature, the shift versus temperature slows down and stops at some point, except for the red sample, which starts to slow down at 42°C and only stops below 35 °C (Figure 5.2a). Below 35 °C entering the smectic phase, no further response of band center is observed but an increase in scattering does take place, thus sealing the plateau of color shift at blue, green, orange and red respectively. Interestingly the RT-red sample that was cured at 40°C has the largest color change (~210 nm) changing from red to blue, while the RT-blue sample cured at 52°C, the range is the smallest (~90nm, light blue to deep blue). During heating, the reverse thermochromic response is observed, reaching a blue reflection at 54°C and disappearance of color when heated further. However, the major bandshift starts later than the curing temperature and has a steeper trend near 54°C. This hysteresis is typical for polymer-stabilized liquid crystals having a smectic-cholesteric phase transition as was also discussed in Chapter 4.

It is interesting that the reflection band shifts of these thermochromic coatings are stopping at higher temperature than the smectic transition point. In contrast, when using a lower network concentration (2wt%), the limit occurs at the smectic transition and when cured at 47°C, the highest reflection wavelength is at 612nm which is over 520nm. It can be surmised that the higher density of network generates a stronger anchoring effect^[23] to the mesogens that pushes the stopping temperature higher. Furthermore, it is beneficial to polymerize the cholesteric sample at temperature that is not too close to the isotropic temperature to obtain a large color change.

Chapter 5

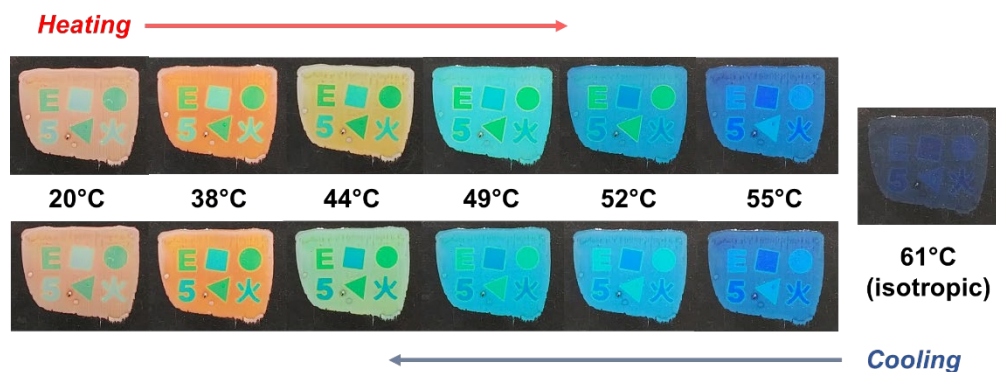


Figure 5.3 Images of the patterned coating at various temperatures during heating and cooling between 20°C and 61°C.

Thermochromic color patterns are created via polymerization at different temperatures using photomasks (Figure 5.1b). The photomasks were made from polyimide tape (Kapton) via laser-cutting. The RT-blue patterns were fabricated at 52°C using a mask containing “square”, “5” and “fire (in Chinese)” shapes, while the RT-green patterns were created at 47°C using a mask having “circle”, “triangle” and “E” shapes. Finally, the RT-red background was polymerized at 40 °C to receive a 3-color pattern at room temperature (Figure 5.3). Upon increasing the temperature, the RT-red background changes color around 40 °C, while the RT-green and the RT-blue patterns retain their colors until the steep blueshift above 52 °C due to the hysteresis. At 55 °C, just below the isotropic transition temperature, the background and the patterns appear in blue colors of different shades. Upon reaching the isotropic temperature at 61 °C, the patterns turn mostly colorless with a slight purple reflection, which is assumed to originate from the polymer network mesogens. The colors reappear with cooling from the isotropic, and the reversed thermochromic response of “square-5-fire”, “circle-triangle-E”, and the background is observed, until they settle in blue, green, and red at 52°C, 47°C, and 35°C, respectively. The thermochromic response in each part of the patterned coating’s different areas is identical to the corresponding non-patterned coatings.

2.2. Thermochromic patterns with light polarization dependent color

We introduced LPL dependency features to our photonic coating by stratification using dichroic initiator 2 following our earlier reported method.^[19] The dichroic initiator aligns with the liquid crystal molecules and preferentially absorbs light with a polarization direction parallel to its molecular orientation (Figure 5.4). As a result, when irradiated by linear polarized UV, polymerization is initiated in the regions with the same molecular alignment director as the light polarization, which is every half a pitch length. The diacrylate network monomers are polymerized in these initiated regions, causing a diffusion of monomers from the non-initiated regions. The stratification process distorts the helical structures by local variation of the concentration of chiral molecules, and forms alternating layers of network-rich and network-poor moieties with different refractive indices along the thickness.

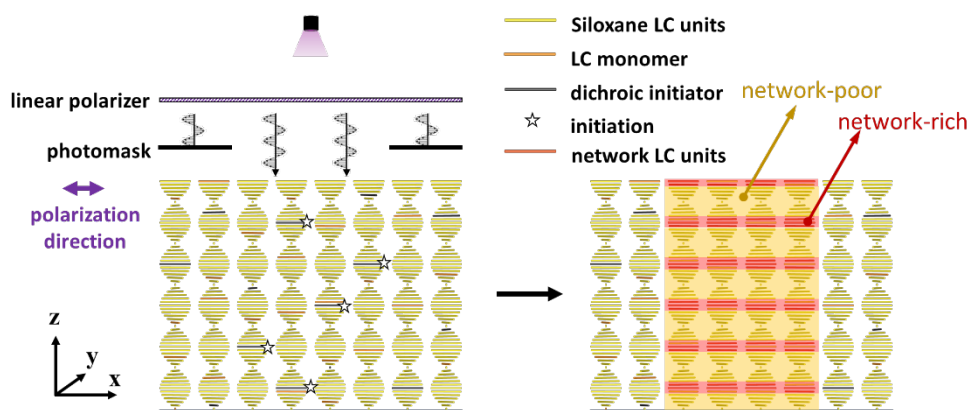


Figure 5.4 Schematic presentation of the stratification process on CLCs, for the fabrication of patterned thermochromic coatings with LPL dependency. Only the areas exposed to linear polarized UV light are stratified, whereas the nonexposed areas maintain a regular chiral nematic helix.

The coating was polymerized with linearly polarized UV light with the polarization direction perpendicular to the coating direction, which from this point on is defined as $0^\circ/180^\circ$ (Figure 5.5a). When stratified at 42°C , a red reflecting coating is obtained at room temperature. The unpolarized transmission spectrum of the coating demonstrates an asymmetric reflection band centered at 600 nm with a minor second peak at 650 nm (Figure 5.5b). Compared to the symmetric reflection band of the non-

Chapter 5

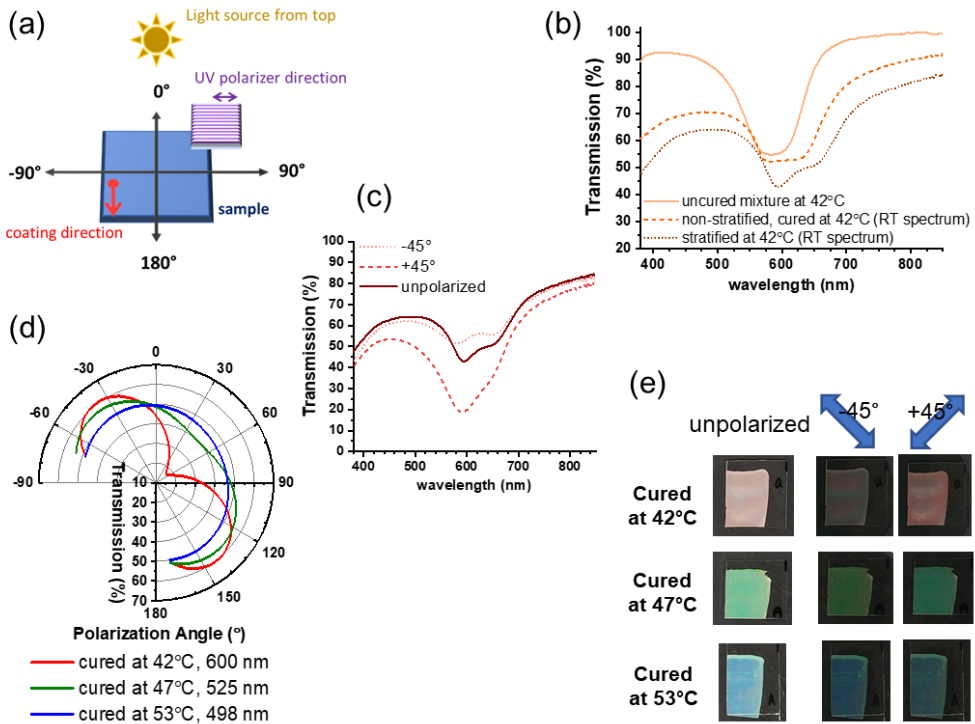


Figure 5.5 (a) Designation of linear polarization angles in the article, defining the direction of coating as 0°/180°, and the UV light polarizer as 90°, when observed from the same side as the light source. (b) Comparison of reflection band shape between the stratified and unstratified coatings cured at 42°C (spectra were recorded at 20°C). The spectrum of the uncured mixture at 42°C is also plotted as a reference. (c) LPL dependent transmission spectra of the stratified coating cured at 42°C in the characteristic angles of -45° and +45°, along with the unpolarized spectra at RT. (d) Polar plots of the transmission at the reflection band center wavelength of the stratified coatings cured at 42, 47, and 53°C, at room temperature. (e) Images of the stratified coatings at room temperature under unpolarized light, linear polarized light at -45° and +45°.

stratified sample cured at the same temperature, this asymmetric reflection band is broader and inclined to higher wavelength (Figure 5.5b), and therefore, its color at RT appears to be red. Linearly polarized light transmission of 600 nm at varied polarization angles shows a “peanut shaped” polar plot (Figure 5.5d, red curve). Transmission at -45° is highest (60%), while at +45° transmission is the lowest (17%). The brightness contrast is clearly seen in photographic images under a linear polarizer, at the directions of -45° and +45° (Figure 5.5e). Apart from the brightness, the reflection color also slightly changes with polarization angle, due to the changed

ratios of reflection band intensity between the two edges of the reflection band (Figure 5c). RT-green and RT-blue samples were successfully prepared as well, via stratification at 47 °C and 53 °C (Figure 5e), where the uncured mixture appears in green and blue reflection, respectively. The reflection center at RT by unpolarized spectra are observed at 525 and 498 nm, respectively. However, the LPL angle dependencies of in these samples are less prominent compared to the red sample (Figure 5.5d). The lowest and highest transmissions of the green coating at its reflection center are 40% and 57%, respectively, whereas for the blue coating this is only 46% and 50%, respectively. The LPL angular contrast of the RT-green sample is minor and that of the RT-blue sample is hardly distinguishable by naked eye (Figure 5.5e). The angles showing the darkest and brightest reflection are still -45° and $+45^\circ$, respectively. We propose that proper stratification is more difficult to achieve for shorter pitches due to a shorter diffusion distance. As the distance between two initiated regions becomes shorter, less monomers are present within half a pitch, and thus the gradient of network concentration is less between network-rich and network-poor regions, resulting in a reduced LPL dependency.

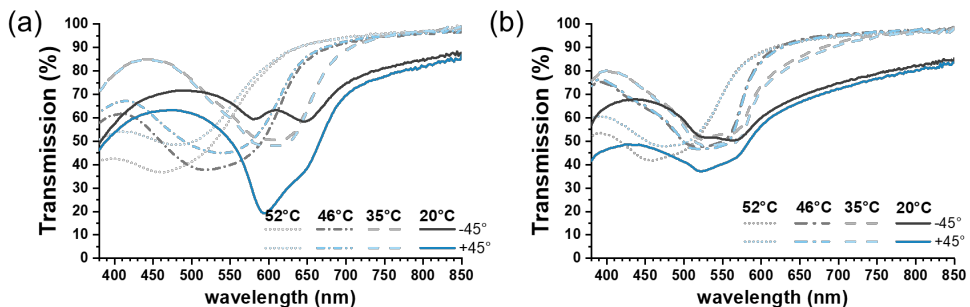


Figure 5.6 LPL dependent transmission spectra (at -45° and $+45^\circ$) of the stratified coatings cured at 42°C (a) and 47°C (b), collected at various temperatures during a cooling from the isotropic phase.

The stratified coatings present a similar type of thermochromic response compared to the unstratified coatings when viewed with unpolarized light. Major reflection band shifts start above their curing temperatures, and they are fully reversible upon cooling from isotropic. We investigated the LPL dependency at elevated temperatures as well (Figure 5.6). It is found that the LPL dependency of the RT-red and RT-green samples diminishes at temperatures higher than 35 °C, but fully recovers when cooled

Chapter 5

to room temperature. The temperature at which LPL dependency disappears is around the smectic-cholesteric transition of the coating. Therefore, it can be inferred that the LPL dependency is highly related to the smectic transition, in which smectic clusters are formed along the anisotropic direction of the network, extending the deformed areas in the helices.

A patterned coating with stratified structures was fabricated using the combination of a linear UV light polarizer and photomasks. The patterns of “circle”, “triangle” and “E” were exposed at 47 °C (green color) with LP UV light, then the patterns of “square”, “5” and “fire” were exposed at 42 °C (red color) with LP UV light, and finally the background area was cured at 42 °C with unpolarized UV (Figure 5.7a). As the “square-5-fire” patterns were cured at the same temperature as the background,

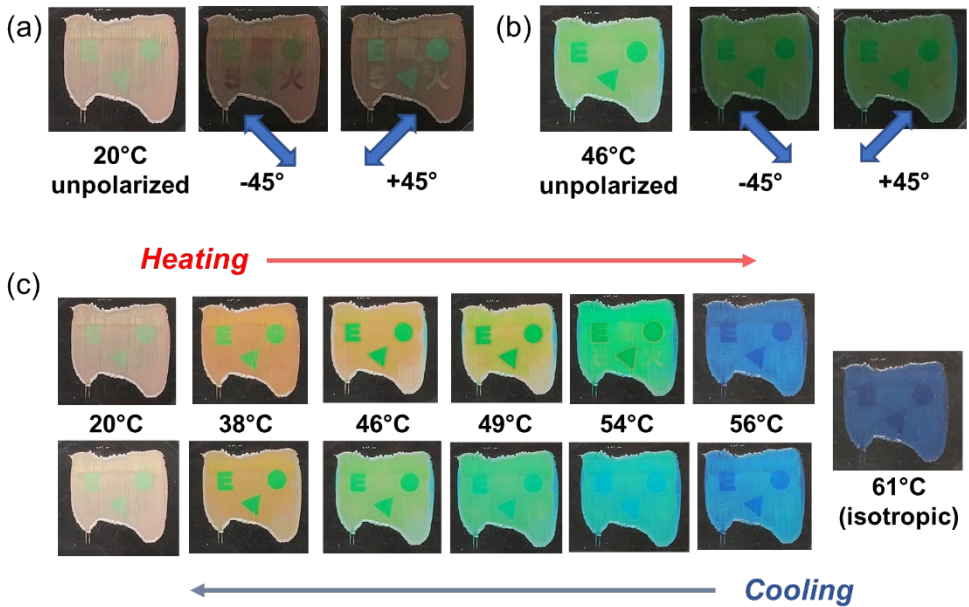


Figure 5.7 Images of the stratified patterned coating, showing (a) red-and-green patterns at room temperature. The red patterns which were stratified are hidden into the unstratified background of the same color under unpolarized light, and reveal under a linear polarizer. Both the stratified red and green patterns show variation in optics with rotating polarization angle, between the darkest reflection angle of -45° and the brightest reflection angle of $+45^\circ$. (b) at elevated temperature (46°C), the angular dependency of the patterns is diminished. The hidden pattern is therefore not clearly revealed with a polarizer. (c) Thermochromic response of the coating at various temperatures during heating and cooling between 20°C and 61°C , under unpolarized light.

these patterns have almost the same color as the background and are therefore hidden with unpolarized light. The hidden red patterns can be clearly revealed under a linear polarizer due to the contrast in color and brightness against the unstratified background. Both the RT-red and RT-green patterns show various shades of colors when rotating the LPL direction between -45° and $+45^\circ$, in good resolution. At elevated temperatures where thermochromic shifts take place, the LPL dependency of both patterns is largely weakened, and the “square-5-fire patterns” are not clearly revealed by LPL anymore (Figure 5.7b).

The coating shows diverse thermochromic response for the different colored patterns, in the same way as the unstratified coatings (Figure 5.7c). Throughout the cycle, the RT-red patterns remained almost invisible under unpolarized light, proving the highly similar thermochromic response between stratified and unstratified parts. In particular, at 54°C during cooling, all 3 parts show a uniform shade of blue color, and therefore, all patterns are hidden. This is different from the unstratified patterns (Figure 5.3). We attribute this phenomenon to the broader reflection bands after stratification, which reflection colors are more impure to be distinguished among different shades. As the hidden patterns could only be clearly revealed under a linear polarizer at room temperature, an interesting scenario of interactive art and information encryption by this patterned sample is therefore presented.

3. Conclusion

In this work are developed thermochromic photonic coating devices that combine features of facile processing, fast response, full reversibility, patternability, and LPL dependent colors. By performing polymerizations at different temperatures ($40\text{-}52^\circ\text{C}$) various reflection colors from red to blue can be obtained. A three-color patterned coating could be prepared by photomasked polymerization at three temperatures. The initially multicolored coating becomes blue at higher temperatures, with each color shifting in sequence instead of all colors shifting simultaneously. Linear polarization dependent color can be achieved using a dichroic photoinitiator in the mixture and cure with LP UV light. The deformed helical structures obtained through this stratification process present color and brightness contrasts of reflection at room temperature when viewed with LPL between the polarization angles of -45° and $+45^\circ$. The LPL dependency mostly disappears at elevated temperatures, but this is fully reversible. In addition, the thermochromic responsiveness of the stratified coatings

Chapter 5

under unpolarized light is identical to the unstratified coatings polymerized at the same temperature, and they are patternable as well. We demonstrate an encrypted coating with some stratified patterns hidden into the unstratified background when viewed with unpolarized light at any temperature. The patterns are only revealed when viewed with LPL at room temperature. These easily-processable, multi-functional coatings would be of interest for products in aesthetics or security purposes. Protective topcoats are feasible upon this CLC coating to enhance mechanical strength of the devices.^[24,25]

4. Experimental

Materials. The network monomer was purchased from Merck. The initiator 1 (Irgacure 184) was purchased from Ciba Specialty Chemicals Inc. The dichroic photoinitiator, (1-(4''-heptyl-[1,1':4',1''-terphenyl]-4-yl)-2-methyl-2-morpholinopropan-1-one), was obtained from Merck. The surfactant, (2-(N-ethylperfluorooctanesulfonamide) ethyl methacrylate), was purchased from Acros. The polyimide Optmer AL 1051 or alternatively, AL 1254, were purchased from JSR Micro.

Synthesis. The cholesteric CP12 was synthesized following the methods in Chapter 4. The feed ratio of P1/P2 precursors in the reaction was adjusted to be 88/12 in mol.

Yield: 3.2192g, 69.2%.

¹H NMR (400 MHz, CDCl₃) δ 8.10, 7.59, 7.52, 7.41, 7.35, 7.28, 7.08, 6.91, 5.93, 3.99, 3.81, 2.07, 1.96, 1.79, 1.48, 1.45, 1.41, 0.97, 0.56, 0.11, 0.05. The average backbone length $(x+y)_{\text{avg}}$ calculated from NMR peak integrals was 6.0 according to Equation 4 ($r = 0$).

GPC (THF, detector: PDA254nm in polystyrene standards): $M_n = 3534\text{Da}$, $M_w = 4295\text{Da}$, $M_z = 5173\text{Da}$, $M_w/M_n = 1.21$.

Phase transitions of CP12 revealed by DSC: G -2 Sm 39.7 Ch 64.9 I.

Preparation of CLC mixtures. In a tan glass vial was weighted the components of CP12 and network monomers. The surfactant and the initiator were then added into the mixture via diluted toluene solution in volumetric flasks. More toluene was added

to dissolve all the components homogeneously. The total solute comprises about 45 wt% of the mixture.

The composition for non-stratified coatings is: CP12/network monomer/surfactant/initiator 1 = 94.6/4/1/0.4, in weight ratio. The initiator 1 ratio in the mixture is lowered to be 0.04 for the patterned, non-stratified coatings.

The composition for stratification is: CP12/network monomer/surfactant/initiator 2 = 94/4/1/1, in weight ratio.

Preparation of rubbed polyimide-coated glass substrates. The glass substrates are of 9×9 cm² size, and the procedure of applying a polyimide layer follows the exact method as the previous literature.^[19]

Preparation of the coatings. An RK PrintCoat Instruments K control coater was used to prepare all coatings. The example of non-stratified, non-patterned coatings is given below: On a 9×9 cm² size glass substrate with rubbed polyimide was loaded 60 μ l of the mixture, and the was placed at 100 °C for 40 min to evaporate the solvent. Afterwards, the substrate was transported to the pre-heated coater, at 52°C on the substrate surface. The coating was applied using a 60 μ m gap (4-sided applicator, 1107/80/1, Sheen), which was pushed forward over the mixture automatically by the coater. The speed of the applicator movement was about 0.5 cm/s, at the direction anti-parallel to the rubbing direction of the polyimide layer. The coating was then cooled down to the desired temperature (recorded at the substrate surface) and was UV-cured using an EXFO Omnicure S2000 mercury lamp at an intensity of 4.5 mW/cm² (unpolarized) for 1 min in nitrogen environment, followed by post-curing for 4min. The coating was let cooled to room temperature. The entire piece of coating was cut into several pieces for different tests, using a glass cutter. All optical measurements including photos of the coatings were started from the second cycle of heating-and-cooling between 20°C and 61°C.

For the stratification process, a high contrast linear polarizer (PUVD260C35S from LOT- QuantumDesign GmbH) was placed between coating and the UV light source during the curing. The polarization direction was perpendicular to the coating direction (Figure 5.5b). The intensity of polarized UV light that reaches the coating surface was ~ 1.5 mW/cm².

Chapter 5

For the patterned coatings, a photomask was placed above the coating during each temperature-stage of UV curing (Figure 5.1b). The photomasks were made by a commercial polyimide tape (Kapton) clung on glasses, and were laser-cut into different patterns. To avoid direct contact to the coating surface, the photomask was attached with the glass substrate using double-sided tapes, which thickness is higher but very close to the coating thickness.

The thickness of all received coatings are 22-27 μm as determined by interferometry.

Characterizations. Proton nuclear magnetic resonance (^1H NMR) spectra were recorded on a 400 MHz Bruker Avance III HD spectrometer. Gel permeation chromatography (GPC) was performed on a Shimadzu LC-2030C.3D instrument equipped with a PDA-254 nm detector, using tetrahydrofuran (THF) as the eluent and monodisperse polystyrene calibration standards. Differential scanning calorimetry (DSC) curves were measured with a DSC Q2000, TA Instruments. Thicknesses of the coatings were examined using a Forgalé Zoomsurf 3D interferometer.

Transmission spectra of unpolarized light were performed in a PerkinElmer LAMBDA 750 UV/vis/NIR spectrophotometer with a 150 mm integrating sphere detector. Temperature control of the samples was realized via a Linkam THMS600 hot-stage with a customized aperture diameter of 6 mm. Heating and cooling of the hot-stage were programmed using a Linkam T96 controller. For linear polarized light transmission spectra and the polar plots, a linear polarizer is equipped in the spectrometer.

Temperature calibrations for transmission spectra and the photographs follows the methods as Chapter 4.

5. References

- [1] C. P. Barrera-Patiño, J. D. Vollet-Filho, R. G. Teixeira-Rosa, H. P. Quiroz, A. Dussan, N. M. Inada, V. S. Bagnato, R. R. Rey-González, *Sci. Rep.* **2020**, *10*, 1.
- [2] E. R. Dufresne, H. Noh, V. Saranathan, S. G. J. Mochrie, H. Cao, R. O. Prum, *Soft Matter* **2009**, *5*, 1792.
- [3] S. Yoshioka, S. Kinoshita, *Forma* **2002**, *17*, 169.
- [4] V. Sharma, M. Crne, J. O. Park, M. Srinivasarao, *Science*. **2009**, *325*, 449.
- [5] L. Fernández Del Río, H. Arwin, K. Järrendahl, *Thin Solid Films* **2014**, *571*, 410.
- [6] P. Wu, J. Wang, L. Jiang, *Mater. Horizons* **2020**, *7*, 338.
- [7] J. Yang, W. Zhao, Z. Yang, W. He, J. Wang, T. Ikeda, L. Jiang, *J. Mater. Chem. C* **2019**, *7*, 13764.

- [8] J. Yang, W. Zhao, Z. Yang, W. He, J. Wang, T. Ikeda, L. Jiang, *ACS Appl. Mater. Interfaces* **2019**, *11*, 46124.
- [9] L. Qin, J. Wei, Y. Yu, *Adv. Opt. Mater.* **2019**, *7*, 1.
- [10] H. Wan, X. Li, L. Zhang, X. Li, P. Liu, Z. Jiang, Z. Z. Yu, *ACS Appl. Mater. Interfaces* **2018**, *10*, 5918.
- [11] M. Anyfantakis, V. S. R. Jampani, R. Kizhakidathazhath, B. P. Binks, J. P. F. Lagerwall, *Angew. Chemie - Int. Ed.* **2020**, *59*, 19260.
- [12] P. Zhang, A. J. J. Kragt, A. P. H. J. Schenning, L. T. De Haan, G. Zhou, *J. Mater. Chem. C* **2018**, *6*, 7184.
- [13] A. Belmonte, M. Pilz da Cunha, K. Nickmans, A. P. H. J. Schenning, *Adv. Opt. Mater.* **2020**, *8*, 2000054.
- [14] B. Zhang, X. Lin, Y. You, X. Hu, L. de Haan, W. Zhao, G. Zhou, D. Yuan, *Opt. Express* **2019**, *27*, 13516.
- [15] S. S. Lee, J. Bin Kim, Y. H. Kim, S. H. Kim, *Sci. Adv.* **2018**, *4*, eaat8276.
- [16] C. Yang, B. Wu, J. Ruan, P. Zhao, L. Chen, D. Chen, F. Ye, *Adv. Mater.* **2021**, 2006361.
- [17] P. Zhang, G. Zhou, L. T. de Haan, A. P. H. J. Schenning, *Adv. Funct. Mater.* **2021**, *31*, 2007887.
- [18] C. Bourgerette, C. Bin, H. Finkelmann, M. Mitov, J. Schmidtke, W. Stille, *Macromolecules* **2006**, *39*, 8163.
- [19] A. J. J. Kragt, D. C. Hoekstra, S. Stallinga, D. J. Broer, A. P. H. J. Schenning, *Adv. Mater.* **2019**, *31*, 1903120.
- [20] D. J. Broer, *Curr. Opin. Solid State Mater. Sci.* **2002**, *6*, 553.
- [21] B. Serrano-Ramón, C. Kjellander, S. Zakerhamidi, C. W. M. Bastiaansen, D. J. Broer, *Emerg. Liq. Cryst. Technol. III* **2008**, *6911*, 691109.
- [22] I. Dierking, L. L. Kosbar, A. C. Lowe, G. A. Held, *Liq. Cryst.* **1998**, *24*, 387.
- [23] X. Yuan, L. Zhang, H. Yang, *Liq. Cryst.* **2010**, *37*, 445.
- [24] S. P. W. Govers, N. Alexander, M. Al-Masri, J. Omeis, L. G. J. van der Ven, G. de With, A. C. C. Esteves, *Prog. Org. Coatings* **2021**, *150*, 105991.
- [25] “RepelFlex® – NBD Nano,” can be found under <https://www.nbdnano.com/solutions/coatings/repelflex/>, accessed: April 2021.

Chapter 6

Technology assessment

The technology of the temperature responsive siloxane coating is assessed. The materials are promising before applications such as infrared smart windows, interactive decoration, security labels, and smart packaging. The advantage as well as challenges are discussed, and possible improvements are proposed.

This chapter is partially reproduced from: Zhang, W.; Froyen, A. A. F.; Schenning, A. P. H. J.; Zhou, G.; Debije, M. G.; de Haan, L. T. Temperature-Responsive Photonic Devices Based on Cholesteric Liquid Crystals. *Adv. Photonics Res.* **2021**, 2 (7), 2100016.

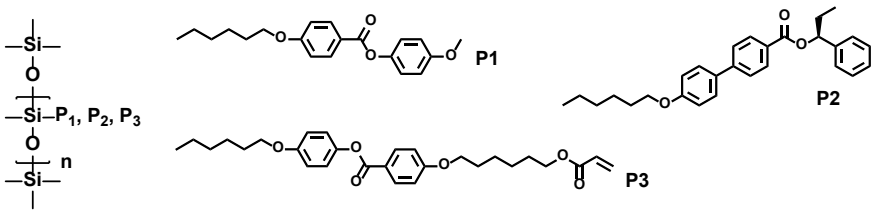
Chapter 6

1. Introduction

The previous chapters have shown the evolution of siloxane-based CLC materials to become easily-processable, stable, temperature responsive photonic coatings. Chapter 2 exhibits the proof of concept that such materials are processible as well-aligned photonic coatings and present temperature responsive reflective color (TR-RC, or thermochromic) behavior as coatings, which is the cornerstone of this thesis. In Chapter 3, crosslinkable units are introduced into the siloxane CLC material in the attempt to produce a much more stable coating with a partially crosslinked, entirely polymeric molecular system. It was proven that with a crosslinked network, siloxane CLCs could still retain a decent temperature response. However, the synthesis and fabrication of the coating is complex and the TR-RC is not fully reversible. In Chapter 4, an alternative PSLC system is adopted in which crosslinked network and the CLC siloxanes are not bonded. Siloxane synthesis is therefore easier, and most importantly the ratio of network in the system can be precisely controlled via monomer dosage. Finally, an optimal network ratio is found where the coating retains a proper TR-RC while gaining full reversibility, fast response speed, and long-term stability. In addition, it is shown that an elastomeric topcoat can be directly applied on top of the PSLC to serve as a good protective layer, which would be beneficial for applications development. Chapter 5 enriches the optical responsiveness of the PSLC system described in Chapter 4, revealing that the reflection color shifting range is also controllable via the polymerization temperature of the network, which enables colorful patterns by masked exposure. In addition, linearly polarized light-dependent color can be built into this patternable and TR-RC PSLC coating to bestow new applications. The characteristics of the molecular systems in each chapter are compared in Table 6.1. To summarize, the siloxane-based CLC molecular systems for TR-RC coatings have evolved to be easily processable, have a fast responsiveness and to be fully reversible, patternable, and complexed optics are also possible.

In this Chapter, potential products, i.e., infrared reflective smart windows and visible light reflecting products such as temperature indicators, derived from these TR-RC coatings are discussed.

Table 6.1. Summary of molecular systems in the main chapters of the thesis.



The image shows a siloxane network design on the left, consisting of a vertical chain of silicon atoms (Si) connected by oxygen atoms (O). The top silicon atom is bonded to a methyl group (represented by a vertical line). The second silicon atom is bonded to three groups: a methyl group, a phenyl ring (represented by a hexagon with a circle inside), and a group labeled P₁, P₂, P₃. The third silicon atom is bonded to a methyl group and a group labeled n. To the right of the network are three chemical structures: P₁ is a phenyl ring with a hexyl chain at the para position and a methoxy group at the other para position; P₂ is a phenyl ring with a hexyl chain at the para position and a chiral center at the other para position; P₃ is a phenyl ring with a hexyl chain at the para position and a vinyl group at the other para position.

	Chapter 2	Chapter 3	Chapter 4-5
Siloxane design	P1 homopolymer	P1+P2+P3 terpolymer	P1+P2 copolymer
Chiral center	Added S811	In P2	In P2
Network design	No network	Polymerizable group in P3 (6 mol%)	Added network monomer
Network fraction	0	40-50% of siloxane chains (rough estimation) in short network segments	Tunable ratios, 3-4wt% are the optimal
TR-RC wavelengths	2350-1250 nm	1363-775 nm	670-400nm, variable by network ratio and curing temperature Linear polarized light dependent color can be built upon
TR-RC temperatures	16-66°C	20-66 °C	20-55 °C
TR-RC Reversibility	Irreversible from isotropic	Irreversible from isotropic	Fully reversible
Coating processability	Simple	Complicated, requiring a mediator	Simple
Chemical stability	S811 loss over storage	Stable	Stable
Mechanical stability	Susceptible to any force	Susceptible to any force at >30°C	Stable when with a topcoat
Application model	IR reflecting windows	IR reflecting windows	Temperature sensor, decorative art, security labels

2. Infrared reflecting coatings for smart windows

The modern era faces a climate challenge requiring the consumption of energy by humans to be reduced. As windows are playing an increasingly important role in the

Chapter 6

modern world (architecture and vehicles), they can be functionalized to reject sunlight energy in order to lower the energy consumption needed for the cooling of interior spaces (Figure 6.1a). As introduced in Chapter 2, coatings or foils that reflect near-infrared light (IR), which are invisible but a major source of sunlight heating, would be of great use for producing energy saving, transparent windows. Compared to absorption based technologies, light reflection is more effective in terms of energy insulation.^[1]

“Smart windows” refer to the on-demand light transmittance modulation of the windows.^[2] Temperature responsive infrared reflectors are one category of materials that can be used for smart windows as they can automatically adjust IR transmittance according to the circumstance, thus regulating heat without manual operation. Such smart window coatings are an appealing application of the siloxane based CLC materials that have been presented in this thesis. The coatings in Chapter 2-3 demonstrated the prototypes of such infrared reflecting smart windows, which

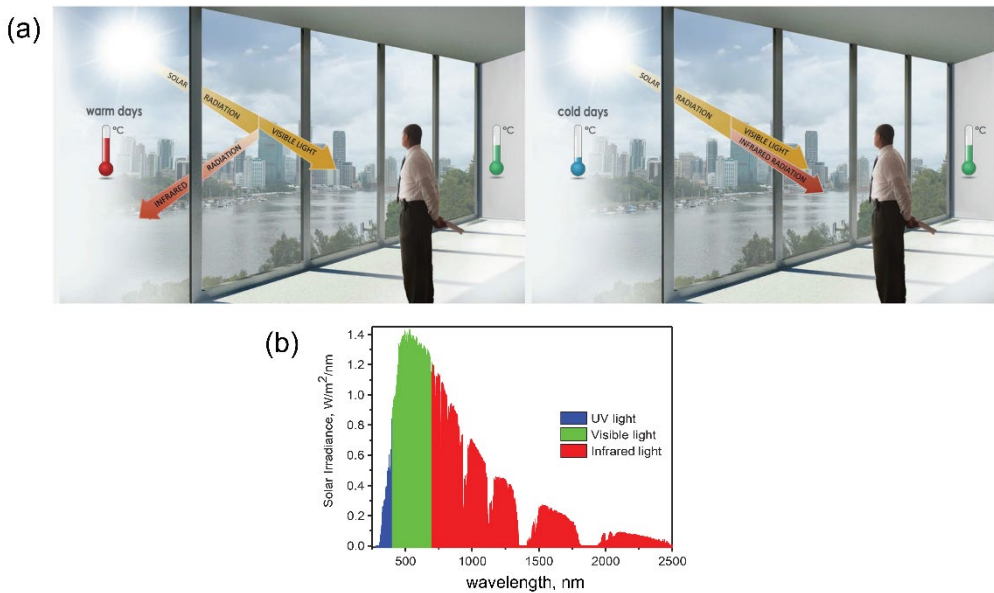


Figure 6.1 (a) The concept of an ideal temperature-responsive smart window reflecting infrared radiations during warm days (left) and allowing it to transmit during cold days (right), while remaining transparent in the visible region. Reproduced with permission.^[1] Copyright 2017, John Wiley and Sons. (b) Solar spectrum on Earth. Data taken from National Renewable Energy Laboratory.^[3]

exhibited good processibility as coatings and large thermal reflection bandshift over the IR region. The system developed in Chapter 4 is suited because of the full reversibility from being heated beyond the isotropic temperature, the fast response speed, and excellent transparency. The easy processibility of the material may allow for larger sized products, too. To adapt the material for smart windows, the concentration of chiral dopant shall be lowered to relocate the reflection bandshift to the IR region.

The reflection band of the coatings shifts towards a lower wavelength in the IR range at higher temperatures, driven by the smectic-cholesteric transition. This characteristic is favorable for smart windows, as sunlight contains more energy in the lower wavelengths of IR (Figure 6.1b).^[3] Furthermore the coating will be transparent in the visible light region. Moreover, the siloxane backbones have a T_g below 0 °C, which allows for responsiveness at warm weathers on Earth.

Despite the potential of the materials, improvements have to be made for the realization of commercial smart window products. Major improvements to focus on are increasing reflection efficiency, scale-up production, robustness, and cost prize.

2.1. Improving heat regulating efficiency

Near infrared light covers a wide wavelength range of 700-2500 nm.^[3] To reject IR light entirely, reflection of these wavelengths needs to be completely covered, with 100% reflection. However, in the materials shown in this thesis, only a single small reflection band is observed instead of a broad reflection band. Furthermore, the CLCs due to the single handedness a maximum of only 50% of reflection can only obtained. Although the direction of the band shift is correct for smart windows, the general heat regulating efficiency in these devices is presumably not high enough for practical usage.

An ideal smart window coating would present a single reflection band at ~2500 nm at low temperature, and broadens to the full IR range when heated. In fact, such a band-broadening type of temperature response has been shown in PSLC systems with small mesogenic molecules.^[4-7] Such broadening stems from anchoring effects (Figure 6.2) that cause the non-reactive CLC molecules near the polymer network to be physically constrained and no longer able to respond to changing temperatures. On the other hand, CLC molecules located further away from the polymer network

Chapter 6

have more freedom of motion, and their temperature response is unaffected by the network. As a result, the reflection band of the system is gradually broadened upon heating.

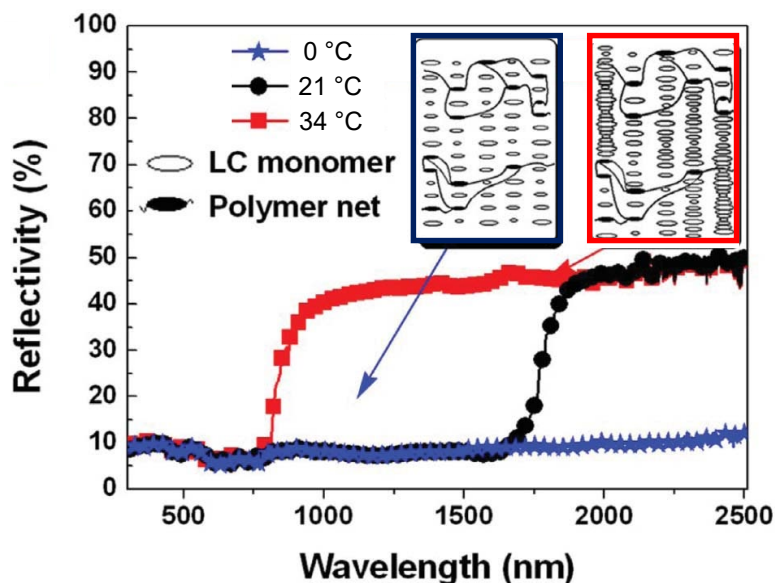


Figure 6.2 The band-broadening type of temperature response of a PSLC cell using HTP changing small molecules. Inset reveals the mechanism of such band broadening, which is due to the inhomogeneity of the network induced during photopolymerization that causes an anchoring effect. Adapted with permission.^[7] Copyright 2010, Taylor & Francis.

However, PSLCs utilizing smectic-cholesteric type CLCs rarely show such broadening effects.^[8–10] The only reported case of band broadening when using PSLCs with a smectic-cholesteric phase transition is seen in a cell with an ultra-thick (203 μm) LC layer containing 11 wt % acrylate network and 88 wt % of a non-reactive smectic-cholesteric phase transition CLC mixture.^[11] For making polymer coatings based on these results, siloxane CLCs with an HTP changing mechanisms could be used. Materials with such properties have been discovered in a few examples^[12,13], the chemical structures of which are drawn in Figure 6.3.

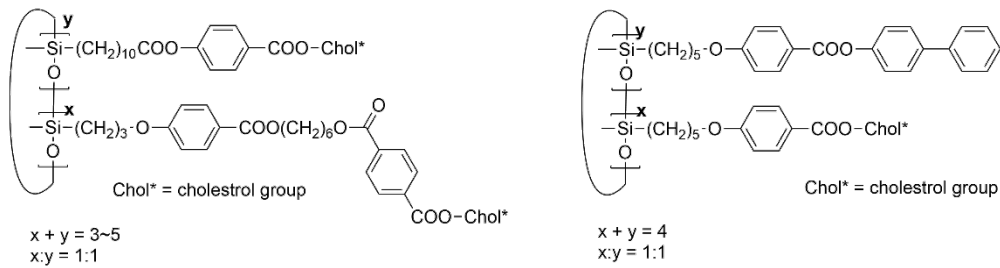


Figure 6.3 Chemical structures of thermochromic siloxane CLCs with an HTP changing mechanism. Cholesterol groups are used as chiral dopants. [12,13]

To achieve 100% of light reflection, both left- and right- handed CLCs have to be present in the coating. This could be achieved by coating two CLC layers of opposite handedness.

2.2. Realizing large scale production

In the previous chapters, the siloxane based CLC materials are proven to be processable via a wire-bar or blade coating method, and the material can adopt a planar CLC alignment upon coating. The maximum sample size prepared in this thesis is seen in the patterned coatings presented in Chapter 5, where the substrate size is 9*9 cm to fit the entire gap applicator, and the pattern size is approximately 4*3 cm, which is large enough for the pattern imprint. Compared to the traditional method of capillary filling into cells to obtain alignment, the bar-coating processing is superior in processing time for more viscous materials and avoiding chromatography effect which causes inhomogeneity issues when applied over large areas. It could be estimated that such lab-scale bar-coat setup should be modified for meter-scale fabrications, as the substrates shall preferably move rather than the gap (Figure 6.4a). Industrial flexography coaters are available for pilot testing (Figure 6.4b).

Apart from the direct application on glass as coatings, adhesive foils could be an attractive route as well, which would be convenient for application to existing windows. Bar-coating, however, may be not efficient for foil fabrication. An alternative way is roll-to-roll fabrication, commonly seen in the production of foils (Figure 6.4c). PDLC foils have been successfully fabricated as meter scale products (Figure 6.4d).^[14,15] Transparency tuning window foils driven by both temperature and electricity have been demonstrated. As friction force between substrates is involved

Chapter 6

in roll-to-roll procedures, planar alignment of our siloxane based CLCs might be possible. Compared to systems with small mesogenic molecules^[16–18] our full-polymer systems could be more robust since leakage or flow of the LCs can be avoided.

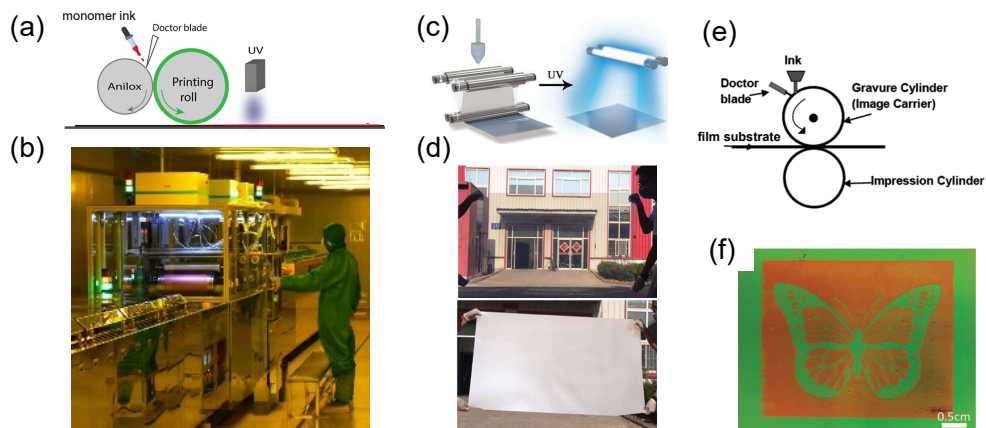


Figure 6.4 (a) Schematic presentation of the flexography technique. Reproduced with permission.^[20] Copyright 2019, Royal Society of Chemistry. (b) Industrial flexographic coater. Picture provided by Guohua Optoelectronics, Shenzhen, China. (c) Schematic presentation of roll-to-roll fabrication of foils. (d) meter scale PDLC foils produced via roll-to-roll methods. The transparent foil turns opaque at higher temperatures. Reproduced with permission.^[14,15] Copyright 2017, Royal Society of Chemistry. (e) Schematic presentation of the gravure technique. Reproduced with permission.^[19] Copyright 2011, IEEE. (f) colored soft film by CLC polymers, produced by gravure printing. Reproduced with permission.^[21] Copyright 2019, John Wiley and Sons.

Flexographic and gravure printing^[19] (Figure 6.4a,e) are also powerful candidates for upscaling flexible substrate devices, as the printing speed can be fast, up to 1.5 m/s. The frictional forces induced by the printing roll could also facilitate planar cholesteric alignment in CLC polymer films (Figure 6.4f).^[20,21] Patterning on these films is possible by designing the plate cylinder. Therefore, these processing techniques are for fabricating TR-RC CLC polymer coatings or foils.

2.3. Enhancing mechanical robustness

The TR-RC PSLC coatings contain largely non-crosslinked oligomers to maintain a proper temperature response. These coatings are not mechanically robust enough for commercial products and easily suffer from mild damage such as touching and light abrasion. If the materials are not coated on the inner sides of the double-glazed

windows, a topcoat must be applied to enhance its robustness. Solvents or low-mass precursors should be avoided when selecting the topcoat material, as they could penetrate into the siloxane CLCs and disturb the alignment.

In Chapter 4, a PDMS topcoat is bar-coated on top of the siloxane CLC layer and shown to provide decent protection against abrasion by finger touching, without harming the TR-RC property of the coating. Tougher topcoats are needed in further product development to provide better protection. Many candidates are available on the market. For instance, transparent and anti-scratch solvent free polymer based materials are promising that would not harm the CLC material during the coating procedure.^[22,23]

2.4. Cost control

The cost of polymer coating in product development. This thesis shows new designs of siloxane CLC oligomers that are suitable for TR-RC coatings. The synthesis of these materials involves multi-step reactions with different mesogenic precursors. Especially the chiral dopant M2 which is not commercially available is expensive to synthesize. For instance, the retail price of (S)-(-)-1-phenyl-1-propanol used to synthesize M2 is 287 € for 1 mL. This would impose a great burden to the cost of large-scale fabrication. To lower the cost, selecting commercially available materials and simplifying synthesis steps is key.

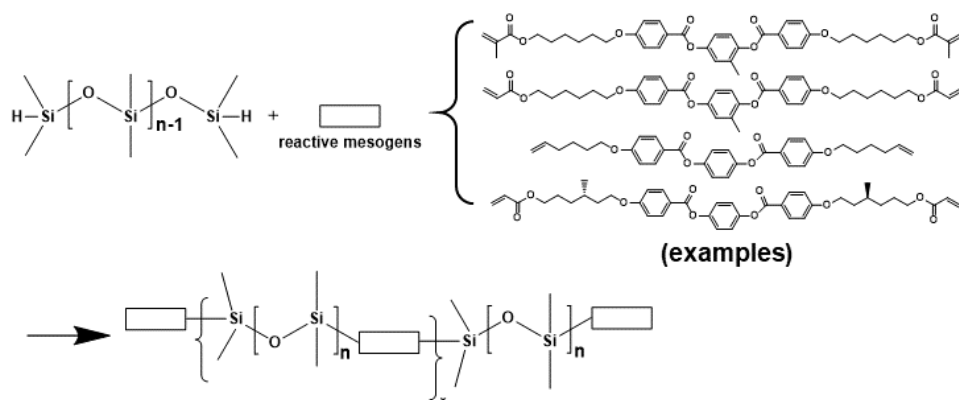


Figure 6.5 Synthesis of main chain siloxane CLC materials. Some examples of mesogenic units are given.

Chapter 6

Main-chain siloxane CLC materials can be considered as one possible solution.^[24,25] Through a hydrosilylation reaction of PDMS with Si-H terminal groups and a mixture of reactive mesogens, the material can be synthesized in one step (Figure 6.5). The selection of mesogenic units can be chosen from a variety of diacrylate nematic mesogens and chiral dopants which have been mass-produced. Main-chain TR-RC CLC oligomers using thiols or amines as chain extenders have been synthesized.^[26,27] By using siloxane as an extender, the responsiveness of the oligomers might be improved, the working temperature can be lowered to ambient temperature conditions, and by stabilization with crosslinked networks, excellent thermal responsiveness similar to that observed in the side-chain polysiloxanes can be achieved.

3. Applications of visible light reflecting coatings

Visible light reflectors have been demonstrated from PSLC coatings with TR-RC CLC siloxanes (Chapter 4). Color patterned coatings have with linear polarization dependent colors been created too (Chapter 5). Potential applications for these colorful TR-RC coatings include interactive decorations, security labels, and temperature indicators. These products could be specially customized and fabricated on a smaller scale, without requirements on full intensity or broadband reflection. The abovementioned issues about processing methods, mechanical robustness and cost control may still apply to their product development, though.

3.1. Interactive decoration

Decorative art such as mood rings and body-temperature sensitive sheets (Figure 6.6a) have been produced from TR-RC CLCs as alleged solvent-based inks.^[28] One could infer from the information provided that these inks are made from PDLC systems in that they are sold as either paintable inks, or breakable sheets.

Compared to PDLC systems or layers with absorption-based colors, the PSLC TR-RC coatings described in this thesis (Chapter 4) have the unique feature of high transparency. This feature would be optimal for decorations where transparency is needed, such as windows, showcases, or containers. Patternability of the coatings as demonstrated in Chapter 5 can extend the option for decorative designs as well. One possible application of the patterns is outdoor decoration or advertisement on architecture windows, like the examples of the patterned luminescent solar concentrator that is shown in Figure 6.6b.^[29] Transparent, removable decorative foils with thermally responsive colors can also be envisioned from our materials.

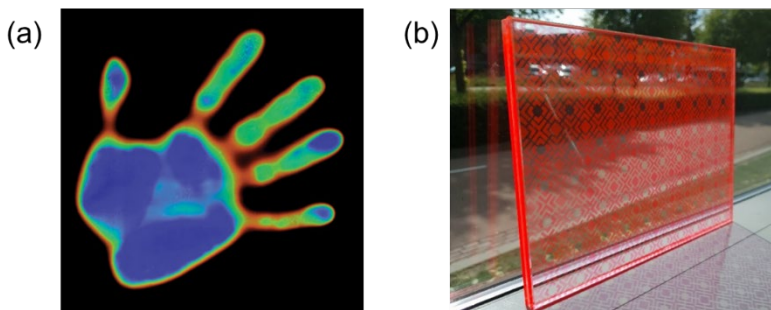


Figure 6.6 (a) An example of thermosensitive CLC sheet that is sensitive to body temperature. (b) patterned luminescent solar concentrator that can be used as window decorations. Reproduced under terms of the CC-BY-NC-ND license.^[29] Copyright 2020, Elsevier.

3.2. Security labels

Chapter 5 shows the hiding and revealing of patterns in the TR-RC coating, created via stratification in the CLC helices. The red stratified patterns are hidden in the unstratified background of the same color, and can be revealed under linear polarized light due to the contrast in color and brightness. This suggests the possibility for applications as security labels, such as anti-counterfeit marks or information encryption. The application scenario would be the identification of genuine products or passwords. Each pattern has a unique temperature responsiveness and is reversible, which would add extra dimensions to the verification or encryption method. Patterns, colors, TR-RC properties, and polarization dependency could all be programmed as the “code”.

Chapter 6

3.3. Temperature indicators

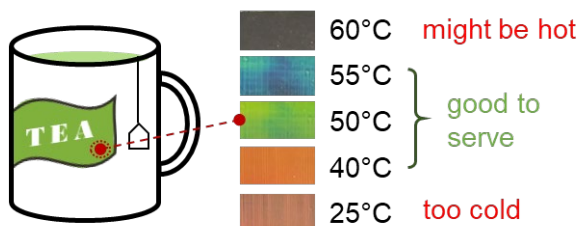


Figure 6.7 A schematic illustration of warm-beverage labels using the CLC-siloxane based thermochromic coatings described in Chapter 4.

Several temperature indicator coatings using CLC materials have been reported. Irreversibly responsive CLC polymer coatings as depicted in Chapter 1 are being developed into smart labels in cold chain transportation or sterilization.^[30,31] The irreversible color change by heat would indicate the temperature history of the target. Furthermore, reversibly TR-RC PDLC sheets to detect fever (Feverscan[®]) are already available on the market.^[32]

The reversibly TR-RC coating introduced in Chapter 4 is ideal for food labels where the working temperature range is of importance. Warm beverages (e.g. coffee, tea) are best served at around 58°C.^[33] Consuming at a higher temperature could be harmful to health.^[34,35] Therefore, this TR-RC system is well suited for showing if a beverage is at a proper serving temperature by a label on the container or package (Figure 6.7). Above 55°C where no color is presented, the food is considered too hot to consume, while below 40°C the reflection shifts to red, indicating a cold drink with reduced flavor. Warning signs could be printed behind the CLC label to alert the possible burns, too, due to the good transparency of the label. If such labels could be fabricated at low cost, they can be produced as single-used food packages.

4. Conclusion

The chapter show a map of potential applications for siloxane-based TR-RC CLC coatings. As can be concluded, the materials introduced in this thesis are promising for coating-based products such as infrared reflective smart windows, temperature indicators, interactive decorations, and security labels. Future researches and

engineering on the material can be dedicated to remove the obstacles to allow these products to reach the market.

5. References

- [1] H. Khandelwal, A. P. H. J. Schenning, M. G. Debije, *Adv. Energy Mater.* **2017**, *7*, 1602209.
- [2] Y. Ke, J. Chen, G. Lin, S. Wang, Y. Zhou, J. Yin, P. S. Lee, Y. Long, *Adv. Energy Mater.* **2019**, *9*, 1902066.
- [3] “Calculated from the data given at the website of National Research Energy Laboratory,” can be found under <http://www.nrel.gov>, **accessed: October 2016**.
- [4] F. Wang, P. Song, H. Yang, X. Shao, *Liq. Cryst.* **2016**, *43*, 1732.
- [5] L. Xiao, H. Cao, J. Sun, H. Wang, D. Wang, Z. Yang, W. He, J. Xiao, H. Ding, H. Yang, *Liq. Cryst.* **2016**, *43*, 1299.
- [6] H. Yang, K. Mishima, K. Matsuyama, K. I. Hayashi, H. Kikuchi, T. Kajiyama, *Appl. Phys. Lett.* **2003**, *82*, 2407.
- [7] X. Yuan, L. Zhang, H. Yang, *Liq. Cryst.* **2010**, *37*, 445.
- [8] J. Sun, H. Wang, L. Wang, H. Cao, H. Xie, X. Luo, J. Xiao, H. Ding, Z. Yang, H. Yang, *Smart Mater. Struct.* **2014**, *23*, 125038.
- [9] B. Zhang, X. Lin, Y. You, X. Hu, L. de Haan, W. Zhao, G. Zhou, D. Yuan, *Opt. Express* **2019**, *27*, 13516.
- [10] X. Wu, H. Cao, R. Guo, K. Li, F. Wang, H. Yang, *Polym. Adv. Technol.* **2013**, *24*, 228.
- [11] W. Huang, X. Zhang, J. Guo, L. Zhang, Z. Bian, D. Zhao, W. He, H. Cao, H. Yang, *Liq. Cryst.* **2009**, *36*, 497.
- [12] J. W. Wang, B. Y. Zhang, *J. Appl. Polym. Sci.* **2013**, *130*, 1321.
- [13] X. Zhang, L. Zhang, J. Tan, X. Wu, B. Li, F. Wang, H. Yang, Z. Yang, *J. Mater. Sci.* **2014**, *49*, 4927.
- [14] X. Liang, C. Guo, M. Chen, S. Guo, L. Zhang, F. Li, S. Guo, H. Yang, *Nanoscale Horizons* **2017**, *2*, 319.
- [15] X. Liang, S. S. Guo, S. S. Guo, M. Chen, C. Li, Q. Wang, C. Zou, C. Zhang, L. Zhang, H. Yang, *Mater. Horizons* **2017**, *4*, 878.
- [16] A. Ranjesh, T.-H. Yoon, *ACS Appl. Mater. Interfaces* **2019**, *11*, 26314.
- [17] H. Khandelwal, E. P. A. Van Heeswijk, A. P. H. J. Schenning, M. G. Debije, *J. Mater. Chem. C* **2019**, *7*, 7395.
- [18] E. P. A. van Heeswijk, T. Meerman, J. de Heer, N. Grossiord, A. P. H. J. Schenning, *ACS Appl. Polym. Mater.* **2019**, *1*, 3407.
- [19] D. A. Alsaïd, E. Rebrosova, M. Joyce, M. Rebroso, M. Atashbar, B. Bazuin, *J. Disp. Technol.* **2012**, *8*, 391.
- [20] D. C. Hoekstra, K. Nickmans, J. Lub, M. G. Debije, A. P. H. J. Schenning, *ACS Appl. Mater. Interfaces* **2019**, *11*, 7423.
- [21] E. P. A. van Heeswijk, L. Yang, N. Grossiord, A. P. H. J. Schenning, *Adv. Funct. Mater.* **2020**, *30*, 1.
- [22] “RepelFlex® – NBD Nano,” can be found under <https://www.nbdnano.com/solutions/coatings/repelflex/>, **accessed: April 2021**.
- [23] “SHIKOH™_Mitsubishi Chemical Corporation,” can be found under https://www.m-chemical.co.jp/en/products/departments/mcc/coating-mat/tech/1205890_9239.html, **accessed: April 2021**.
- [24] Y. Shoji, R. Ishige, T. Higashihara, J. Watanabe, M. Ueda, *Macromolecules* **2010**, *43*, 805.
- [25] M. Amela-Cortés, D. W. Bruce, K. E. Evans, C. W. Smith, *J. Mater. Chem.* **2011**, *21*, 8436.
- [26] P. Zhang, A. J. J. Kragt, A. P. H. J. Schenning, L. T. De Haan, G. Zhou, *J. Mater. Chem. C* **2018**, *6*, 7184.
- [27] A. Kotikian, R. L. Truby, J. W. Boley, T. J. White, J. A. Lewis, *Adv. Mater.* **2018**, *30*, 1706164.

Chapter 6

- [28] “Special FX Creative- Inks, Paints, Pigment, Plastic and Print – SFXC _ Special FX Creative,” can be found under <https://www.sfxc.co.uk/>, accessed: **January 2021**.
- [29] J. ter Schiphorst, M. L. M. K. H. Y. K. Cheng, M. van der Heijden, R. L. Hageman, E. L. Bugg, T. J. L. Wagenaar, M. G. Debije, *Energy Build.* **2019**, *207*, 109625.
- [30] K. Nickmans, D. A. C. van der Heijden, A. P. H. J. Schenning, *Adv. Opt. Mater.* **2019**, *7*, 1900592.
- [31] Y. Foelen, D. A. C. Van Der Heijden, M. Del Pozo, J. Lub, C. W. M. Bastiaansen, A. P. H. J. Schenning, *ACS Appl. Mater. Interfaces* **2020**, *12*, 16896.
- [32] “Color Changing Thermometer Strips & Temperature Indicator,” can be found under <https://www.hallcrest.com/>, accessed: **January 2021**.
- [33] F. Brown, K. R. Diller, *Burns* **2008**, *34*, 648.
- [34] D. Loomis, K. Z. Guyton, Y. Grosse, B. Lauby-Secretan, F. El Ghissassi, V. Bouvard, L. Benbrahim-Tallaa, N. Guha, H. Mattock, K. Straif, *Lancet Oncol.* **2016**, *17*, 877.
- [35] F. Islami, H. Poustchi, A. Pourshams, M. Khoshnia, A. Gharavi, F. Kamangar, S. M. Dawsey, C. C. Abnet, P. Brennan, M. Sheikh, M. Sotoudeh, A. Nikmanesh, S. Merat, A. Etemadi, S. Nasseri Moghaddam, P. D. Pharoah, B. A. Ponder, N. E. Day, A. Jemal, P. Boffetta, R. Malekzadeh, *Int. J. Cancer* **2020**, *146*, 18.

Summary

Temperature Responsive Photonic Coatings based on Siloxane Liquid Crystals

Temperature-responsive photonic polymers are able to change their structural reflective color upon temperature fluctuations. These “smart” materials have potential applications as temperature indicators, aesthetics, and heat-regulating windows. For these applications, polymer coatings are desired that are easily processable, robust, and have a reversible response. However, the fabrication of such thermochromic coatings remains challenging. This thesis aims at preparing temperature responsive reflective-color coatings from cholesteric liquid crystal (CLC) polymer materials, pursuing easy processability, fast and reversible responsiveness, and good mechanical robustness. In the Chapters 2-5 are shown the evolution of material system design based on siloxane CLC materials with smectic transitions to induce a temperature responsive color change. Chapter 2 shows the proof of concept that a siloxane-based CLC material can be bar-coated, using a simple mixture of nematic homopolymer and a chiral dopant. In Chapter 3 a crosslinkable terpolymer CLC is synthesized in order to achieve a polymer-stabilized coating with a high crosslink ratio. Temperature responsiveness of this coating is remained in this polymer stabilized liquid crystal (PSLC) system. Chapter 4 modifies the PSLC system such that the crosslinked network is not covalently bonded to the siloxane CLC. By using the optimal network concentration, the PSLC coating shows full reversibility in responsiveness from both isotropic and smectic transitions. It is also shown that a topcoat can be used to provide mechanical protection to the PSLC coating. Chapter 5 enriches the optical responsiveness of the PSLC system, showing that its responsiveness can be controllable via polymerization temperature of the network, which enables colorful patterns by masked exposure. In addition, linearly polarized light-dependent colors can be built upon this coating as well.

Through these generations of material systems, the siloxane-based temperature responsive CLC coatings are evolved to be simple in fabrication, fast and fully reversible response, tunable wavelength range, and mechanically robust. It is

foreseen that these coatings can be developed further into various applications including IR reflective smart windows and temperature indicators.

Acknowledgements

This thesis has been in preparation for more than four years with all-out, day and night effort concentrated on performing research work in both Eindhoven and Guangzhou. Hundreds of wrong directions and failed experiments have been attempted before each chapter finally took shape. So, first of all, I would like to thank you for reading my thesis. All that sweat pays off if you enjoy reading it.

My PhD project was made possible by Device Integrated Responsive Materials (DIRM), a joint lab between South China Normal University (SCNU) and Eindhoven University of Technology. Therefore, I would like to express my special gratitude to my co-promotor Prof. Guofu Zhou, the director of DIRM group. You offered me this opportunity to start my PhD project, and supported me in resources and funds. The idea of bringing science to the application frontier, which is one mission of DIRM, inspires me a lot and has become my personal ambition, too. It is sad that my wish of pilot line testing of the coatings in my last year was not fulfilled due to the difficulty in travelling to China, but I am looking forward that a nice smart coating product from DIRM can become reality in the future.

I would like to present my biggest thanks to my daily supervisors Albert and Laurens. We completed the research projects hand in hand, overcoming the difficulties of remote co-supervising to finally work out an effective path. Under your supervisions, I now deeply understand what good research entails. You cared for all perspectives of my academic growth, from initiating a research idea to planning experiments, from data analysis to presenting and writing. I am a slow learner, but with your patient help I have been able to walk progress very far from where I started. The Dutch spirit of equality, passed down to me through myriad meetings, have also helped adapt my outlook. I feel lucky to have you as my supervisors and as friends.

I would also like to thank prof. dr. Dirk Broer for enlightening me with the world of liquid crystals, introducing me to the DIRM group, and spark inspiration during my beginning stages. You are a hero I look up to. Johan, many thanks for the professional advice on organic synthesis. The successful synthesis of the important compounds in the thesis, for example M2 and TP, owes much to your expertise. The liquid crystal

library you created also opened a lot of options for my selection in chemicals. Dr. Michael & Audrey Debije, thanks to your assistance in writing of journal articles and the thesis: they became much more concise and readable by your magic hands. Dr. Danqing Liu, thank you for the always friendly talks and the tips regarding work and life in academia. In addition, I would like to thank prof. dr. Rint Sijbesma, dr. Catarina Esteves, and prof. dr. Jingxia Wang for being members of the defense committee.

The SFD group provides me a platform for freely conducting my research. I enjoyed every moment working in the SFD labs as well as joining in special events and mingling with people. I am grateful to all the former and current SFD members that I have met. Marjolijn, you have been taking care of my general arrangements for working in the Netherlands since I was a visitor student in 2015. As I often move between places, all kind of troubles came up to me regarding my visa, residence and travelling, but you handled them all perfectly. My PhD could not have gone so smoothly without your help. Tom, you are always very helpful in any favor that I asked, including technical support and ordering materials. We also had so many good times in playful chit-chats. Stijn, you were my supervisor during my Master exchange student period, and we collaborated a lot during my PhD. You are creative while staying rigorous and focused, which I set as a good model for a researcher to learn from. We also hung out a lot in China and the Netherlands, and had a lot of enjoyable moments that I can clearly remember. Jeroen Sol, my office mate, we have been very eager to share thoughts with each other over work, life, and everything, especially cultures and languages, which I could not help but to share my knowledge. These conversations were always a good way to bring ease and peace of mind during times of busy work. Your online animation software course with Alberto during the pandemic introduced me a new skill of advanced drawing, too. To Arne, also my office mate, since we all worked on cholesterics, we could hold useful brainstorming sessions on the topic. We collaborated together on the very nice review paper which has been adapted to be part of my thesis. Thanks for your input. A lot of my experiments and writings were finished over the weekends, which are non-regular hours. I cherish these quiet, but not lonely, times with the accompany by the "OT guys", namely Xiaohong, Xinglong, Yuanyuan, Li Liu, Pei Zhang, Wei Feng. With you guys, these 'overtimes' felt pleasant and secure.

I would also say a big 'thank you' to other people who had helped me greatly with experiments, and who I spent happy times with: Koen, Kamlesh, Cees, Anne-Hélène, Dirk-Jan, Hitesh, Monali, Lihua, Hao Liu, Huub, Jeroen ter Schiphorst, Sander, Sarah, Matthew, Anping, Wanshu, Shaji, Sterre, Daniëlle, Roel, Yari, Fabian, Davey, Simon, Gilles, Alberto, Dongyu, Rob, Marina, Yi-ru, Henk, Damian, Nadia, Ellen, Sean, Sebastian, Shajeth, Niki, Marc, Ievgen, Stathis, Thierry. I will be missing you after leaving the group. Hope to see everyone again in the future (the World is becoming smaller!).

My PhD was initiated in SCNU, Guangzhou, the city where I was born, and the university where I studied for my Bachelor and Master degrees. It was my pleasure to join the DIRM team and begin the TU/e story. This will be an important page of my life. In DIRM, we frequently discussed each other's progress through regular meetings, which I benefited a lot from. My gratitude to the DIRM teachers, who are so kind and friendly: Xiaowen, Dong Yuan, Wei Zhao, Huapeng, Zhen Zhang. DIRM secretaries Joey Zhou, Qiuxia, Peggy Liang, Huishan, and the administrators of the institute, thanks for great support during my stay in SCNU, and making my PhD journey to TU/e possible. I would like to thank technician Jinhong and Tingting for solving troubles big and small in the laboratory and assisting me in building a new synthesis room. Additionally, I would specially thank the groups of Hao Li, Yao Wang, LingLing, and Pengfei in our institute. You offered equipment and lab space to me at the early stage when our lab did not have a lot yet.

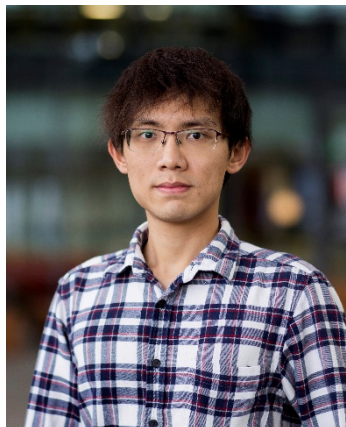
Of course, I will not forget the colleges and students in SCNU. We stick together like a big family, creating a friendly and easy environment. Some of you have also got the chance to come to TU/e for an exchange, making me feel like a "small family" back home. My sincere thanks to all of you. Just to name a few: Wei Liu, Zixuan, Sunqian, Yuxin, Pengrong, Xiuyi, Lansong, Beibei, Lingyun, Hui Yu, Xinmin, Xiulan, Xiao Wang, Yong Zhou, Jialin, Shuting, Zhenping... Special thanks to Yuanyuan, who walks a similar PhD to me. We supported each other in tackling all the matters related to the PhD track. Your dedication to science and daring to open new fields also impressed me a lot, which I have been trying hard to model myself.

During the past years, I have met with friends in both China and the Netherlands, which have enriched my life and spirit. Acknowledgements are given to you: Chao Zhang, Yichen, Yuan Liao, Yingbo, Baoping, Juan Wang, Hao Wu, Jie Zheng, Ting

Liang, Xiao Meng, Bojia, Long Zhang, Xianhong, Xianwen, Lusi, Jian Liu, Lanhui, Guoxiu, Jiaxin, Feibo, Huiyi, Shidong, Danwen, Wanshi, Yiwei, Diederik, Patri, Koen, Justinas, Jitesh, Eser, Joey, Douwe, Job... I will always remember the shining points of you that leave sparks in me.

At last, a credit to my parents and family. 衷心感谢我的父母以及家人，在并不宽裕的条件下仍然支持我读博的决定。为了能让我专心地顺利完成博士的攻读，在背后默默付出了许多。是你们的辛劳才造就了现在的我。相信我们的生活一定会越来越好，未来的路一定越走越宽。祝你们平安，健康，快乐！

Curriculum Vitae



Weixin ("Wilson") Zhang was born in on January 15th, 1992 in Guangzhou, China. After graduating from high school in 2010, he studied in South China Normal University (SCNU), Guangzhou, China, and received his bachelor's degree in Materials Chemistry in 2014. He continued to study for his master's degree in SCNU, in the group SCNU-TUE Joint Lab of Device Integrated Responsive Materials (DIRM), under supervision of Prof. Guofu Zhou and Dr. Laurens de Haan. During his Master study, he visited the Stimuli-responsive Functional Materials and Devices group in Eindhoven University of Technology (TU/e) for 9 months as an exchange student from DIRM, with scholarship from SCNU. In May 2017, he successfully defended his Master thesis in SCNU, titled *"Preparation and Study of Temperature Responsive Composite HP/S811 Based on Polysiloxane Liquid Crystalline for Application in Infrared Reflectors"*. In July 2017, he joined the group of Stimuli-responsive Functional Materials and Devices in TU/e for his PhD studies, and became a member of DIRM. His PhD project focuses on temperature-responsive photonic coatings based on siloxane cholesteric liquid crystals, under the supervision of Prof. Albert Schenning, Dr. Laurens de Haan, and Prof. Guofu Zhou. The most important results of Weixin's PhD research are summarized in this thesis.

List of Publications

Zhang, W.; Kragt, S.; Schenning, A. P. H. J.; De Haan, L. T.; Zhou, G. Easily Processable Temperature-Responsive Infrared-Reflective Polymer Coatings. *ACS Omega* **2017**, 2 (7), 3475–3482.

Zhang, W.; Lub, J.; Schenning, A. P. H. J.; Zhou, G.; de Haan, L. T. Polymer Stabilized Cholesteric Liquid Crystal Siloxane for Temperature-Responsive Photonic Coatings. *Int. J. Mol. Sci.* **2020**, 21 (5), 1803.

Zhang, W.; Schenning, A. P. H. J.; Kragt, A. J. J.; Zhou, G.; de Haan, L. T. Reversible Thermochromic Photonic Coatings with a Protective Topcoat. *ACS Appl. Mater. Interfaces* **2021**, 13 (2), 3153–3160.

Zhang, W.; Kragt, S.; Schenning, A. P. H. J.; De Haan, L. T.; Zhou, G. Patternable thermochromic photonic coatings with light polarization dependencies. *Adv. Mater. Interfaces* (submitted).

Zhang, W.; Froyen, A. A. F.; Schenning, A. P. H. J.; Zhou, G.; Debije, M. G.; De Haan, L. T. Temperature-responsive photonic devices based on cholesteric liquid crystals. *Adv. Photonics Res.* **2021**, 2 (7), 2100016.